

**GEOSTATISTICAL EVALUATION OF THE EASTERN ORE FIELD ONE (EF1) OREBODY,  
ROSH PINAH ZINC MINE, NAMIBIA.**

Sheron Tjiuavioye Kaviua

A Dissertation submitted to the Faculty of Engineering and the Built Environment,  
University of the Witwatersrand, Johannesburg, in fulfilment of the requirements  
for the degree of Master of Science in Engineering.

Signed on 16 May 2018 in Johannesburg

## DECLARATION

I declare that this Dissertation is my own unaided work. It is being submitted for the Degree of Master of Science in Engineering at the University of the Witwatersrand, Johannesburg. It has not been submitted before for any degree or examination to any other University.



---

(Signature of candidate)

16<sup>th</sup> day of May 2018 in Johannesburg

## **ABSTRACT**

The geometry, size and quality of a deposit are key parameters required for decision-making regarding mining methods, capital investments or divestments, economic viability and processing methods. The dissertation uses a quantitative approach to assess three geological modelling methods for orebody geometry. It applies Principal Components Analysis (PCA) in order to understand the variability and correlation in the data. The dissertation aims to determine the significance of increasing the composite size to 3 m for grade estimation and to estimate the tonnes and grades of the Eastern Ore Field 1 in-situ resource as on 31 December 2016.

A MineSight, a Leapfrog and a hybrid of MineSight and Leapfrog modelling method were assessed, aiming to reduce the modelling time. The Minesight and Leapfrog hybrid model is recommended for modelling complex sedimentary exhalative deposits. The PCA was carried out using Matlab. Based on the correlation of 0.998, the first principal component increases with increasing Ag, Zn and Pb and it correlates most strongly with Ag. The second principal component increases with Zn, with a correlation of 0.985. With a correlation of 0.927, the third component increases with Mg. A 3 m composite size is recommended for estimating EF1 because the generated block-model estimates have lower means, standard deviations, variances and numbers of extreme outliers. The 3 m composite size is closer to the SMU at Rosh Pinah, and produces a better block estimate than 1.5 m composites, the later gives more tonnes and higher grade due to the volume-variance effect, which ultimately leads to overestimation of the mineral deposit. The total in-situ EF1 resource estimated using the Ordinary Kriging interpolation method as on 31 December 2016 was 814,100 tonnes at 8.58% Zn, 3.19% Pb and 79.22 ppm Ag.

In memory of my grandmother

Gustafine Sauku Kaviua

1925 - 1993

## **ACKNOWLEDGEMENTS**

The dissertation is the result of the work of many people that helped and sacrificed resources and time throughout the different projects. I would like to acknowledge Rosh Pinah Zinc Mine for sponsoring the tuition fees and providing the dataset and software used. Special thanks to my supervisor, Professor Richard Minnitt who helped me with the best of his knowledge and Mr. Eric Mouton for the motivation. I acknowledge Mr. Christo Horn for adding the dissertation as a key performance indicator on my performance contract. I am thankful to my partner and best friend Martin Shipanga for helping out with the kids and all household activities. To Taylor, Shannaze and Jamilah thanks for understanding that mother had to spend long hours at work. Special thanks to my parents, Razikua, Puree and friends (Linus, Solomon, Annakleta and Liina) for the emotional support.

## CONTENTS

DECLARATION.....	ii
ABSTRACT.....	iii
ACKNOWLEDGEMENTS .....	v
CONTENTS .....	vi
LIST OF FIGURES.....	xi
LIST OF TABLES .....	xiv
NOMENCLATURE .....	xv
CHAPTER 1: INTRODUCTION .....	1
1.1 Problem statement .....	1
1.2 Objectives of this research.....	3
1.3 Rosh Pinah Zinc Corporation.....	4
1.4 Project location .....	4
1.5 Organization of the dissertation.....	7
CHAPTER 2: RESEARCH METHODOLOGY .....	9
2.1 Introduction.....	9
2.2 Project data .....	9
2.3 Methods .....	10
2.3.1 Quality assurance quality control .....	11
2.3.2 Data validation .....	11
2.3.3 3D grade and lithological solids .....	12
2.3.4 Exploratory data analysis .....	13
2.3.5 Resource estimation .....	13
2.3.6 Model validation .....	14

<b>CHAPTER 3: LITERATURE REVIEW .....</b>	<b>15</b>
<b>3.1 Introduction.....</b>	<b>15</b>
<b>3.2 History and development of geostatistics.....</b>	<b>15</b>
<b>3.3 Significant work done in geostatistics .....</b>	<b>17</b>
3.3.1 Geological modelling .....	17
3.3.2 Sample size .....	18
3.3.3 Top cut/Outliers .....	18
<b>3.4 Geological setting.....</b>	<b>20</b>
<b>3.5 The Geology of the EOF.....</b>	<b>23</b>
<b>3.6 Previous estimations of the EF1 .....</b>	<b>28</b>
<b>3.7 Ordinary Kriging .....</b>	<b>29</b>
3.7.1 Development of OK equation .....	29
3.7.2 The Lagrange Parameter.....	33
3.7.3 Minimizing the Error Variance .....	33
3.7.4 OK using $\gamma$ or $\rho$ .....	35
<b>3.8 Block Kriging .....</b>	<b>36</b>
3.8.1 Introduction .....	36
3.8.2 Advantage and disadvantage of block kriging .....	38
<b>3.9 Quantified Kriging Neighbourhood Analysis .....</b>	<b>38</b>
<b>CHAPTER 4: DATA COLLECTION AND VALIDATION.....</b>	<b>40</b>
<b>4.1 Drilling .....</b>	<b>42</b>
<b>4.2 Drilling data and accuracy of borehole information.....</b>	<b>43</b>
<b>4.3 Logging.....</b>	<b>44</b>
<b>4.4 Sampling techniques .....</b>	<b>44</b>

<b>4.5 Sample preparation</b> .....	45
<b>4.6 Mapping information</b> .....	45
<b>4.7 Data aggregation methods</b> .....	46
<b>4.8 Data validation</b> .....	46
4.8.1 Collars .....	46
4.8.2 Lithology .....	47
4.8.3 Assays .....	47
4.8.4 Conflicting grade and lithologies.....	47
<b>4.9 Certified Referenced Material</b> .....	48
4.9.1 AMIS0147 .....	49
4.9.2 AMIS0149 .....	50
4.9.3 AMIS0153 .....	51
4.9.4 AMIS0157 .....	52
4.9.5 AMIS0158 .....	53
<b>4.10 Blanks</b> .....	55
<b>4.11 Field Duplicates</b> .....	58
<b>4.12 QAQC Summary</b> .....	61
<b>CHAPTER 5: MODELS</b> .....	<b>63</b>
<b>5.1 Introduction</b> .....	63
<b>5.2 Minesight models</b> .....	63
5.2.1 Advantages of Minesight solid (A).....	67
5.2.2 Limitations of Minesight solid (A).....	67
<b>5.3 Leapfrog model</b> .....	69
5.3.1 Advantages of Leapfrog solids (Model B–D) .....	72
5.3.2 Limitations of Leapfrog solids (Model B –D).....	73



5.4 Modeling EF1 sedimentary exhalative deposit .....	74
5.5 Summary.....	76
<b>CHAPTER 6: STATISTICAL ANALYSIS OF ASSAY DATA AND COMPOSITES.....</b>	<b>77</b>
6.1 Introduction.....	77
6.2 Compositing data .....	78
6.3 Comparison of assay data and composites .....	78
6.4 Skewness and Kurtosis.....	79
6.5 Histograms.....	80
6.6 Assessing normality using probability plots.....	85
6.6.1 Z-Score .....	85
6.6.2 Normal probability plots .....	85
6.7 Population mean of the LN (2), $N > 40$ for Zn, Pb and Ag .....	86
6.8 Principal Component Analysis .....	87
6.9 Outlier detection using Quantile Regression .....	89
6.10 Summary.....	90
<b>CHAPTER 7: GEOSTATISTICAL ESTIMATION PARAMETERS.....</b>	<b>92</b>
7.1 Introduction.....	92
7.2 Interpolation method.....	92
7.3 Dealing with outliers .....	93
7.4 Domaining .....	93
7.5 Contour plots.....	95
7.6 Variograms .....	97
7.7 Ellipsoid validation .....	101
7.8 Interpreting variograms .....	101

<b>CHAPTER 8: GEOSTATISTICAL ESTIMATION .....</b>	<b>104</b>
<b>8.1 Block size and statistical grade estimation .....</b>	<b>104</b>
<b>8.2 EOF resource classification .....</b>	<b>105</b>
8.2.1 The PRED system.....	106
8.2.2 Results PRED system .....	108
8.2.3 Results of Mineral Resource estimation .....	109
8.2.4 Grade distribution .....	115
<b>8.3 Grade tonnage curves .....</b>	<b>117</b>
<b>8.4 Model validation .....</b>	<b>120</b>
<b>8.5 Evaluating Kriging.....</b>	<b>124</b>
8.5.1 Slope of regression .....	124
8.5.2 Kriging standard deviation.....	125
8.5.3 Results of the QKNA .....	125
<b>8.6 Summary.....</b>	<b>126</b>
<b>CHAPTER 9: CONCLUSIONS.....</b>	<b>127</b>
<b>9.1 Research questions and main findings.....</b>	<b>127</b>
<b>9.2 Relationship to previous research .....</b>	<b>128</b>
<b>9.3 Limitations of the study.....</b>	<b>129</b>
<b>9.4 Recommendations .....</b>	<b>130</b>
<b>CHAPTER 10: REFERENCES .....</b>	<b>132</b>

## LIST OF FIGURES

Figure	Page
1 Rosh Pinah Zinc Mine location (Crowther, 2014) .....	5
2 Locations of RPZC Exclusive Prospecting License and Mining License (Crowther, 2014) ..	6
3 Layout plans of in-situ mineral resources of the Rosh Pinah Mine. The project area is demarcated with the black square .....	6
4 Longitudinal section of RPZC resources and production focus.....	7
5 Locality of the Rosh Pinah Zn-PB deposit and its stratigraphic setting within the Pan-African Gariep belt. After Frimmel and Frank (1998) .....	22
6 Rosh Pinah Mine Stratigraphy. Source: Mouton (2006) .....	23
7 Schematic cross-section indicating the EOF structure around the Rosh Pinah Mine with development of D2 backfolds and possible backthrusts. Source: Alchin and Moore (2005).....	24
8 Eastern Orefield structural section indicating the western syncline and the eastern anticline as well as major faults cross-cutting the orebody. Source: Watkey (2001) .....	25
9 Rosh Pinah Mine genetic model; mainly a SEDEX with subordinate VMS and BHT depositional and deformational characteristics.....	27
10 A sedimentary exhalative (SEDEX) ore deposition model (modified after Alchin and Moore (2005)).....	27
11 EF1, EF2 and 90 Off Main grids .....	43
12 A. EOF -030 level map indicating lithological contacts. B. EF1 -1080 section interpretation indicating the triangulated carbonate mapping as lines .....	46
13 AMIS0147 Ag Total (ppm) standard analyses by sequence.....	49
14 AMIS0153 Ag (ppm) standard analyses by sequence .....	51
15 AMIS0157 Zn Total (%) standard analyses by sequence.....	52
16 AMIS0158 Zn Total (%) standard analyses by sequence.....	54
17 AMIS0158 Pb Total (%) standard analyses by sequence .....	54
18 SS_BLANK Zn Total (%) standard analyses by sequence .....	56
19 SS_BLANK Zn Total (%) standard analyses by sequence; zoomed in around the acceptable minimum and maximum value .....	56
20 SS_BLANK Ag (ppm) standard analyses by sequence .....	57
21 Original sample versus repeat sample analyses for Zn.....	59

22 Minesight lithological and grade solids A. Carbonate solid. B. Microquartzite solid. C. Footwall breccia solid. D. Arkose solid. E. All lithological solids. F. Zn Equivalent above 4% grade solid.....	66
23 Plan view of the EOF fold hinge on the -030 level .....	68
24 Leapfrog settings. A. Surface resolution of five and wireframe snapped to drilling data only. B. Ignored segments shorter than 0.5 were converted to ore if flagged by ore on either side; interior segments shorter than 1 m were filtered out and all exterior segments were excluded. C. Interior lithology is the high-grade ore above 4% and all other lithologies were treated as exterior. D. Trend data and composites from borehole information.....	70
25 A. Minesight solid of Zn equivalent grade above 4%. B. Leapfrog model created from Minesight sections and level plans. C. Leapfrog model created from Minesight sections, level plans and borehole data. D. Leapfrog model created from boreholes information only .....	71
26 EF1 Section -1020 interpretation of Leapfrog solid created from borehole information and the mineralisation trend. B. The images display solids that were over-interpolated because of a wide snapping window.....	74
27 Field mapping sheet of EF1_-030 level sill.....	75
28 A. Histogram of the sample length. B. Histogram of the composite length.....	78
29 Plan view of Domain 1 and Domain 2 .....	94
30 Domain 1 rotation or New North, plunge and dip for Zn .....	95
31 Domain 1 rotation or New North, plunge and dip for Pb .....	96
32 Two structured spherical model (Anon., n.d.) .....	99
33 Lag distance, lag tolerance and band width (Anon., n.d.) .....	99
34 Lag distance, directions, window angle, and band widths for the EOF estimation.....	100
35 Zn search ellipsoid for Domains 1 and 2 .....	101
36 A vertical section (-1020) displaying the model estimates assays (blue – model estimates from 1.5 m composites; green–model estimates from 3 m composites) and borehole assays (shown in white) .....	105
37 Ellipsoidal search parameters for resource classification of Zn and Pb for Domains 1 and 2 .....	107
38 A. Number pass for blocks to be populated with Zn values (PZn). B. PRED value for resource classification .....	109

39 Zn histogram of the model estimate (Domain 1) calculated from 1.5 m composites. B. Zn histogram of the model estimate (Domain 1) calculated from 3 m composites. C. Pb histogram of the model estimate (Domain 1) calculated from 1.5 m composites. D. Pb histogram of the model estimate (Domain 1) calculated from 3 m composites .....	111
40 A. Zn grade distribution. B. Pb grade distribution .....	115
41 EOF faults and their association with high-grade mineralisation .....	116
42 Zn grade tonnage curves for models obtained from 1.5 m and 3 m composites.....	118
43 Pb grade tonnage curves for models obtained from 1.5 m and 3 m composites .....	119
44 Ag grade tonnage curves for models obtained from 1.5 m and 3 m composites .....	119
45 Zn swath plot along the elevation .....	120
46 Pb swath plot in the easting direction .....	122
47 Pb composites showing many lower-grade composites.....	122
48 IDW estimate (red) compared to the OK estimates (green) from the 1.5 m model and 3 m model.....	123

## LIST OF TABLES

Table	Page
1 EF1 total resources from 2002 to 2015 .....	28
2 EF1 QC samples .....	40
3 Rosh Pinah Mine CRMs – Expected values, Lower and Upper Limits .....	48
4 AMISO158 – Ag standard descriptive statistics .....	53
5 Analytical values for blank samples analysed .....	55
6 Standard material properties for geological modelling .....	65
7 Lithological and grade solid sizes and tonnes (density of 3.46).....	65
8 The width, length, volume and tonnages of experimental ore solids .....	72
9 Comparison of assay data and 1.5 m composites for Zn, Pb, Cu and Fe variables.....	81
10 Comparison of assay data and 1.5 m composites for Ag, Mn, Mg and Rd variables.....	82
11 Summary statistics of 3 m Composites for Zn, Pb, Cu, Fe, Ag, Mn, Mg and Rd variables .....	83
12 Comparison of Skewness and Kurtosis of Assay, 1.5 m composites and 3 m composites .....	84
13 Estimating the parameters of the LN (2), $N > 40$ .....	87
14 Principal component analysis results.....	88
15 Top cut grades used for Domain 1 and Domain 2 .....	89
16 Summary of rotations, plunge and directions for both Domain 1 and 2 as well as the different ranges, nugget effects and sills .....	103
17 Classification criteria according to the PRED system.....	108
18 EF1 insitu Mineral Resource estimate as at December 31, 2016 .....	110
19 Domain 1 model statistics estimated from 1.5 m and 3 m composites .....	112
20 Domain 2 model statistics estimated from 1.5 m and 3 m composites .....	112
21 EF1 Measured Resources estimated from 1.5 m composites .....	113
22 EF1 Indicated Resources estimated from 1.5 m composites.....	113
23 Measured Resources estimated from 3 m composites .....	114
24 EF1 Indicated Resources estimated from 3 m composites.....	114
25 QKNA statistics for EF1.....	125

## NOMENCLATURE

Capping: To truncate the extreme high values to some threshold or top-cut value.

Coefficient of variation: The ratio of the standard deviation to the mean value

$$CV = \text{Standard deviation} / \text{mean}$$

Cross-validation: Is a model validation technique for assessing how the results of a statistical analysis will generalize to an independent data set.

Geostatistics: A collection of numerical techniques that deal with the characterization of spatial attributes.

Inverse Distance Weighting: A type of deterministic method for multivariate interpolation with a known scattered set of points. The assigned values to unknown points are calculated with a weighted average of the values available at the known points.

Kriging: Optimal interpolation that generates best linear unbiased estimate at each location.

Mean: Is the sum of all the sample values divided by the number of samples.

$$\text{Mean} = \text{Sum of sample values} / \text{number of samples}$$

**Median:** The middle value, determined by sorting the data into ascending order and selecting the middle value. The median is the same as the 50<sup>th</sup> percentile, where half the data lies below this sample value and half the data lies above this sample value.

**Mode:** The most frequently occurring sample value.

Mode = highest frequency value

**Nearest Neighbour interpolation:** A simple method of multivariate interpolation in one or more dimensions which selects the value of the nearest point and does not consider the values of neighboring points at all, yielding a piecewise-constant interpolant.

**Nugget effect:** Describes the expected difference between samples when the separation distance is almost negligible.

**Range:** The difference between the highest and lowest sample value.

Range = maximum value – minimum value

**Semi-variogram:** Characterization of spatial correlation. The semivariogram,  $\gamma(h)$ , of a stationary and intrinsic random variable,  $Z(x)$ , is the mean of the squared differences between all pairs of data values separated by lag  $h$ :

**Standard deviation:** The square root of the variance.



Swath plots: A graphical display of the grade distribution derived from a series of bands, or swaths, generated in several directions through the deposit.

Total sill: The total variability inherent in the data.

Variance: Measures the typical difference between the actual sample values and the overall average value.

$$\text{Variance} = \frac{\text{Sum of (sample value - mean value)}^2}{\text{Number of samples} - 1}$$

Variogram range: The lag or separation distance at which the variability reaches the sill.

## **CHAPTER 1: INTRODUCTION**

The project is a quantitative study that uses statistical and geostatistical analyses to optimize, understand and document the Eastern Ore Field (EOF) estimation. The project aims to estimate the in-situ tonnes and grades of the EF1 as on 31 December 2016, to determine the principal components of the EOF ore, to assess different modelling methods and to determine the significance of increasing the composite size from 1.5 m to 3 m on grade estimation. Rosh Pinah Zinc Corporation (RPZC) data of the EOF, MineSight and Leapfrog software was used for modelling and estimation. Glencore, the major shareholder of RPZC, needs to make well-informed decisions on capital investments or divestments and thus requires accurate information about the orebodies and the processes used to define characteristics of resources and reserves.

Chapter 1 presents the problem statement and the objectives of the project. It further introduces RPZC and identifies the project location. The chapter concludes with the organization of the dissertation.

### **1.1 Problem statement**

Exploration and mining companies make decisions regarding mining methods, production rates, capital investments or divestments, economic viability, work force required, equipment selection, and processing methods. Decisions are mainly aimed at improving the existing systems, increasing efficiency and decreasing cost, thus the management requires timely quality information on which to base their decisions. The geometry, size and quality of a deposit, amongst others, are some of the key parameters required for decision-making.

To increase the net present value of RPZC, Glencore has embarked on a series of investigational projects that aim to improve the existing systems, increase efficiency and decrease cost. The Technical Services Department is tasked to

increase the resources and reserves, optimize the drilling and improve the current resource evaluation processes. Before embarking on increasing the resources, it is important for the Technical Services Department to determine, with confidence, the quantity and quality of current resources. In line with the above, this dissertation aims to determine the in-situ EF1 resources as reported on 31 December 2016, the grades and tonnages, and also to optimize the resource estimation process at the Rosh Pinah Mine.

In 2009 and 2010, Golder Associates Africa (Pty) Ltd conducted audits on the Rosh Pinah Mine resources and made recommendations that were never implemented because further test work on increasing composite size was required. The author tested these recommendations, and by doing so the author assessed and improved the current evaluation processes. The EF1 orebody has been estimated several times before (Table 1); however, no estimation report has been written on the orebody. Hence, there is a need for assessing previous estimations and documenting the geostatistical studies of the EF1 orebody.

The fundamental assumptions of geostatistics, listed below, are used during the estimation. The following are taken from the Geostatistical Methods in Mineral Resource Evaluation class notes by Dohm (2010):

- Sample values are measured precisely and are reproducible.
- Sample values are measured accurately and represent the true value at that location.
- The samples are collected from a physically continuous, homogeneous population of all possible samples.
- Values at unsampled locations are related to values at sampled locations.

## 1.2 Objectives of this research

The dissertation objectives are:

- To assess the different modelling methods, determine the tonnage difference and recommend the best method for modelling complex sedimentary exhalative deposits.
- To conduct a Principal Components Analysis (PCA) and determine the outliers of the EF1 population.
- To assess the significance of increasing the composite size from 1.5 m to 3 m on grade estimation.
- To estimate the tonnes and grades of the in-situ EF1 resources using mapping, exploration and production drilling data collected from 1998 to end December 2016.

Technological advances in modelling allow fast and easier creation of lithological and grade solids, but it is essential to assess whether these models are accurate and adhere to key fundamental concepts of geostatistics. It is imperative to assess the different modelling methods in order to reduce the time geologists spend on modelling and to allow them to attend more to production issues.

Based on the volume variance effect, the effect that the variance decreases with increasing volume, the significance of increasing the composite size to 3 m instead of 1.5 m will be determined. The aim is to have a more conservative grade model with lower variances.

The EF1 orebody was selected as a case study for the dissertation for two main reasons. Firstly, it is the largest orebody mined at the Rosh Pinah Mine so far, it is currently the main source of ore, and it will continue to be a key contributor of ore for another eight years based on the current resources and mine plan. Secondly, Zone 2 material (moderate Zn, high Pb, low Fe and Cu) of the recently discovered Western Orefield Three (WF3) orebody is mineralogically and geochemically similar to the EF1 orebody. Production from the WF3 orebody is

planned to commence in the third quarter of 2016. Furthermore, the EF1 data set is big and dynamic. This, coupled with recent advances in modelling and validation techniques, creates an ideal opportunity for the author to investigate if recent advances are materially significant and geostatistically correct.

### **1.3 Rosh Pinah Zinc Corporation**

Rosh Pinah Zinc Corporation (RPZC) is an underground mine, producing Zn and Pb concentrates, with Cu, Ag and Au as by-products. The main ore minerals are galena (PbS) and sphalerite (Zn,Fe)S. The mine produces about 100,000 tons of Zn concentrate and 16,000 tonnes of Pb concentrate annually.

The mine is 80.08% owned by Glencore and the Namibian Broad-based Empowerment Groupings own the remainder. As part of Glencore's strategy to continue to leverage the geographic scope and diversification of operations, the Glencore group acquired a majority share in RPZC on the 11<sup>th</sup> of June 2012 (Glencore International plc, 2012).

### **1.4 Project location**

The mine is located in the southern part of Namibia, as shown in Figure 1, and it is 800 km south of the capital city of Namibia, Windhoek, and about 100 km north-east of the southern coastal town of Oranjemund. The Skorpion Zinc Mine (Figure 2) that hosts zinc oxide mineralisation is located 20 km north-west of the project area.

The dissertation project area is on the Rosh Pinah Exclusive Prospecting License (EPL) 2616 within the mining grant area Mining License (ML) 39, as shown in Figure 2. The project area (Figure 3) consists of the EF1 and EF2 limbs. The EF1 is

the western limb of the EOF sheath fold and EF2 is the eastern limb. The dissertation focuses mainly on EF1.

Figure 4 indicates a longitudinal section of the mined out and in-situ resources as well as the major production shift taking place in the last quarter of 2016 to 2018. The resources in the upper levels are mainly mined out. The exploration potential is mainly down depths, below the EF1, AAB, SF3 and WF3 orebodies. Further exploration potential is present to the north of the WF3 orebody where the mineralisation is open. The EF1 orebody gets smaller at larger depths and thus production is expected to shift towards the last quarter of 2016 to the recently discovered WF3 orebody.

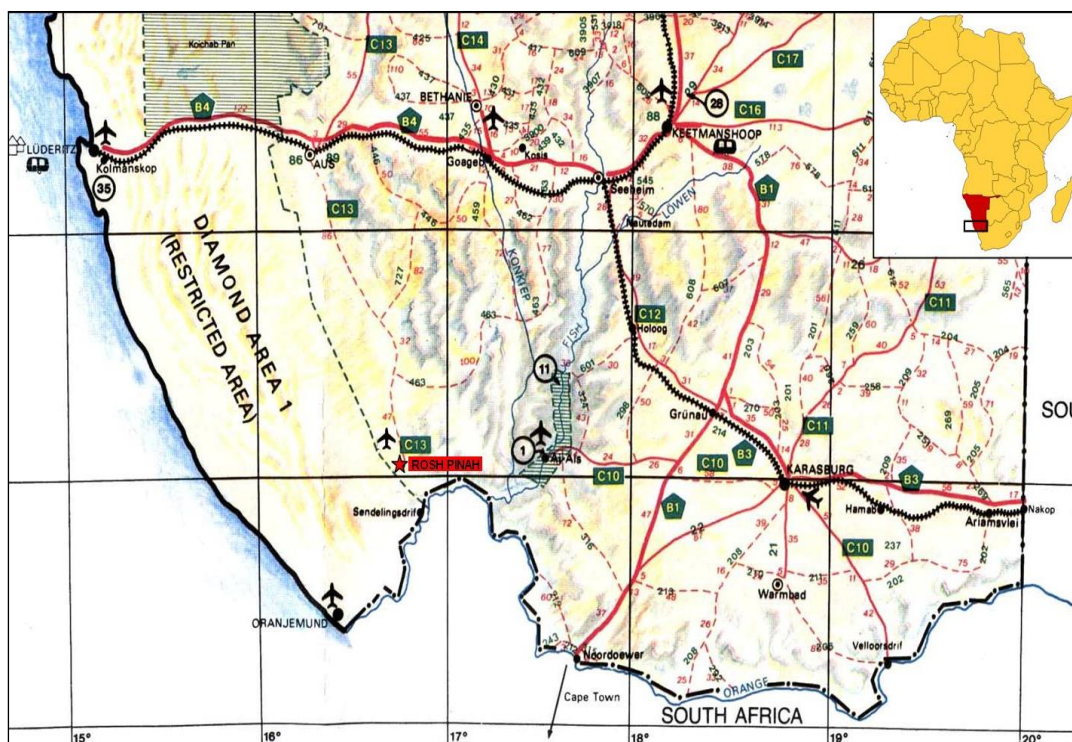
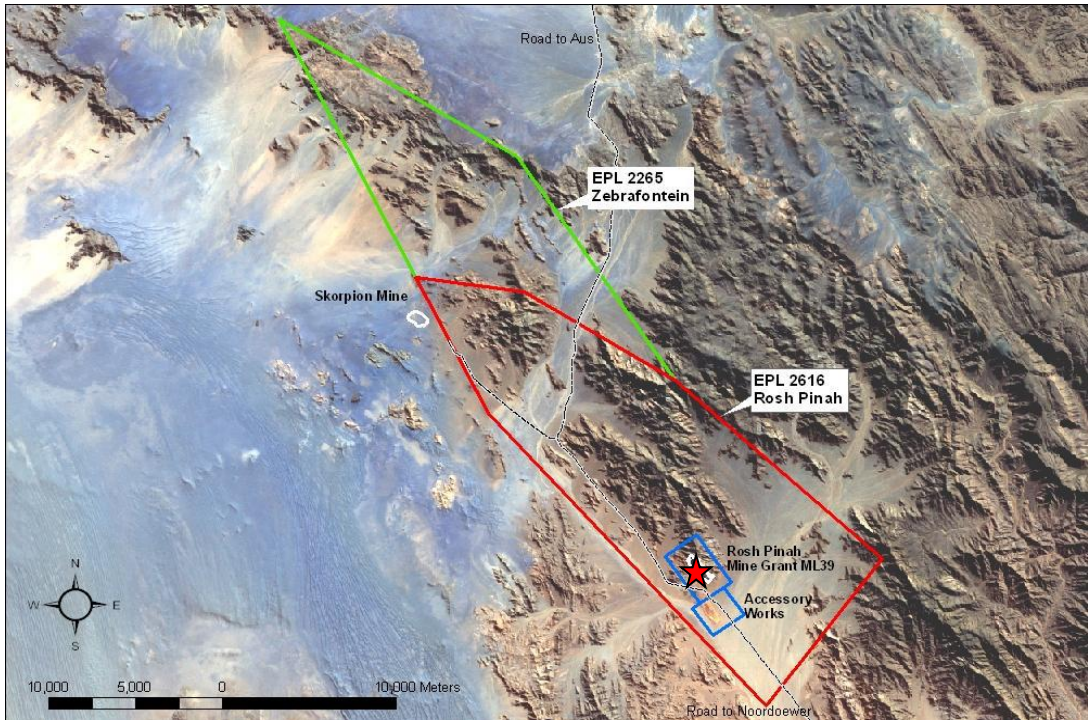
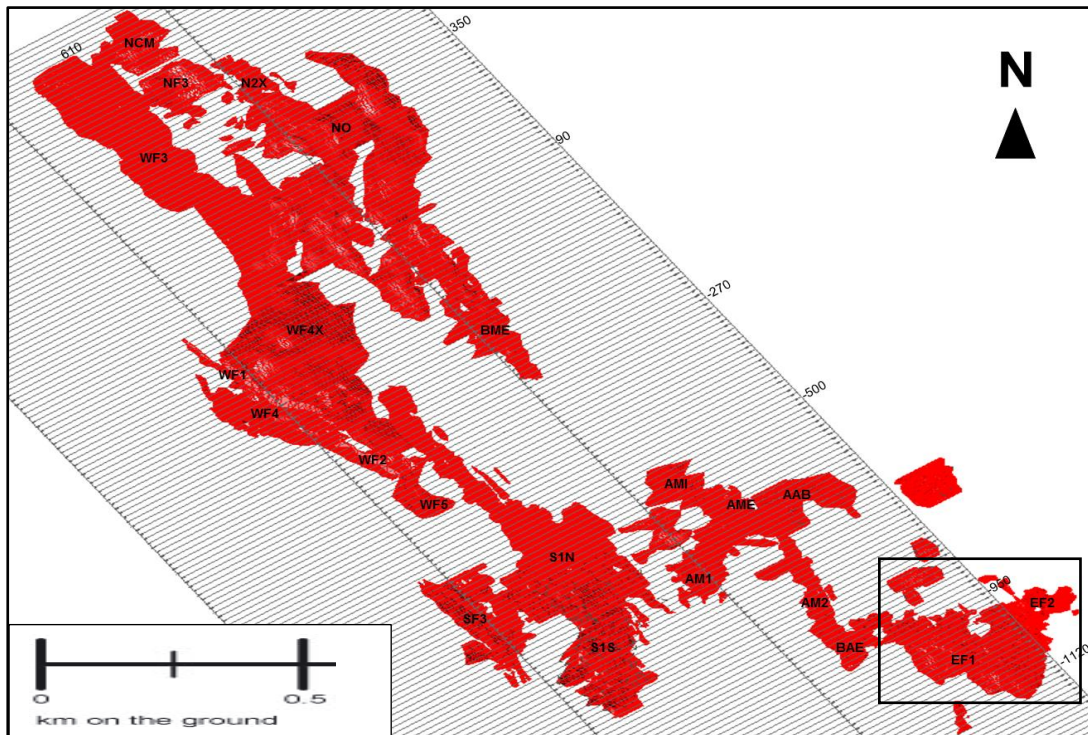


Figure 1 Rosh Pinah Zinc Mine location (Crowther, 2014)





**Figure 2 Locations of RPZC Exclusive Prospecting License and Mining License (Crowther, 2014)**



**Figure 3 Layout plans of in-situ mineral resources of the Rosh Pinah Mine. The project area is demarcated with the black square**

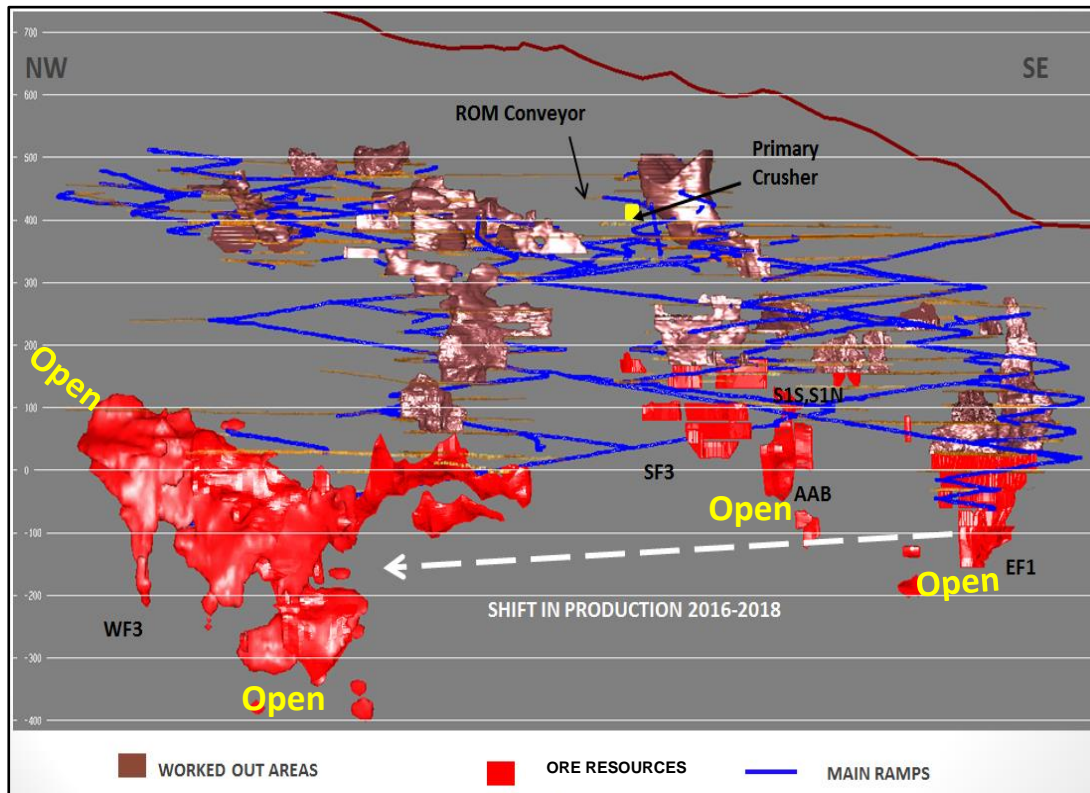


**Figure 4 Longitudinal section of RPZC resources and production focus**

## 1.5 Organization of the dissertation

The dissertation consists of nine chapters. **Chapter 1** starts by highlighting the research problem statement, mainly focusing on the need for management to obtain timely quality information to base their decision on. It includes the fundamental assumptions of geostatistics and the four research objectives.

**Chapter 2** covers the research methodology.

**Chapter 3** covers the literature review; it includes the history and development of geostatistics, significant work done in geostatistics, the geology of EOF and previous estimations. The chapter also presents in detail the theory of Ordinary Kriging (OK) and the development of the OK equations.

There is no use in applying sophisticated techniques to inferior data, as the saying goes “garbage in garbage out”. **Chapter 4** presents the data validation results and a summary of the quality assurance and quality control (QAQC) analyses.



**Chapter 5** presents the geometries, sizes and limitations of the grade and lithological models and finally presents the recommended method for modelling complex sedimentary exhalative deposits.

As a picture is worth a thousand words, **Chapter 6** presents a graphical display of information and the statistical evaluations of the variables.

**Chapter 7** explains and presents the preparatory work or estimation parameters required for kriging interpolation.

The estimation and model validation results are presented in **Chapter 8**. Model validation is possibly the most important step in the model building sequence and it is often overlooked or not done at all. Use of a model that does not fit the data well cannot provide good answers to the questions under investigation.

**Chapter 9** brings the dissertation to conclusion. A review of what was studied in the preceding eight chapters is presented, and limitations of the study and the author's recommendations are given.

## **CHAPTER 2: RESEARCH METHODOLOGY**

### **2.1 Introduction**

The dissertation uses a quantitative approach to address the key objectives. This section presents the project data, the methods applied and reasons why the methods were selected. The dissertation involved QAQC analyses, data validation, 3D grade and lithological solids, exploratory data analysis, resource estimation and model validation. The subsequent subsections define each method in detail.

### **2.2 Project data**

The EOF data set consists of 1607 boreholes drilled from a volume of 275 m in the east, 285 m in the north and 455 m in depth over the course of 13 years (2003 to October 2016). The drilling was done during the production and exploration phases. A total of 1241 holes are production (grade control) boreholes while 366 are exploration holes. The borehole designs are fan-shaped and drilled on 10 m sections for production holes aimed at intersecting the ore outline on 10m spacing. The exploration holes on the other hand are drilled on 30 m sections aimed to intersect the ore outline on 30 m drill spacing.

A total of 18 755 samples were available for this study area, all of them taken from drill cores with sample lengths varying from 40 cm to 1.5 m. The lithologies were respected, thus samples were not taken across lithological contacts. The samples were composited to 1.5 m composite samples, which yielded a total of 18 527 composites. The composites were subdivided into Domain 1 and Domain 2, based on the two structural orientations of the EOF limbs. Domain 2 consists of 9248 composites whilst Domain 1 has 9279 composites. The composites were also composited to 3 m composites.

Geological mapping data were collected on mining benches, which varied in height from 20 to 30 m. Mapping data from 14 levels were used, ranging from the -30 to the 290 level. The mapping information and borehole data were used to construct 23 sections on the Main Geology grid and 16 sections on the EF2 grid. These sections and the mapping information were triangulated and used to interpret 44 level plans every 10 m from the -150 level to the 290 level.

With regard to QAQC (Chapter 4), the duplicates, blanks and five Rosh Pinah Mine certified reference materials were analyzed. A total of 314 blanks, 449 duplicates, 26 AMIS0147, 122 AMIS0149, 123 AMIS0153, 72 AMIS0157 and 55 AMIS0158 were analyzed.

### **2.3 Methods**

This section systematically explains the methods followed and reasons why the methods were chosen. The modelling and estimation process at Rosh Pinah Mine involves the following:

- 1) Data collection: mapping of underground tunnels and gathering of drilling information;
- 2) Data validation: ensuring that all required information is captured, and within the acceptable limits and that the geology is within context.
- 3) QAQC: quality assurance refers to the policies and activities that are conducted to ensure a defined level of data accuracy and quality, whilst quality control is the prevention of unwanted data errors (Hoffman, 2003).
- 4) Sectional interpretations of lithologies and grade: 2D graphical representations of vertical and horizontal slices through the deposit.
- 5) Orebody modelling: 3D representation of the lithologies and grade models, a logical model of the mineralization which forms the foundation of any geostatistical analysis (Krige, 2000).

- 6) Descriptive statistics and graphical display of Zn, Pb, Ag, Cu, Fe, Mn, Mg and specific gravity (SG).
- 7) Plotting contours to determine the major, intermediate and minor directions of continuity.
- 8) Experimental semi-variograms to determine the nuggets, sills and variogram ranges.
- 9) Grade interpolation.
- 10) Model validation and reporting of resources.

### **2.3.1 Quality assurance quality control**

A detailed QAQC analysis was done before the data were used. The QAQC samples are stored in the acQuire database, in which their analyses were done. The analyses were done on Zn, Pb and Ag only because these are the payable metals. The descriptive statistics summary and scatter plots of the Rosh Pinah Mine certified reference material and blanks were presented. Scatter plots of duplicates versus their parent samples were also done.

### **2.3.2 Data validation**

The first step of validation was carried out in Microsoft Excel; it involved ensuring that all required borehole data were captured. Secondly, validations were done in AcQuire by running the AcQuire built-in scripts. The collar, survey, lithology and assay files were validated. The scripts compared the collar depths to the sample, geology and survey depths; it also identified overlapping geology intervals and boreholes with no coordinates. Thirdly, the collar files were exported from the AcQuire database into Leapfrog software and further validations were performed in Leapfrog. In Leapfrog, the following audits were done: missing X, Y, and Z coordinates in the RPZ\_Mine\_Surveyed column, missing section/grid line in the

collar file. Furthermore, the survey table was audited for holes with negative depths, non-numeric values in dip and azimuth columns, holes doubling on themselves (with both positive and negative dip and azimuths) and holes plotting on top of each other. Finally, the assay and lithology tables were audited for intervals with the “From” depth greater or equal to the “To” depth.

### **2.3.3 3D grade and lithological solids**

The section (Figure 12.B) and level plan interpretations were done in MineSight 3D (MS3D) module using borehole information and mapping information. The mapping information contained geological structures and polygons obtained from the mapping of tunnels developed in the EOF orebody. The polygons were triangulated to enable viewing in 2D during section interpretations. The section and level plan interpretations were then used to construct the 3D lithological and grade solid models (Figures 22 and 25) using partial linking in MS3D.

The above-mentioned process of solid generation in MS3D is tedious; in order to produce timely lithological and grade solids, the section and level plan interpretations were uploaded into Leapfrog. Additionally, a third solid was created by using borehole information and MS3D sections and level plan interpretations. The tonnes and outlines of the three solids were compared (Table 8).

The advantage of creating models in Leapfrog is that models that take weeks or months to develop manually can be ready in days or hours. Geological scenarios can be tested in rapid succession, including user-defined geological trends. The superior power of Leapfrog is changing the way geologists use data. With Leapfrog one can access and use large volumes of data and combine more disparate data types. One can evolve models as the data dictates, ultimately reducing costs and increasing the chance of success.

#### **2.3.4 Exploratory data analysis**

Statistical data analyses of Zn, Pb, Ag, Fe, Cu, Mn, Mg and SG were done in the MineSight Data Analyses (MSDA) module. Data analyses involved a summary of each element's descriptive statistics, scatter plots, histograms, probability plots and box plots. Furthermore, Domain 1 and Domain 2 descriptive statistics of the 1.5m composites were compared to the 3 m composites.

The PCA was carried out using Matlab to determine the principal components of the EF1 population. Additionally, the outliers were detected using quantile regression methods and compared with outliers obtained from histograms and cumulative probability plots.

#### **2.3.5 Resource estimation**

The geostatistical estimation involved modelling semi-variograms for Zn, Pb, Ag, Cu, Fe, Mn, Mg and SG. Semi-variograms were modelled in MSDA and estimations were made in the MineSight Compass module. The omni-directional semi-variograms of elements were used to determine the nugget and sill. Directional semi-variograms were then used to determine the ranges in the major, intermediate and minor directions.

The OK method was used for grade interpolation. OK was preferred because all elements have significantly skewed distributions with long tails. The grades were interpolated into 5 x 5 x 5 m blocks.

### **2.3.6 Model validation**

Swath plots plotted in Microsoft Excel and MSDA were used to validate the means of the models estimated from the 1.5 m and 3 m composites against the means of the composites.

## **CHAPTER 3: LITERATURE REVIEW**

### **3.1 Introduction**

The literature review starts by explaining the history and development of geostatistics, including some significant work done in geostatistics. The chapter then introduces the geological setting and the geology of the project area. The geology of EOF includes the structures, the ore mineralogy and the genetic model. A sound understanding of the relationship between the mineralisation and the geological processes that govern its geometry is essential as it improves the quality of the resource estimation (Dohm, 2010). The chapter further presents a summary of the previous studies done and it highlights the limitations of previous estimations. It also presents the theory of OK and the development of the OK equations.

### **3.2 History and development of geostatistics**

Geostatistics originated in the mining industry in the 1950s and early 1960s (Leuangthong et al., 2008). Krige (1951, 1952) developed the concept by correlating ore block estimates to internal follow-up block averages obtained as a block was mined out. His work provided the first direct evidence of spatial correlation and structure, which further led to the concept of the variance-size of the area relationship (Krige, 1952). In the 1960s his approach was formalized by Matheron, as cited by Oliver & Webster (2014).

“Geostatistics has become increasingly popular for numerical modelling and assessing uncertainty in the earth sciences” (Wang et al., 2013; Leuangthong et al., 2008). This is because predictions of shape, orientation and distribution of mineral deposits on a local and regional scale present fundamental challenges to the professionals within the mining industry. The success of exploration



programmes and mining operations depend on the shape, orientation and distribution of mineral resources and is greatly influenced by the accuracy of their predictions. This is even more important in matured mining districts, where mineral exploration at great depths has been accompanied by increased costs and the risk of targeting deposits that require more detailed data and more expensive data acquisition methods (Wang et al., 2013, 2011).

Similarly, Srivastava (2013) states that more research is required by the coal industry because it will encounter greater technical and economic difficulties due to increased variability in coal quality. Current papers that contributed to geostatistics by the coal industry are by Cornah et al., 2013; Saikia and Sarkar, 2013; de Souza and Costa, 2013; Hohn & Britton, 2013; Srivastava, 2013; Zawadzki, Fabijanczyk & Badura, 2013; Webber et al., 2013; Ertunç et al., 2013; Tercan et al., 2012; Heriawan and Koike, 2008. The metal industry is facing similar challenges and recent contributions to the research in geostatistics are provided by Jimenez-Espinosa & Chica-Olmo, 1999; Maleki et al., 2013; Monteiro et al., 2004; Wang & Huang, 2012; Wang et al., 2011, 2013; Daya, 2012; Marinoni, 2003.

The application of geostatistics has expanded into other industries as highlighted by Oliver & Webster (2014), and now it is widely applied in reservoir characterization, agriculture, geophysics, geohydrology, environmental studies, soil sciences, precision, pollution control, public health, fishery, planning, plant and animal ecology, engineering, remote sensing and meteorology. Oliver & Webster present a review that aims to educate and to ensure the understanding of geostatistics techniques and principles by those who have easy access to geostatistical software but lack the fundamentals of geostatistics.

### **3.3 Significant work done in geostatistics**

This section reviews the significant work done in geostatistics, from geological models and support sizes to the final stages of estimation that involve computing variograms, kriging and model validations.

Krige (2000) reiterated the importance of the following workflow of geostatistics regardless of the technique being used:

- a logical model of mineralization,
- logical orebody subdivisions based essentially on geological input,
- the effects of changes in support sizes and types,
- no cutting of high grades unless fully justified,
- block valuations without conditional bias and with lowest error variances,
- model validations.

#### **3.3.1 Geological modelling**

Three-dimensional geological modelling is an important technology in quantitative assessment and prediction of mineral resources on a district scale. It integrates geological, geochemical and geophysical data for the delineation of metallogenesis of mineral deposits and exploration of targets (Wang et al., 2013). Recent 3D geological modelling by Wang (2011, 2012, 2013) acknowledged the work done by Calcagno et al., 2008; Fallara et al., 2006; Kaufman and Martin, 2008; Lemon and Jones, 2003; Mallet, 2002. These works focused on geological modelling when the available data are sparse. Only a few papers (Monteiro et al., 2004) have been published on a mature mining environment where abundant information is available and mining is progressing at a fast pace such that the time it takes to complete a model is a serious constraint.

### **3.3.2 Sample size**

Oliver and Webster (2014) emphasized sample size as the most important factor for determining the reliability or accuracy of the empirical variogram. In general, the more data one has the greater the accuracy. This is in line with Webster and McBratney's (1987) finding, which shows that the spherical model fits well when the sample size is bigger but the model is erratic and appears poor when the sample size is small.

### **3.3.3 Top cut/Outliers**

An outlier is an observation that is located "far enough" from most of the other observations in a data set for it to be considered anomalous. Causes of outlying observations include inherent variability and measurement errors. Outliers can have a significant impact on estimates and inference, so it is important to detect them and decide whether to remove them (top/bottom cut) or consider a robust analysis.

Similarly, the issue of dealing with long-tailed distributions is a huge problem because it may cause high-grade areas to be underestimated and low-grade areas to be overestimated or vice versa. However, a study done by Maleki et al. (2013) on capping and kriging grades with long-tailed distributions found that estimates were globally and conditionally unbiased. They therefore concluded that the top-cut model achieves a trade-off between accuracy, simplicity of use and robustness against extreme high values.

### **3.3.4 Experimental variograms**

De Souza and Costa (2013) focus on improving experimental variograms so that the pattern of spatial variation is clear, allowing easy identification of the parameters of the variogram model required for kriging. In their study they used clustered data, declustered data, and set out to determine how clustering affects the uncertainty and the inventory of resources. They managed to establish that clustering can lead to inefficient classical variogram estimates even for data arising from a stationary random field. On the other hand, Oliver and Webster (2013) cautioned against coarse grids and suggested extra sampling within the grid to improve the short-range variation. They caution against grids because even if grids give unbiased Krige estimates, when coarse they might miss the short-range variation.

Pardo-Iqúizquiza et al. (2013) did a study on the additional uncertainty that is introduced in the absence of the “true” underlying variogram due to scattered data. Similarly, Wang et al. (2013, 2012) relied on scattered information to predict and delineate mineral resources through district scale exploration and potential exploration targets.

### **3.3.5 Model validation**

Concerning cross-validation, Jiménez-Espinosa and Chica-Olmo (1999) temporarily discarded the value at a particular sample location from the sample data set and then estimated the value at the same location using the remaining samples. Thereafter, they compared the estimate to the true sample value that was initially removed from the sample data set. The method of cross-validation described above is tedious and impractical to test all sample locations when dealing with a big data set but it is however a good test for carrying out spot checks. One more

drawback of this method is that it yields a variety of results that are not always consistent (Falivene et al., 2010).

Another validation method widely practiced in the industry is comparing the means of composite to the means of estimate by subdividing the sampling area into swaths. The latter method, done in Microsoft Excel, caters for big data sets but it is also tedious. Most software provides a function for swath plots as a means of validating different models; these are widely used in the industry. Wang et al. (2012) state that 3D Kriged modeling and improved 3D IDW modeling can be used for cross-validation. Now that many softwares are available that do kriging, any geostatistician can produce a Krige estimate without understanding and as a result may produce unreliable and even misleading results (Oliver and Webster, 2014). Thus, it is imperative to cross-validate the estimation results.

In addition, Abedini et al. (2012) assessed the significance of data domaining on cross-validation. They defined domain analysis as the organization of a collection of patterns into clusters based on similarity. Their finding was that optimum number of domains gave the best cross-validation statistics.

### **3.4 Geological setting**

The Rosh Pinah Mine deposit is located within the north-south trending Neoproterozoic Gariiep Belt (Alchin and Moore, 2005). Alchin and Moore state that the belt represents the tectonic framework in which the supercontinent, Rodinia, started to break apart ~741 Ma. Alchin and Moore further state that rifting occurs within basement granites and gneisses of the Mesoproterozoic Namaqua province. They also state that the Gariiep belt is subdivided into a western allochthonous, oceanic Marmora Terrane, which has been thrust over the eastern, parautochthonous sedimentary Port Nolloth Zone (Figure 5). The Rosh Pinah deposit is hosted by the Port Nolloth Zone in the Rosh Pinah Formation.

The Rosh Pinah Formation conformably overlies the massive diamictites of the Kaigas Formation as a typical rift-fill sequence, characterized by predominantly siliciclastic and calcareous succession (Alchin and Moore, 2005). At the base, the Rosh Pinah Formation is a thick footwall arkosic/sandstone succession (Figure 6) characterized by brecciation (Alchin and Moore, 2005). They further state that the footwall succession is overlain by the ore equivalent horizon, which is characterized by carbonaceous mudstone (argillite) containing interbedded carbonate lenses and microquartzite. Furthermore, the carbonates are strongly attenuated and structurally confined to the troughs and crest of D2 folds and comprise of dolomitic carbonates and subordinate barium-rich carbonates. On the other hand, the microquartzites are black, thinly laminated and dense fine-grained lithological units.

A 130 m thick sandstone-mudstone succession conformably overlies the ore equivalent horizon and forms the upper Rosh Pinah Formation (Alchin et al., 2005). The Rosh Pinah siliciclastics were accompanied by contemporaneous, bimodal but predominantly felsic magmatism dated at a Pb-Pb age of  $741 \pm 6$  Ma (Alchin and Moore, 2005). They further state that the volcanism may have provided the heat engine for driving hydrothermal convection to form contemporaneous sedimentary-exhalative and hydrothermal replacement mineral deposits in the deep rift during a cooler regressive period in which the basin was isolated from the open ocean. The Rosh Pinah rift graben infill was terminated during an interpreted sea level drop induced by global cooling prior to the major ~640 to ~590 Ma Marinoan glacial event, during which the glaciogenic Numees Formation was deposited. The sedimentary evolution of the Pan-African Gariiep Belt finally ended during the closure of the Adamastor Ocean at about 545 Ma as a result of subduction and continental collision. The area is overprinted by low- to upper-grade greenschist to lower amphibolite facies metamorphism as cited by Alchin and Moore (2005).

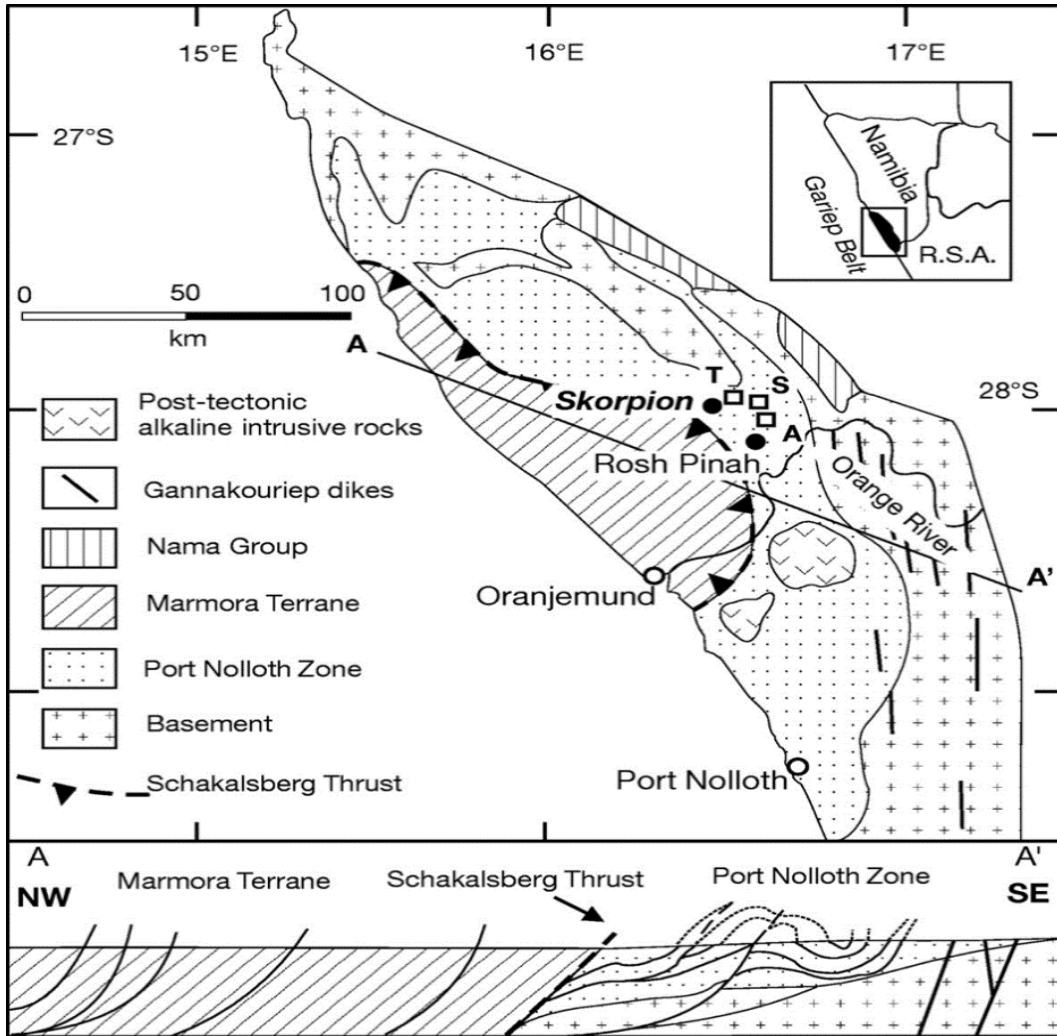


**Figure 5** Locality of the Rosh Pinah Zn-PB deposit and its stratigraphic setting within the Pan-African Gariep belt. After Frimmel and Frank (1998)

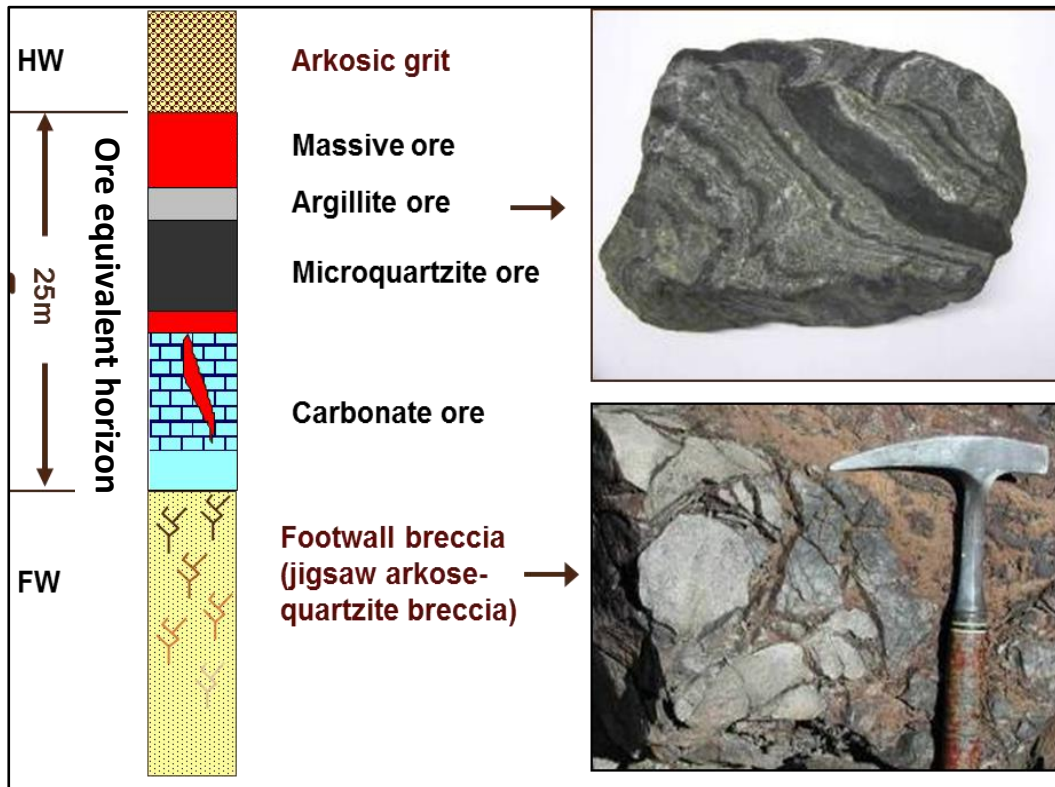


Figure 6 Rosh Pinah Mine Stratigraphy. Source: Mouton (2006)

### 3.5 The Geology of the EOF

Section 3.4 described the EOF geological setting and associated lithology. This section discusses in detail the EOF structure, mineralogy and the genetic model.

#### 3.5.1 Structure

Alchin and Moore (2005) state that during continental collision and oceanic closure, north-northwest trending oblique thrust ramps were produced during the south-east-directed transpressive phase (D1). They further state that orebodies that were originally isoclinally folded and thrust-faulted during early D1 deformation were subsequently refolded during D2 deformation into upright to slightly westerly overturned non-cylindrical folds.



In Watkeys (2001) the EOF orebody (Figure 8) is considered to be situated in a Z-fold, consisting of a western syncline and an eastern anticline, flanked by two steeply dipping sinistral faults, the A–E and the Dennis faults, with the central part cross-cut by the Martina fault (Figure 7). He envisages the EOF fold to be a D2 synclinal subsidiary fold with a steep southerly plunge (64° towards 052°) situated on the limbs of the Rosh Pinah anticlinorium. D2 deformation in the Rosh Pinah Mine area consists of folds with NNW–SSE orientated axes which plunge in both directions (Watkeys, 2001). It is further stated that the D2 folds axial planes are upright to slightly westerly overturned, striking 326° and dipping at 65°. The D3 comprises E–W to SW–NE folds.

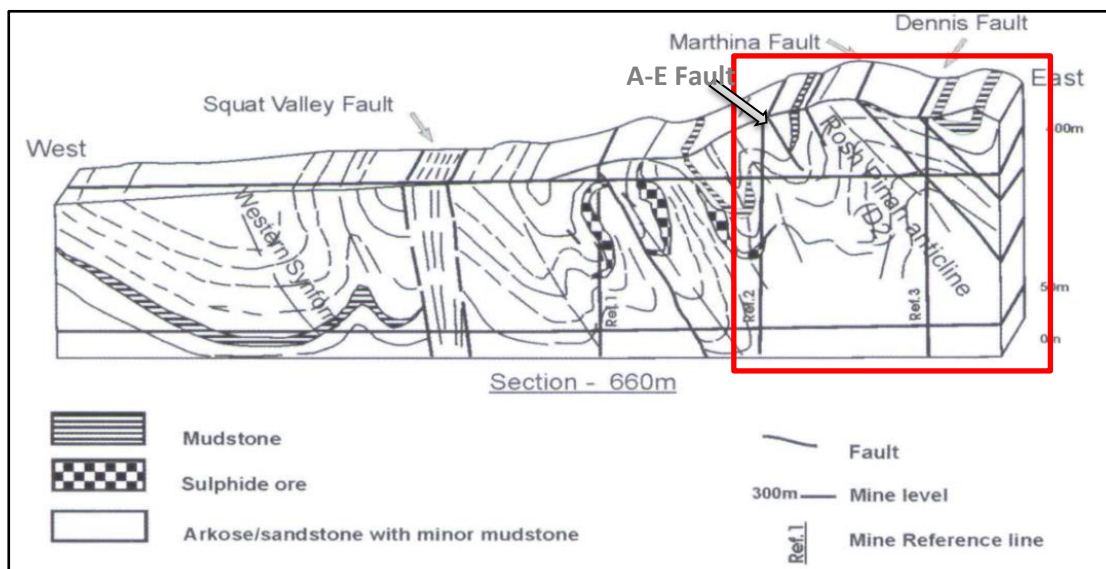


**Figure 7 Schematic cross-section indicating the EOF structure around the Rosh Pinah Mine with development of D2 backfolds and possible backthrusts. Source: Alchin and Moore (2005)**

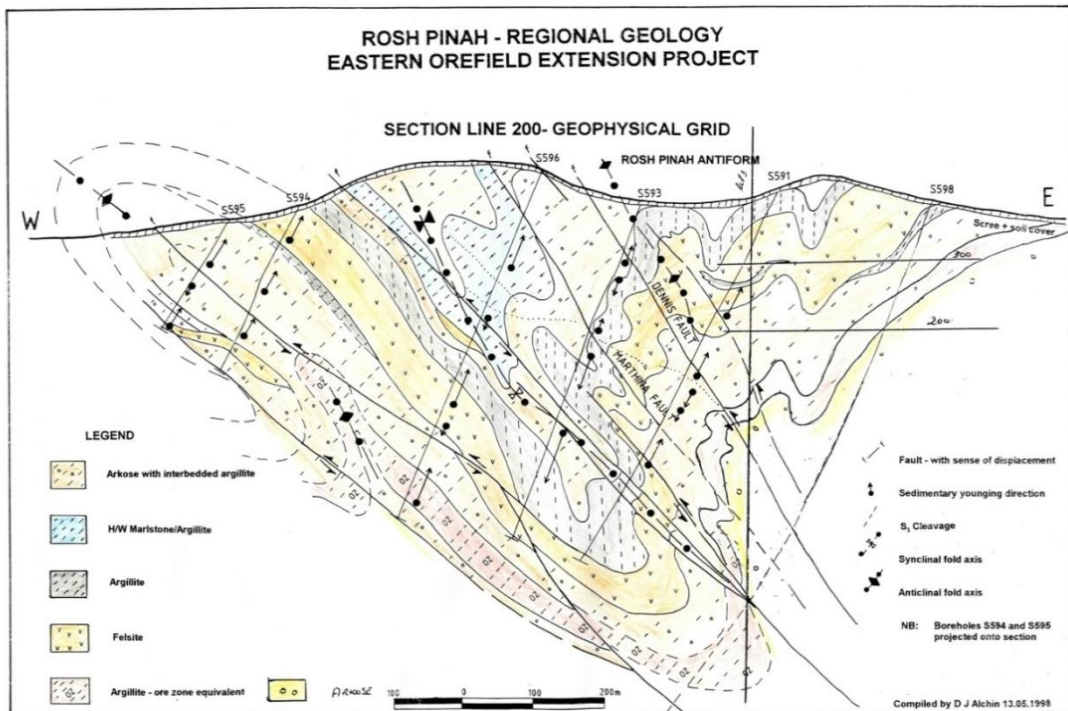


**Figure 8 Eastern Orefield structural section indicating the western syncline and the eastern anticline as well as major faults cross-cutting the orebody. Source: Watkey (2001)**

### 3.5.2 Ore mineralogy

A mineralogical investigation of 34 core samples from the EOF was done in 2003 by Lakefield Research Africa Pty Limited (Richard and Martin, 2003). The investigation aimed at predicting metallurgical response to EOF ore types. They found that the majority of core samples were dolomites, with minor microquartzites, arkoses and graphitic rocks. The Zn and Pb mineralisation occurs mainly in the dolomite and to a lesser extent in microquartzites. Similarly, Alchin and Moore (2005) grouped the EOF orebodies into the predominantly carbonate-hosted type.

Zinc occurs almost entirely as the mineral sphalerite and small amounts as zincian dolomite. The chemistry of the sphalerite varies according to its colour based on

the Mn and Fe contents. An orange-red to dark brown sphalerite are rich in Fe but poor in Mn whilst the orange-to-yellow types are poor in Mn and rich in cadmium. The Pb occurs mainly as galena. Pyrite is the dominant sulphide gangue, with small amounts of chalcopyrite occurring as inclusions in sphalerite and as discrete grain. They also described that the mineralisation varies from a relatively common, coarsely grained, massive variety to a less common, disseminated or laminated type.

Alchin and Moore (2005) state that small amounts of bornite, tennantite-tetradedrite, stromeyerite, acanthite, arsenopyrite, argentite and free gold are present. They also state that bands of massive sulphide generally contain a combined Zn + Pb + Cu content ranging between 25 to 30% and may occur in any stratigraphic position in the ore zone, but are mostly restricted to localities near hanging-wall sequences in microquartzite, argillite or carbonate host rocks.

### **3.5.3 Genetic model**

The Rosh Pinah Mine deposits are classified as a sedimentary exhalative (SEDEX) deposit (Figure 9 and 10) with subordinate volcanogenic massive sulphide (VMS) and Broken Hill-type (BHT) depositional and deformational characteristics (Alchin and Moore, 2005). Watson (1980) states that these deposits have a syngenetic origin. Indicators of a SEDEX origin are its association with basin-margin rifting, anoxic sediments, barite and the finely laminated nature of the ore. The presence of felsic volcanic rocks in the Rosh Pinah Formation has however resulted in the deposit being equated to a distal VMS deposit, like the Skorpion (Alchin and Moore, 2005; Corrans et al., 1993; van Vuuren, 1986). A common feature of SEDEX and VMS deposits is the zonation of metals (Figure 10) in which copper and iron sulphides are deposited in a more proximal setting relative to the fluid sources with Pb and Zn more distal, while Fe + Mn + Ba occur on the ore zone periphery.

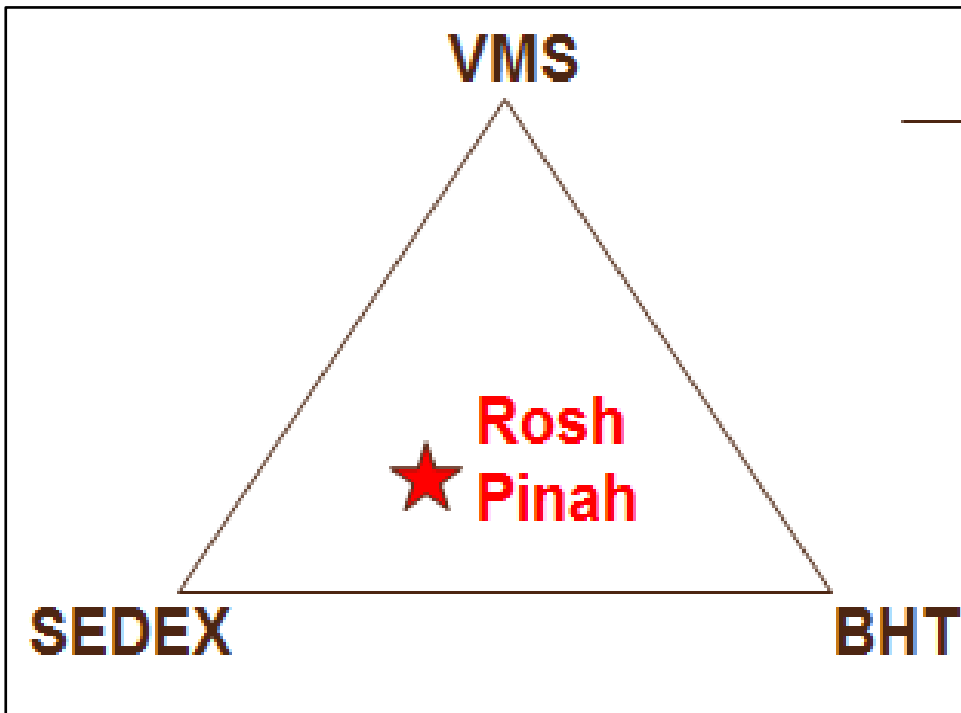


Figure 9 Rosh Pinah Mine genetic model; mainly a SEDEX with subordinate VMS and BHT depositional and deformational characteristics

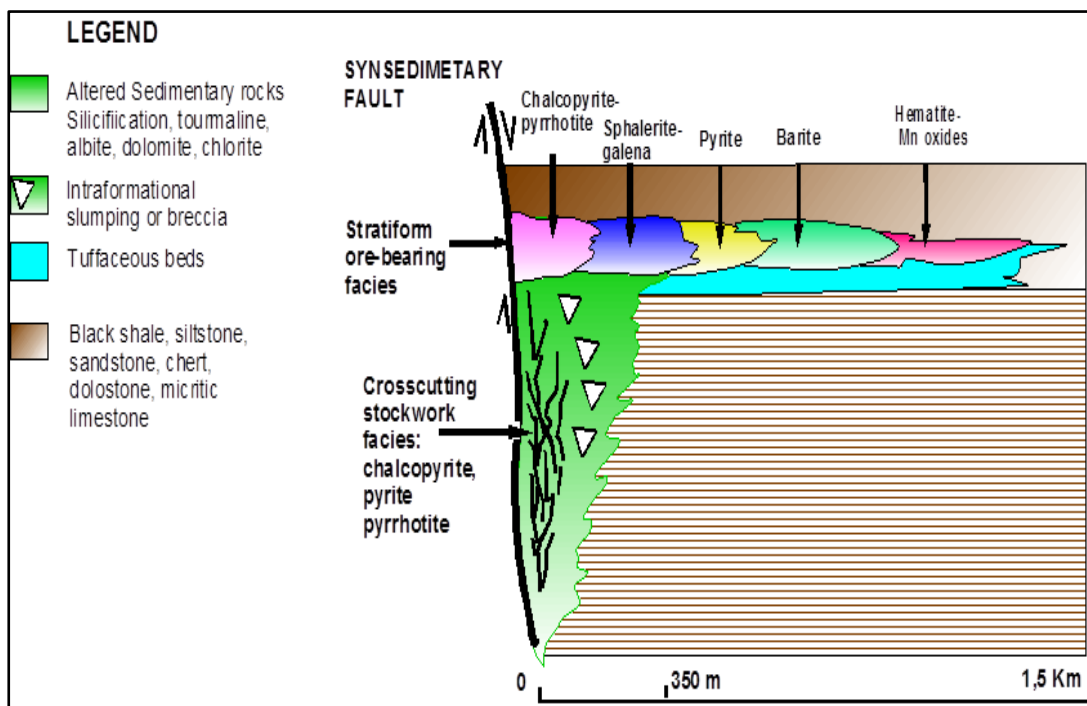


Figure 10 A sedimentary exhalative (SEDEX) ore deposition model (modified after Alchin and Moore (2005))

### 3.6 Previous estimations of the EF1

The orebody was mined since 1999, and by December 2013 about 3 million tonnes were extracted from the EF1 orebody. By December 2013 the in-situ resources of EF1 were about 3.6 million tonnes, and an additional 0.8 million tonnes were moved to the inventory and about 0.5 million tonnes have been mined since then. Resources were moved to the inventory because they are remnants sitting as slivers around the open stope that cannot be economically extracted in the near future.

The EF1 orebody was estimated previously but none of the estimations are well documented, let alone published. Table 1 shows a summary of the different estimations carried out from 2002 to 2015.

**Table 1 EF1 total resources from 2002 to 2015**

EOF estimates				
Year	Total Resource			
	In-situ ore (MT)	Zn (%)	Pb (%)	Ag (ppm)
2002	2.47	14.12	2.93	-
2004	3.95	11.76	2.62	-
2007	6.20	10.68	2.29	54.19
2008	6.20	10.87	2.12	53.6
2010	7.31	10.73	2.38	63.3
2012	5.12	10.54	2.23	61.2
2014	5.58	11.84	2.50	64.3
2015	5.72	12.25	2.61	67.7

The 2010 and 2014 estimations were made using spherical model variograms and the OK interpolation method. Estimations done before 2015 used very small lag

distances of less than 2.5m. The small lag distances resulted in variograms with very low nuggets and ranges (less than 30m). These models are conditionally biased; grades greater than the mean grade are significantly higher and those lower than the mean grade significantly lower. This implies that previous estimations overestimated the high grades and underestimated the low grades.

### **3.7 Ordinary Kriging**

OK was selected as the interpolation method. This section defines OK and the evolution of the OK equations for point estimates. The section further includes the application of OK on block estimates and it concludes with introducing Quantified Kriging Neighbourhood Analysis (QKNA).

OK is often associated with the acronym B.L.U.E., which stands for Best Linear Unbiased Estimator (Isaaks & Srivastava, 1989; Dohm, 2010). Isaaks & Srivastava further explain that OK is linear because its estimates are weighted linear combinations of the available data. It is unbiased since it tries to have the mean residual or error equal to zero. It is best because it aims at minimizing the variance of the errors. It provides the optimum set of weights, smallest standard error, narrowest confidence interval and minimum estimation variance. It is a local estimation technique that is based on the variogram to determine the value of the weights and the estimation variance (Dohm, 2010).

#### **3.7.1 Development of OK equation**

This section discusses the development of the OK equation based on the random function model and unbiasedness as well as the error variance.

### 3.7.1.1 Random function Model and Unbiasedness

Isaaks & Srivastava (1989) pointed out that the unknown true value at unsampled points is estimated using a weighted linear combination of the available samples, i.e.,

$$\hat{v} = \sum_{j=1}^n w_j \cdot v \quad (3.1)$$

If the error,  $r$ , is the difference between the estimated value and the true value at that location, then the error of the  $i$ th estimate is

$$r_i = \hat{v}_i - v_i \quad (3.2)$$

Then the average error of a set of  $k$  estimates is

$$m_r = \frac{1}{k} \sum_{i=1}^k r_i = \frac{1}{k} \sum_{i=1}^k \hat{v}_i - v_i \quad (3.3)$$

The above equation has many unknown quantities thus the solution is to conceptualize the unknown values as the outcome of a random process and solve the problem for the conceptual model. The estimate is also a random variable since it is a weighted linear combination on the random variables at the available sample locations:

$$\hat{V}(x_0) = \sum_{i=1}^n w_i \cdot V(x_i)$$

Similarly, the estimation error is also a random variable, i.e.,

$$R(x_0) = \hat{V}(x_0) - V(x_0)$$

By substituting the previous equation, which expressed our estimate in terms of other random variables, the estimation error can be expressed in terms of the original  $n + 1$  random variables in the random function model as follows:

$$R(x_0) = \sum_{i=1}^n w_i \cdot V(x_i) - V(x_0) \quad (3.4)$$

Assuming that the random function is stationary, all expected values can be expressed as  $E\{V\}$  as follows:

$$E\{R(x_0)\} = \sum_{i=1}^n w_i E\{V\} - E\{V\}$$

Setting the expected value of the error at any location to 0 to ensure unbiasedness results in the following conclusion:

$$\sum_{i=1}^n w_i = 1$$

### 3.7.1.2 Random function Model and Error Variance

In Isaaks & Srivastava (1989), it is alluded that OK attempts to produce a set of estimates with minimum errors of the variance. The error variance,  $\sigma$ , of a set of  $k$  estimates can be written as

$$\begin{aligned} \sigma_R^2 &= \frac{1}{k} \sum_{i=1}^k (r_i - m_R)^2 \\ &= \frac{1}{k} \sum_{i=1}^k \left[ \hat{v}_i - v_i - \frac{1}{k} \sum_{i=1}^k (\hat{v}_i - v_i) \right]^2 \end{aligned}$$

Assuming a mean error of 0, then



$$\begin{aligned}\sigma_R^2 &= \frac{1}{k} \sum_{i=1}^k (r_i - 0)^2 \\ &= \frac{1}{k} \sum_{i=1}^k [\hat{v}_i - v_i]^2\end{aligned}$$

The variance of a weighted linear combination is:

$$\text{Var}\left\{\sum_{i=1}^n w_i \cdot V_i\right\} = \sum_{i=1}^n \sum_{j=1}^n w_i \cdot w_j \cdot \text{Cov}\{V_i V_j\} \quad (3.5)$$

Using formula 3.5 and equation 3.4, we can express the variance of the error, as stated in Isaaks and Srivastava (1989), as

$$\begin{aligned}\text{Var}\{R(x_0)\} &= \text{Cov}\{\hat{V}(x_0)\hat{V}(x_0)\} - \text{Cov}\{\hat{V}(x_0)V(x_0)\} \\ &\quad - \text{Cov}\{V(x_0)\hat{V}(x_0)\} + \text{Cov}\{V(x_0)V(x_0)\} \\ &= \text{Cov}\{\hat{V}(x_0)\hat{V}(x_0)\} - 2\text{Cov}\{\hat{V}(x_0)V(x_0)\} \\ &\quad + \text{Cov}\{V(x_0)V(x_0)\}\end{aligned} \quad (3.6)$$

The first term in 3.6 is the covariance of  $\hat{V}(x_0)$  with itself, which is equal to the variance

$\hat{V}(x_0)$  of

$$\text{Var}\{\hat{V}(x_0)\hat{V}(x_0)\} = \text{Var}\left\{\sum_{i=1}^n w_i \cdot V_i\right\} = \sum_{i=1}^n \sum_{j=1}^n w_i w_j \tilde{C}_{ij}$$

The second term can be written as:

$$2\text{Cov}\{\hat{V}(x_0)V(x_0)\} = 2 \sum_{i=1}^n w_i \tilde{C}_{i0}$$

The third term is the covariance of the random variable  $V(x_0)$  with itself and it is equal to the variance of  $V(x_0)$ , so

$$\text{Cov}\{V(x_0)V(x_0)\} = \bar{\sigma}^2$$

Combining the three terms, the error variance (Isaaks and Srivastava, 1989) becomes

$$\sigma_R^2 = \bar{\sigma}^2 + \sum_{i=1}^n \sum_{j=1}^n w_i w_j \tilde{C}_{ij} - 2 \sum_{i=1}^n w_i \tilde{C}_{i0} \quad (3.7)$$

Equation 3.7 gives an expression for the error variance as a function of  $n$  variables, but based on the unbiasedness condition the set of  $n$  weights must be restricted to possible solutions that sum to 1. The problem of constrained optimization can be solved by the technique of Lagrange parameters, described in the next subsection.

### 3.7.2 The Lagrange Parameter

Equation 3.7 has  $n+1$  equations and  $n$  unknowns. To solve the problem a new variable, the Lagrange parameter  $\mu$ , was added. The parameter is equal to 0 due to the unbiasedness condition thus it is safe to add the variable. The Lagrange parameter is required to convert the constrained minimization problem into an unconstrained one.

Then equation 3.7 becomes

$$\sigma_R^2 = \bar{\sigma}^2 + \sum_{i=1}^n \sum_{j=1}^n w_i w_j \tilde{C}_{ij} - 2 \sum_{i=1}^n w_i \tilde{C}_{i0} + 2\mu \left( \sum_{i=1}^n w_i - 1 \right) \quad (3.8)$$

### 3.7.3 Minimizing the Error Variance

The error variance (equation 3.7) is minimized by calculating the  $n+1$  partial first derivative of the error variance with respect to the weights (Isaaks & Srivastava, 1989). Then we obtain

$$\frac{\partial(\bar{\sigma}_R^2)}{\partial w_1} = 2 \sum_{j=1}^n w_j \tilde{C}_{1j} - 2\tilde{C}_{10} + 2\mu$$

Setting this equation to 0 produces the following equations:

$$2 \sum_{j=1}^n w_j \tilde{C}_{1j} - 2\tilde{C}_{10} + 2\mu = 0$$

$$\sum_{j=1}^n w_j \tilde{C}_{1j} + \mu = \tilde{C}_{10}$$

(3.9)

This system of equations, referred to as the OK system, can be expressed in matrix notation as

$$\underbrace{\begin{bmatrix} \tilde{C}_{11} & \cdots & \tilde{C}_{1n} & 1 \\ \vdots & \ddots & \vdots & \vdots \\ \tilde{C}_{n1} & \cdots & \tilde{C}_{nn} & 1 \\ 1 & \cdots & 1 & 0 \end{bmatrix}}_{(n+1) \times (n+1)} \cdot \underbrace{\begin{bmatrix} w_1 \\ \vdots \\ w_n \\ \mu \end{bmatrix}}_{(n+1) \times 1} = \underbrace{\begin{bmatrix} \tilde{C}_{10} \\ \vdots \\ \tilde{C}_{n0} \\ 1 \end{bmatrix}}_{(n+1) \times 1}$$

(3.10)

To solve for the weights, equation 3.10 can be multiplied with the inverse of the left-hand side covariance matrix. Then,

$$\mathbf{w} = \mathbf{C}^{-1} \cdot \mathbf{D}$$

(3.11)

Multiplying each of the  $n$  equations given in equation 3.9 by the weights produces the following:

$$\sum_{i=1}^n \sum_{j=1}^n w_i w_j \tilde{C}_{ij} = \sum_{i=1}^n w_i \tilde{C}_{i0} - \mu$$

Substituting this into equation 3.8 allows the minimized error variance to be expressed as

$$\begin{aligned}\tilde{\sigma}_R^2 &= \tilde{\sigma}^2 + \sum_{i=1}^n w_i \tilde{C}_{i0} - \mu - 2 \sum_{i=1}^n w_i \tilde{C}_{i0} \\ &= \tilde{\sigma}^2 - \left( \sum_{i=1}^n w_i \tilde{C}_{i0} + \mu \right)\end{aligned}\tag{3.12}$$

Or, in terms of the matrices, to be expressed as:

$$\tilde{\sigma}_R^2 = \tilde{\sigma}^2 - \mathbf{w} \cdot \mathbf{D}\tag{3.13}$$

This minimized error variance is referred to as the OK variance used with the notation  $\sigma_{OK}^2$ .

### 3.7.4 OK using Y or p

It is assumed that the random variables in the random function model all have the same mean and variance. Therefore, based on this assumption there is a relationship between the model variogram and the model covariance Isaaks & Srivastava (1989) gives:

$$\gamma_{ij} = \tilde{\sigma}^2 - \tilde{C}_{ij}\tag{3.14}$$

In terms of the variogram, the OK system can be written as:

$$\sum_{j=1}^n w_j \tilde{\gamma}_{ij} - \mu = \tilde{\gamma}_{i0} \quad \forall i = 1, \dots, n\tag{3.15}$$

There is also a relationship between the model correlogram and the model covariance, i.e.,

$$\tilde{\rho}_{ij} = \frac{\tilde{C}_{ij}}{\tilde{\sigma}^2} \quad (3.16)$$

In terms of the correlogram, the OK system can be presented as:

$$\sum_{j=1}^n w_j \tilde{\rho}_{ij} + \mu = \tilde{\rho}_{i0} \quad \forall i = 1, \dots, n \quad (3.17)$$

With the modelled error variance given by:

$$\tilde{\sigma}_R^2 = \tilde{\sigma}^2 \left( 1 - \left( \sum_{i=1}^n w_i \tilde{\rho}_{i0} + \mu \right) \right) \quad (3.18)$$

### 3.8 Block Kriging

#### 3.8.1 Introduction

The previous section focused on point kriging, but often in mining, a block estimate or an estimate of the average value of a variable within a prescribed local area is required. One method of block estimates is to discretize the local area into many points and then to average the individual point estimates to get the average over the area.

The block kriging system is similar to the point kriging system given by equation 3.10. The mean value of a random function over a local area is the average of all the point random variables contained within the local area (Isaaks and Srivastava, 1989). Thus, the mean value over a local area can be described as follows:

$$V_A = \frac{1}{|A|} \sum_{j|j \in A} V_j \quad (3.19)$$

Where  $V_A$  is a random variable corresponding to the mean value over an area  $A$  and  $V_j$  are random variables corresponding to the point values within  $A$ .

In equation 3.10, the OK equation, the construction of the covariance matrix  $C$  is independent of the location at which the estimate is required thus the matrix  $C$  does not require any modifications for block kriging. "However, the covariance vector  $D$  consists of covariance values between the random variables at the sample locations and the random variables at the location that we are trying to estimate" (Isaaks and Srivastava, 1989). For block estimation, the covariance values required for the covariance vector  $D$  are the point-to-block covariance, which is expressed as follows:

$$= \frac{1}{|A|} \sum_{j|j \in A} Cov\{V_j V_i\}$$

Isaaks and Srivastava further state that the covariance between the random variable at the  $i$ th sample location and the random variable  $V_A$  representing the average value of the phenomenon over the area  $A$  is the same as the average of the point-to-point covariances between  $V_i$  and the random variables at all the points within  $A$ . The block kriging system can therefore be expressed as:

$$\begin{array}{c}
 \mathbf{C} \quad \cdot \quad \mathbf{w} = \mathbf{D} \\
 \underbrace{\begin{bmatrix} \bar{C}_{11} & \cdots & \bar{C}_{1n} & 1 \\ \vdots & \ddots & \vdots & \vdots \\ \bar{C}_{n1} & \cdots & \bar{C}_{nn} & 1 \\ 1 & \cdots & 1 & 0 \end{bmatrix}}_{(n+1) \times (n+1)} \cdot \underbrace{\begin{bmatrix} w_1 \\ \vdots \\ w_n \\ \mu \end{bmatrix}}_{(n+1) \times 1} = \underbrace{\begin{bmatrix} \bar{C}_{1A} \\ \vdots \\ \bar{C}_{nA} \\ 1 \end{bmatrix}}_{(n+1) \times 1}
 \end{array} \tag{3.20}$$

With the bar above the covariances on the right-hand side indicate that the covariance is the average covariance between a particular sample location and all the points within  $A$ :

$$\bar{C}_{iA} = \frac{1}{|A|} \sum_{j|j \in A} \tilde{C}_{ij} \quad (3.21)$$

The block kriging variance is given by:

$$\bar{\sigma}_{OK}^2 = \bar{C}_{AA} - \left( \sum_{i=1}^n w_i \bar{C}_{iA} + \mu \right) \quad (3.22)$$

Where:  $\bar{C}_{AA}$  is the average covariance between pairs of locations within A.

### 3.8.2 Advantage and disadvantage of block kriging

Isaaks and Srivastava (1989) further state that the advantage of using the block kriging system is that it produces an estimate of the block average with the solution of only one kriging system. The disadvantage is that the calculation of the average covariances involves slightly more computation than the calculation of the point-to-point covariances in the point kriging system.

### 3.9 Quantified Kriging Neighbourhood Analysis

Quantified Kriging Neighbourhood Analysis (QKNA) is a method that quantitatively assesses the suitability of a kriging neighbourhood. Vann et al. (2003) argue that QKNA is a mandatory step in setting up any kriging estimate. The results of QKNA, mainly focusing on the kriging standard deviation, are presented in section 8.5.

Kriging only gives the best linear unbiased estimate with low variances if the block size and the neighbourhood are properly defined. Bigger blocks with low nugget effects will have better Krige estimates. Vann et al. (2003) state that, in general,

the block size needs to increase as the nugget increases and that block sizes smaller than half the drilling grid dimensions are not suitable for QKNA unless the grade continuity is very high (very low nugget and long ranges).

Vann et al. (2005), and Krige (1994, 1996a) state that the definition of the ranges in Kriging can have a significant impact on the outcome of the Kriging estimate. They also state that neighbourhoods should not be too restrictive, as this results in conditional bias. Furthermore, they state that conditional bias causes estimated grades greater than the mean grade to be significantly higher and those lower than the mean grade to be significantly lower, so high grades will be overestimated and low grades underestimated.

Vann et al. (2003) state that if long ranges are selected, negative weights may be drawn in, but this causes problems if they are many. Especially at margins of an optimized search, Kriging weights should be very small or even slightly negative. However, in the case of a pure nugget, every sample found gets an equal weight ( $1/N$ ), no matter how far the search.

Vann et al. (2003) further state that the following criteria should be considered when evaluating a particular kriging neighbourhood:

- the slope of the regression of the “true” block grade on the estimated block grade;
- the distribution of kriging weights themselves (including the proportion of negative weights);
- the Kriging variance.



## CHAPTER 4: DATA COLLECTION AND VALIDATION

Quality assurance (QA) connotes protocols and procedures that ensure that the sampling and assaying are completed to a certain quality, while, quality control (QC) is the use of QAQC samples and statistical analyses to ensure that the assay results are reliable (Snowden, 2009). QC is a multifaceted process that starts with ensuring that the drilling and sampling methodologies are in place, appropriate and undertaken according to best practices. The next stage in the process involves planned task observations to ensure drilling and sampling methodologies are adhered to.

In order to obtain high confidence in the field sample collection, preparation and analysis, QC samples are inserted into the sample batches that are submitted to the laboratory for assaying. Out of the 19 916 EOF samples, a total of 1161 are QC samples and 18 755 are field samples. The QC samples (Table 2) represent 5.8% of the total samples and they include blanks, duplicates, AMIS0147, AMIS0149, AMIS0153, AMIS0157 and AMIS0158.

**Table 2 EF1 QC samples**

<b>QC Standards</b>	<b>Total</b>
Blanks	314
Duplicates	449
AMIS0147	26
AMIS0149	122
AMIS0153	123
AMIS0157	72
AMIS0158	55

**1161**

Data validation is carried out in order to clean the data set, and a clean data set is the basis for reliable estimation. Hence, much time has been dedicated to data

validation. At Rosh Pinah Mine, the Standard Sampling QAQC Standard Practice Instruction (Mukumbi, 2014) governs the QAQC samples. The QAQC samples are manually or automatically inserted within the field samples during sample sheet generation. For boreholes with more than 15 samples, the QA/QC samples are automatically inserted after the 15th field sample such that the 16th, 17th and 18th sample constitute a duplicate, a certified standard and a blank, respectively. For boreholes with less than 15 samples the QAQC samples are inserted manually at any interval, maintaining the sequence, such that the  $n$ th sample is split to form the duplicate  $n + 2$ , whilst  $n + 3$  is the certified standard and  $n + 4$  is a blank. Certified standards are used to identify analytical bias and to identify sample swaps or mislabeling of samples and/or QAQC samples, whilst, the coarse blank checks for contamination included at the crushing stages of sample preparation. QAQC samples were only introduced in 2009 at Rosh Pinah Mine, thus the trends of historical samples analysed prior cannot be explained by the QAQC analysis.

This chapter describes the drilling and sampling techniques applied during exploration, the type of data collected during borehole logging and data validation methods put in place. The chapter further summarizes the EOF QAQC analyses of the certified reference material (CRM), blanks and duplicates. Spurious QC samples and pulp samples that plot outside the acceptable limits are listed. The aim of the QAQC analyses was to identify spurious QC samples, to correct them and if they cannot be corrected to exclude them from the estimation data set. Boreholes were excluded from the data set if:

- They did not have coordinates.
- There were missing assay results.
- They had conflicting geology or grade information.

#### **4.1 Drilling**

The EOF was diamond-drilled using BQ (60 mm and 36.5 mm hole and core diameter, respectively) sized core. Three drilling programs are run based on the drill spacing; primary drilling is done on sections that are 60 m apart, followed by the secondary and tertiary drilling, which are done on 30 m and 10 m sections, respectively.

The grid for EF1 sections is in the 55 – 235° direction aimed to intersect the NW-SE striking EF1 limb perpendicular whilst the EF2 grid is drilled in the 119 - 299° direction with the aim to intersect the NE - SW limb, as shown in Figure 11. The 90 Off Main Grid is drilled in the 145 - 325° direction and it aims to intersect the fold hinge at 90°.

Drill locations for underground drill holes are marked by the Rosh Pinah Survey Department. Surveyors mark the grid lines and azimuth on the tunnel walls. Drillers are given drill instruction sheets showing the section lines, the direction of drilling, the depth and the dip of the borehole. The drill foreman and geologist check the machine set-up before drilling starts.

The drill core is logged by a geologist for lithological, structural and geotechnical information as per standard. Core recovery and orientation surveys of the boreholes are done by technical assistants on all boreholes and sampling of the core is done on instruction by the geologist. The geologist, as the responsible person, oversees the sampling procedure and ensures that the density of the core is measured before samples are submitted to the laboratory.

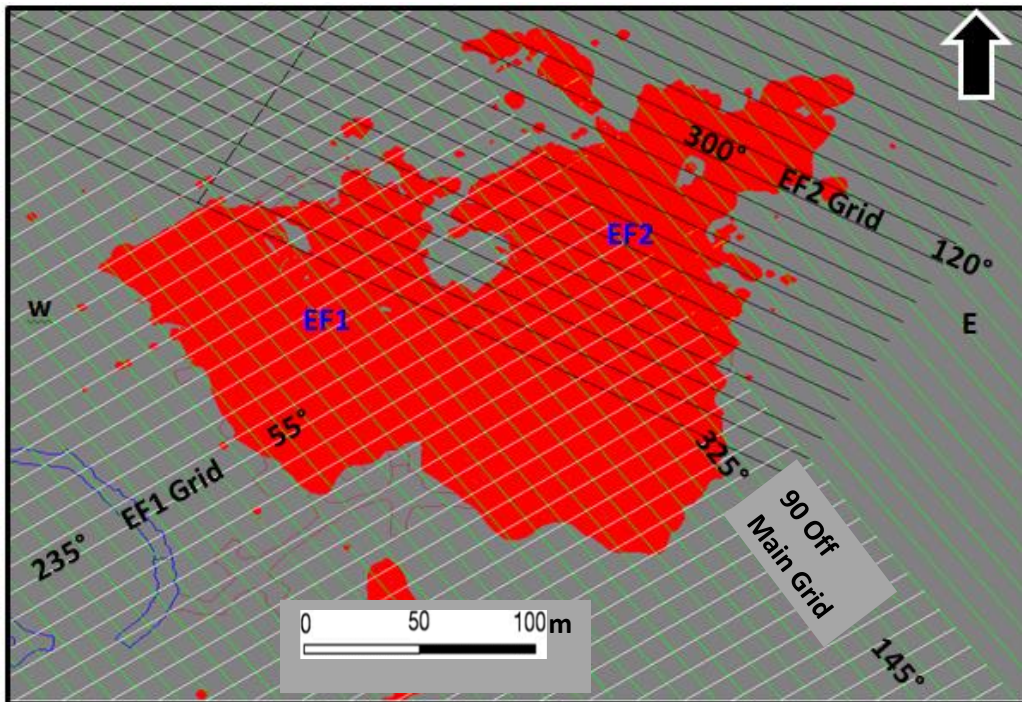


**Figure 11 EF1, EF2 and 90 Off Main grids**

#### **4.2 Drilling data and accuracy of borehole information**

A total of 1607 boreholes were drilled in EOF, of which 1241 are tertiary exploration holes whilst 366 are underground exploration (primary and secondary) holes. The following information is collected during borehole logging; collar surveys, coordinates, lithologies, structural information, bedding grading, water readings, downhole surveys and core recoveries.

Planned drillhole information (collar coordinates, dip, azimuth and depth) can be extracted using the MineSight software. All drillholes deeper than 50 m are down-hole surveyed. The orientation survey is conducted with a Reflex tool, or historically by the Electronic Multi Shot (EMS), the Sperry sun or the Eastman. On completion of every section, an instruction sheet is issued to the Survey Department, to survey the final collar position of the drill-hole and the dip at the collar. Core recovery is measured and imported into MineSight via the acquire database software for every borehole drilled.

### **4.3 Logging**

Core logging at Rosh Pinah Mine is done on the surface using a standard form in “Pocket AcQuire” software designed for the Compaq Palmtop computers which is totally compatible with the geological acQuire (SQL) database on the mine. The capture screen in Pocket acQuire is designed such that the software prompts the geologist to select descriptions of fields, lithology, colour, sedimentary grading, structure (folding, faulting, cleavage, etc.), alteration and mineralisation, already stored for each field (validation tables). When logging, the geologist records all collar and survey data for the drillhole, lithological, structural and grading data using the Palmtop computers. Only values which are present in the validation tables can be entered into the database, except for fields such as depth, comments, hole number, etc. Information is then imported into the MineSight software via acQuire.

### **4.4 Sampling techniques**

Only drill core data are used for the resource and grade estimation. Sampling standards used when sampling mineralised intersections are:

- maximum sampling length of 150cm,
- a minimum sampling length of 40cm,
- no sampling across lithological boundaries,
- no sampling across different alteration zones,
- no sampling across different mineralogical assemblages,
- all included waste is sampled, and

- 1.5m of waste is sampled on either side of the mineralised interval.

Sampling intervals are clearly marked on the core. The primary and secondary drill cores are split in half. One half is stored with the rest of the core and the other half is sent to the laboratory for analysis. The tertiary drill core is wholly sampled.

#### **4.5 Sample preparation**

Samples are packaged at the core shed, registered into Laboratory Information Management System (LIMS) by assistants in the Mineral Resource Management Department and then dispatched daily to the laboratory.

On arrival, samples are checked, sorted and then activated in LIMS. Thereafter the samples are crushed using a jaw crusher to about 5.5 mm before splitting, using a Jones Riffler, to obtain a representative sample of approximately 100 g. Samples are mill-pulverized prior to wet chemical preparation.

#### **4.6 Mapping information**

Another set of information used is the mapping information; the level maps for each lithology were triangulated and viewed in section view during section interpretations, especially to mark out the lithological contacts. Figure 12 demonstrates how the mapping information was used.

The mapping information and borehole data were used to construct 23 sections on the Main Geology grid (EF1) and 16 sections on the EF2 grid. These sections were triangulated and based on the triangulated sections 44 level plans were interpreted on every 10 m level from the -150 level to the 290 level.

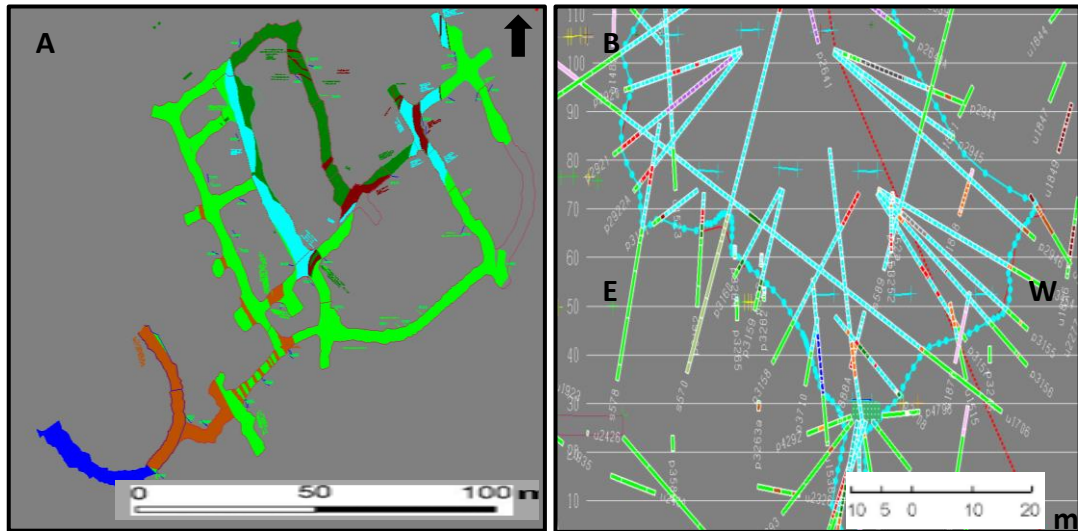


**Figure 12 A. EOF -030 level map indicating lithological contacts. B. EF1 -1080 section interpretation indicating the triangulated carbonate mapping as lines**

#### 4.7 Data aggregation methods

The grade model was modelled based on a 4% Zn equivalent cut-off. The Zn equivalent was calculated using the following formula:

$$\text{Zinc equivalent} = \text{Zn} + (1.01 \times \text{Pb}) + (0.026 \times \text{Ag}) + (\text{Au} \times 0.817)$$

(Crowther, 2014).

#### 4.8 Data validation

This section presents the validation of collars, lithologies, assays, conflicting grades and lithologies.

##### 4.8.1 Collars

Out of the 1607 collars, nine collars did not have surveyed or planned coordinates. These nine collars are presented in Appendix A and were excluded from the dataset. An additional 66 production holes were not collar-surveyed but

had planned coordinates. Survey coordinates may not be recorded if boreholes are underwater or if the geologist forgets to request the collar surveys from the surveyors, as occasionally happens. These 66 holes were included in the dataset, and their planned coordinates were used.

#### **4.8.2 Lithology**

Borehole p3582 and p4657 are missing lithological data, so both were not logged. The core was disposed before logging. These two boreholes were also excluded from the dataset.

#### **4.8.3 Assays**

Appendix B shows a list of 17 boreholes that were sampled, but however these samples were submitted to the laboratory, the results have not been reported. They were also excluded from the dataset. A total of 298 boreholes were drilled but not sampled because they did not intersect economic mineralisation. These boreholes are included in the dataset and are used for interpretations.

#### **4.8.4 Conflicting grade and lithologies**

A total of 70 boreholes, listed in Appendix C, were excluded from the dataset and interpretations because of conflicting geology or grade due to spurious borehole orientations.



#### 4.9 Certified Referenced Material

All five referenced materials used were supplied by EXXARO from the Rosh Pinah Mine zinc–lead sulphide ore. Table 3 summarizes the five reference materials with their expected values and their lower limits and upper limits at two standard deviations for the inductively coupled plasma (ICP) analysis.

**Table 3 Rosh Pinah Mine CRMs – Expected values, Lower and Upper Limits**

Name	Zn			Pb			Ag		
	Expected	Lower Limit	Upper Limit	Expected	Lower Limit	Upper Limit	Expected	Lower Limit	Upper Limit
AMIS0147	29.05	27.85	30.25	3.32	3.17	3.47	62.8	57.8	67.8
AMIS0149	15.37	14.83	15.91	1.71	1.63	1.79	30.1	27.8	32.4
AMIS0153	8.84	8.5	9.18	1.02	0.97	1.07	19.9	18.6	21.2
AMIS0157	3.03	2.91	3.15	0.3432	0.3208	0.3656	6.7	5.5	7.9
AMIS0158	1.62	1.56	1.68	0.2162	0.197	0.2354	5.6	4.7	6.5

The CRM analyses show that the analyses are dominantly acceptable, though some assays returned results outside the acceptable limits due to contamination and dilution. The Ag analysis for all CRMs displayed higher variability, possibly due to an unreliable or inaccurate analytical method or inherit variability. The CRMs indicate that the laboratory reported an acceptably high bias during October 2011. The subsequent subsections summarize the Zn, Pb and Ag analyses for each CRM in detail.

#### 4.9.1 AMISO147

A total of 24 AMISO147 Zn samples, presented in Appendix D, were analyzed at EF1, of which 10 (41.67%) plot outside the acceptable limits and 14 plot within two standard deviations. A total of 26 AMISO147 – Pb samples, presented in Appendix F, were analyzed, of which 6 (23.08%) plot outside the acceptable limits and 16 plot within two standard deviations. Only two AMISO147 – Ag standards (Figure 13) were analyzed and both plot far outside the acceptable limits, which could be due to an unreliable or inaccurate Ag analytical method.

A list of all AMISO147 standards that returned unacceptable assay values is presented in Appendix E. They returned unacceptable values because of contamination; most of the samples were analysed during October 2011 and Dec 2013. This implies that the laboratory staff did not clean equipments well during these periods. Reanalysis should have been requested.

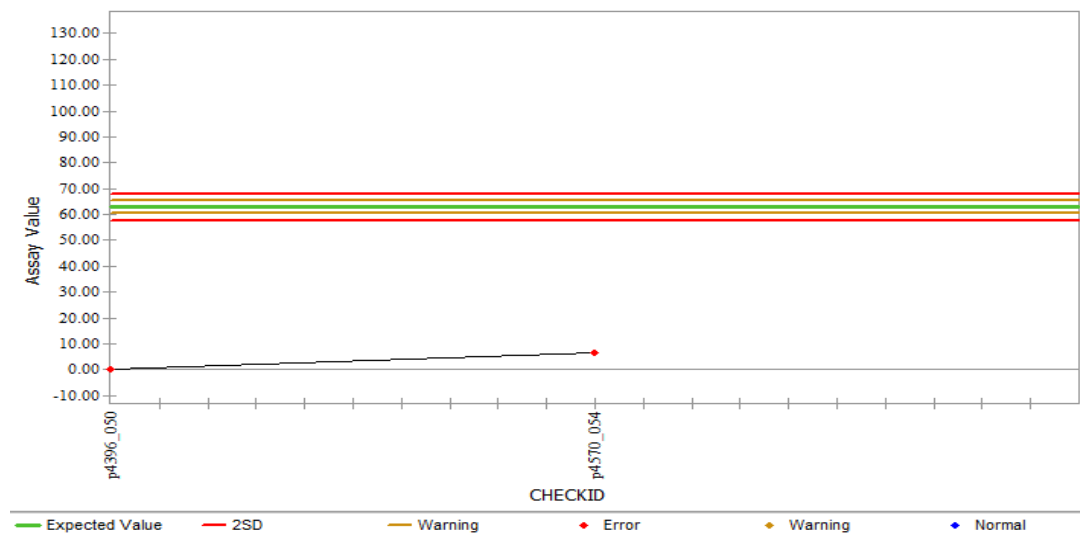


Figure 13 AMISO147 Ag Total (ppm) standard analyses by sequence

#### 4.9.2 AMISO149

A total of 122 AMISO149 standards (Appendix G and H) were analyzed at EF1, of which 71 (58.20%) Zn standards plot outside the acceptable limits and 51 plot within two standard deviations. The AMISO149 Zn has an expected value of 15.37% and a calculated mean of 15.70%, which is 0.39% higher than the expected value. Returning assays indicate an unacceptably high bias during October 2011 and in January 2013. The ICP was not well calibrated during those periods. Some of the standards returned assays outside the acceptable limits because of contamination and reanalysis should have been requested.

Four standards listed below were wrongly labelled as AMISO149 (Appendix G); these were corrected as follows:

- p4819\_017 is AMISO158,
- p4554\_035 is AMISO153,
- p4356\_017 and p4410\_017 is AMISO57.

Of the 122 standards analysed, 42 (34.43%) Pb standards plot outside the acceptable limits and 80 plot within two standard deviations, as shown in Appendix H. A total of 118 AMISO149 – Ag standards (Appendix I) were analyzed, of which 64 (54.24%) plot outside the acceptable limits and 54 plot within two standard deviations. Appendix I also indicates that Ag analyses done before sample p4557\_007 (October 2011) were highly erratic, which could be a result of a poor Ag analytical method being used by the laboratory during that period.

### 4.9.3 AMISO153

A total of 123 AMISO153 Zn and Pb standards (Appendix J and K) were analyzed, of which 51 (41.46%) Zn standards plot outside the acceptable limits and 72 plot within two standard deviations. A total of 48 (39.02%) Pb samples plot outside the acceptable limits and 75 plot within two standard deviations.

No sample swaps were observed. Zn samples analysed before p4367\_084 (October 2011) and Pb samples before January 2013 were highly erratic which could be due to a poor analytical method or contamination.

A total of 113 AMISO153 – Ag standards were analyzed, of which 68 (60.18%) plot outside the acceptable limits and 45 plot within two standard deviations. Figure 14 indicates that AMISO153 Ag analyses done before sample p4923\_017 (January 2013) were highly erratic, which could be because of a poor Ag analytical method. Between sample p4923\_017 and p4916\_011, the laboratory reported an unacceptable low bias of around 15 ppm.

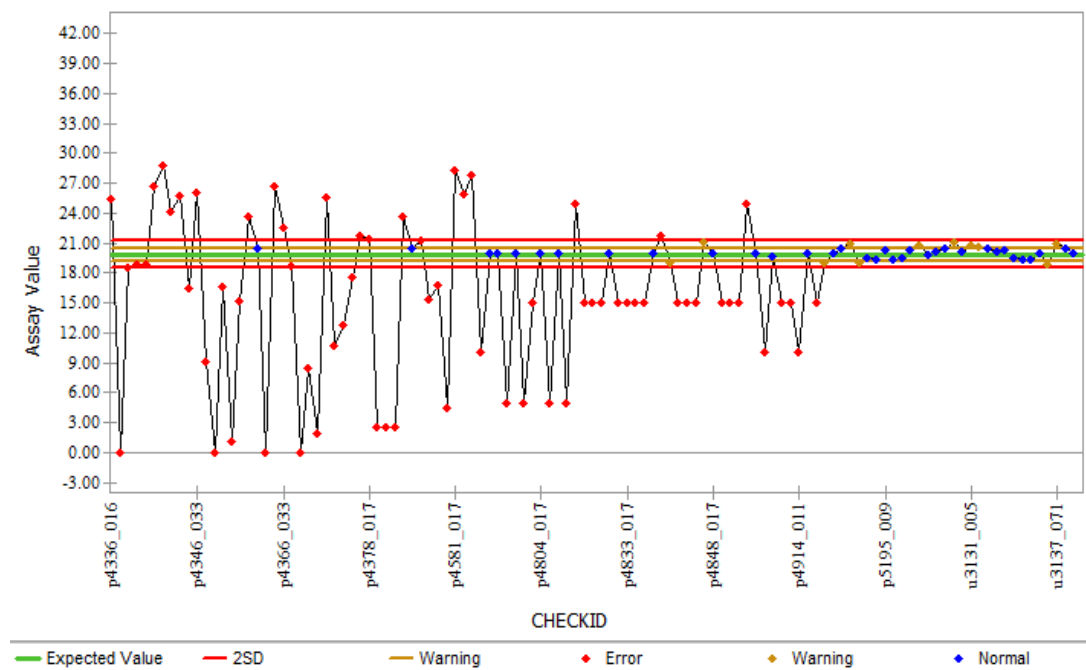
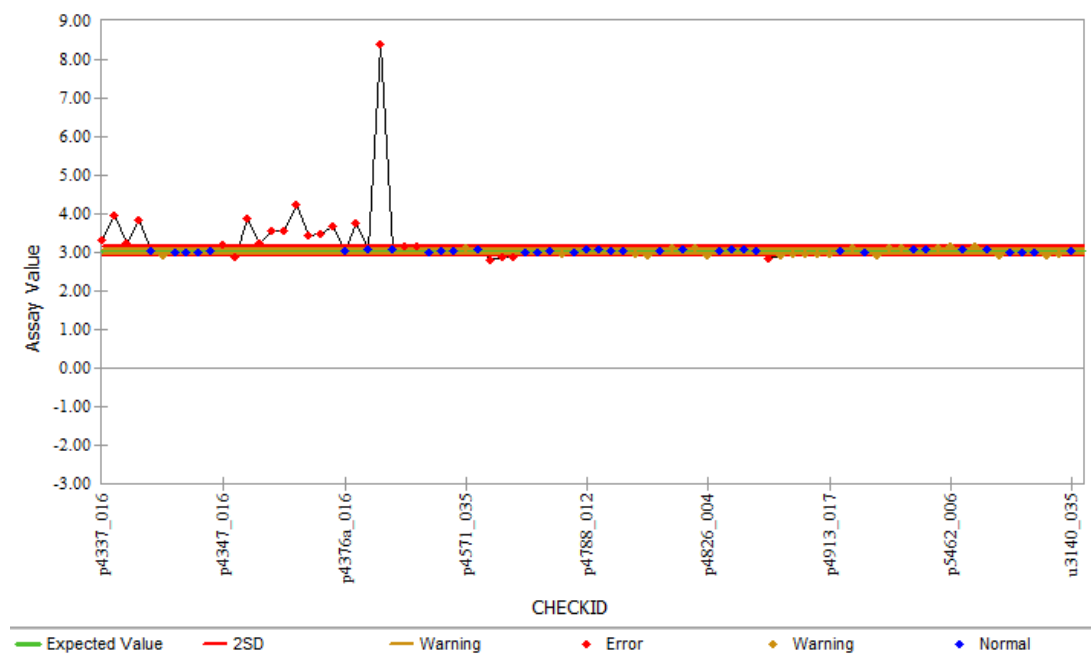


Figure 14 AMISO153 Ag (ppm) standard analyses by sequence

#### 4.9.4 AMIS0157

A total of 72 AMIS0157 – Zn and Pb standards (Appendix L) were analyzed, of which 27 (37.50%) Zn standards plot outside the acceptable limits and 45 plot within two standard deviations. A total 22 (30.56%) Pb standards plot outside the acceptable limits and 50 plot within two standard deviations. Sample p4395\_033 was wrongly labelled as AMIS0157 (Figure 15); it is in fact AMIS0153 and this was corrected. Figure 15 also indicates that samples analysed between October 2011 to January 2013 showed an unacceptably high bias.



**Figure 15 AMIS0157 Zn Total (%) standard analyses by sequence**

A total of 63 AMIS0157 Ag standards (Appendix M) were analyzed, of which 45 (71.43%) plot outside the acceptable limits and 18 plot within two standard deviations. AMIS0157 Ag analyses done before sample p4923\_017 (January 2013) were highly erratic, which could be because of a poor Ag analytical method. The laboratory also reported an unacceptably low bias of around 0ppm during October 2011.

#### 4.9.5 AMISO158

A total of 55 AMISO158 Zn (Figure 16), Pb (Figure 17) and Ag standards were analyzed. A total of 22 (39.29%) Zn standards plot outside the acceptable limits and 33 plot within two standard deviations. Figure 16 indicates that samples between p4346a\_016 and p4365\_033, which were analysed during October 2011, returned assay values above the acceptable limits. Figure 16 also shows that the standard often reported an unacceptably low bias.

A total of 23 (41.82%) Pb standards plot outside the acceptable limits and 32 plot within two standard deviations. Figure 17 also confirms that samples between p4346a\_016 and p4365\_033, which were analysed during October 2011, returned assay values above acceptable limits. AMISO158 Pb analysis reported a mean bias of 6.71%, which is supported by Figure 17, which shows that the Pb standard often reported an unacceptably and acceptably high bias.

A total of 31 (56.36%) Ag standards plot outside the acceptable limits and 24 plot within two standard deviations. The AMISO158 Ag standard has an expected value of 5.6ppm and the returning assays yield a calculated mean of 4.53 ppm (Table 4), which is 1.07 ppm lower than the expected value. The laboratory reported an unacceptably low bias of 2.5 ppm during 2012, until January 2013. AMISO158 Ag analyses done before sample p4908\_017 (January 2013) were highly erratic, which could be because of a poor Ag analytical method.

**Table 4 AMISO158 – Ag standard descriptive statistics**

# of Analyses above Threshold	# Outside Error Limit	% Outside Error Limit	Mean	Median	Min	Max	Standard Deviation	Standard Error	Total Bias
55	31	56.36	4.53	5.02	0	62.12	15.85	2.00	0.70

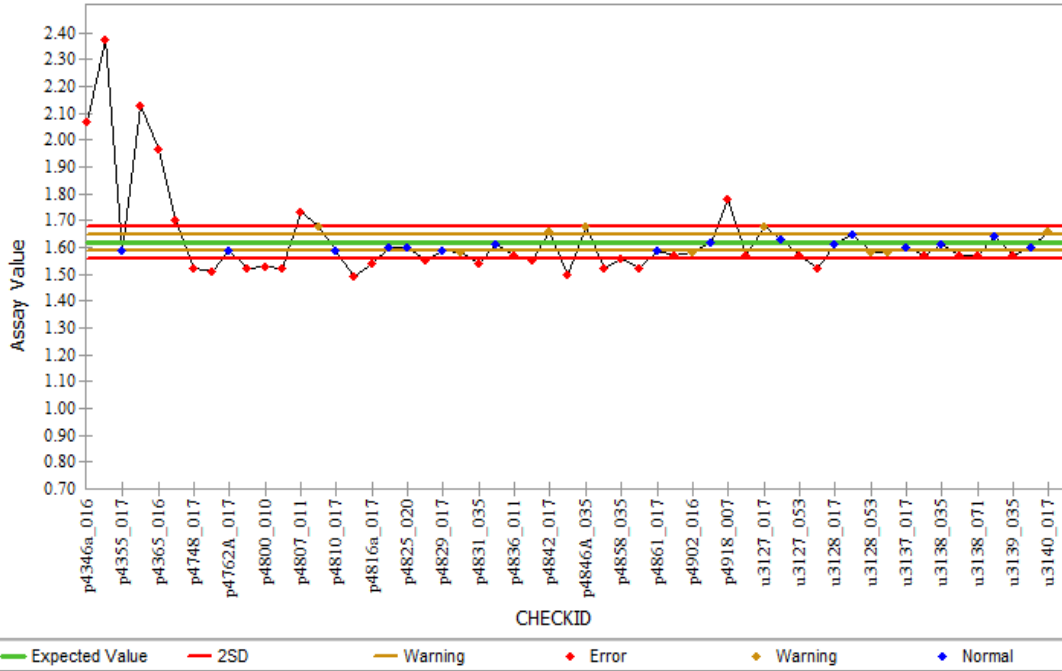


Figure 16 AMIS0158 Zn Total (%) standard analyses by sequence

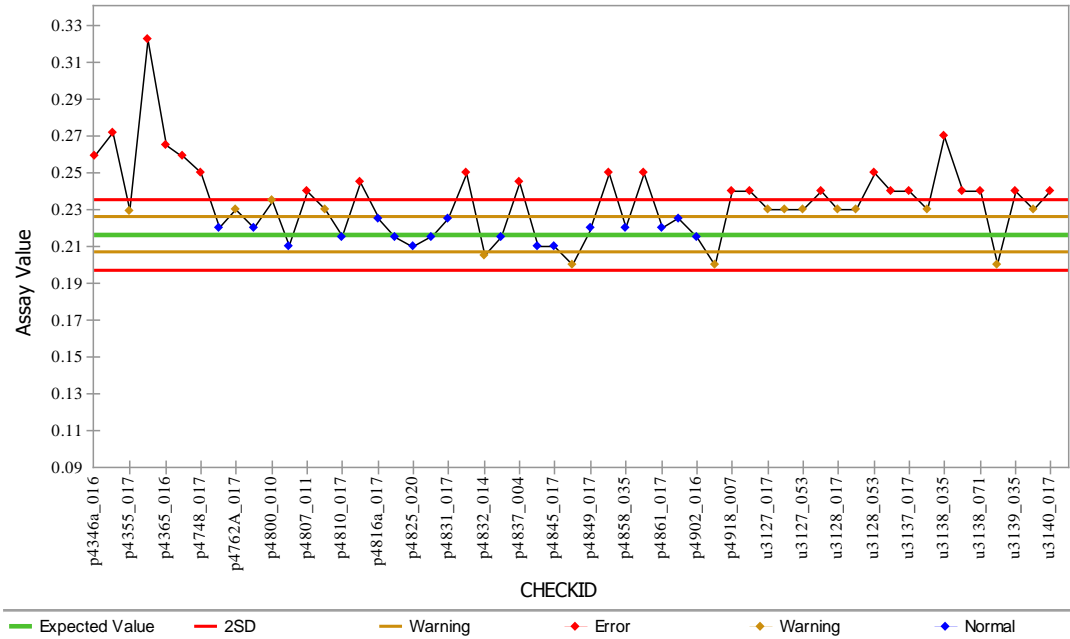


Figure 17 AMIS0158 Pb Total (%) standard analyses by sequence

#### 4.10 Blanks

Rosh Pinah Mine blanks are interlaminated sandstone and limestone collected from the Pickelhaube Formation at a locality approximately 4 km west of Rosh Pinah. The aim of inserting blanks is to determine contamination errors introduced during the sample handling process. The acceptable limits of Pb, Zn, and Ag analyses for the blanks are summarized in Table 5.

**Table 5 Analytical values for blank samples analysed**

Name	Element	Expected value	Lower Limit	Upper Limit
SS_BLANK	Zn (%)	0.05	0.00	0.10
SS_BLANK	Pb (%)	0.05	0.00	0.10
SS_BLANK	Ag (ppm)	2.5	0.00	5

A total of 314 Zn blank samples (Figure 18) were analyzed, of which 126 (40.13%) plot outside the acceptable limits and 188 plot within two standard deviations. Five sample swaps occurred whereby primary samples were swapped with blanks, namely, p5191\_006 was swapped with p5191\_007; p5193\_004 with p5193\_007; p4591\_018 with p4591\_015; p5462\_001 with p5462\_009; p4570\_052 with p4570\_055. Figures 19 and 21 also confirm that samples analysed during October 2011 were less reliable.

A total of 311 Pb blank samples were analyzed, of which 157 (50.48%) plot outside the acceptable limits and 154 plot within two standard deviations. A total of 313 Ag blanks (Figure 20) were analyzed, of which 242 (77.32%) plot outside the acceptable limits and 71 plot within two standard deviations. Figure 20 also indicates two sets of low bias, at 0 ppm and 2.5 ppm; this is because some samples that returned assays below the detection limit were captured with an assay value of 0 whilst others were assigned the half detection limit of 2.5 ppm.



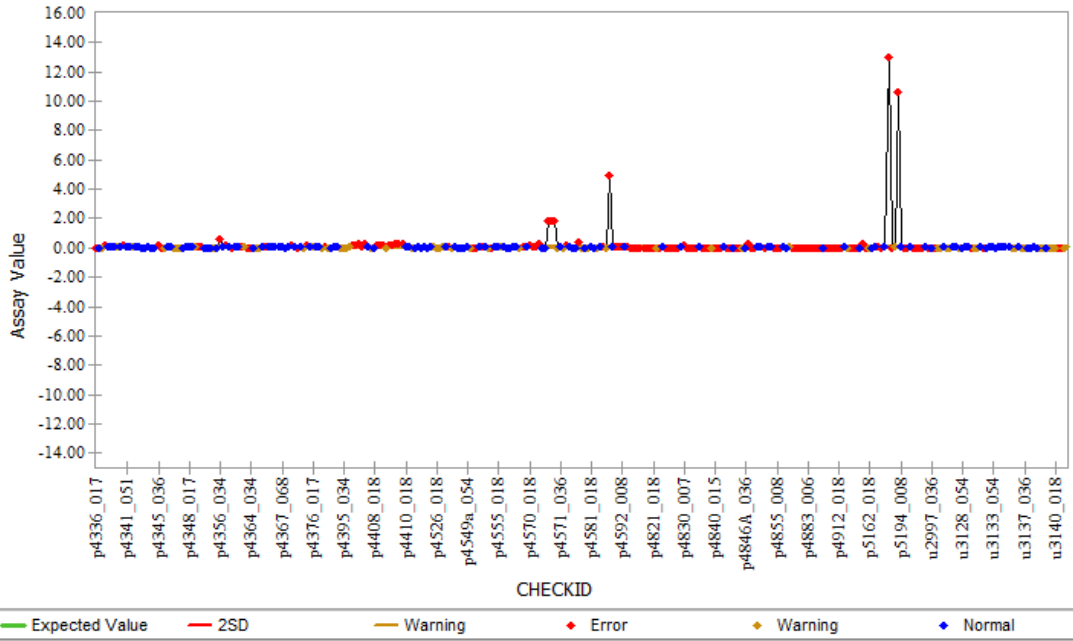


Figure 18 SS\_BLANK Zn Total (%) standard analyses by sequence

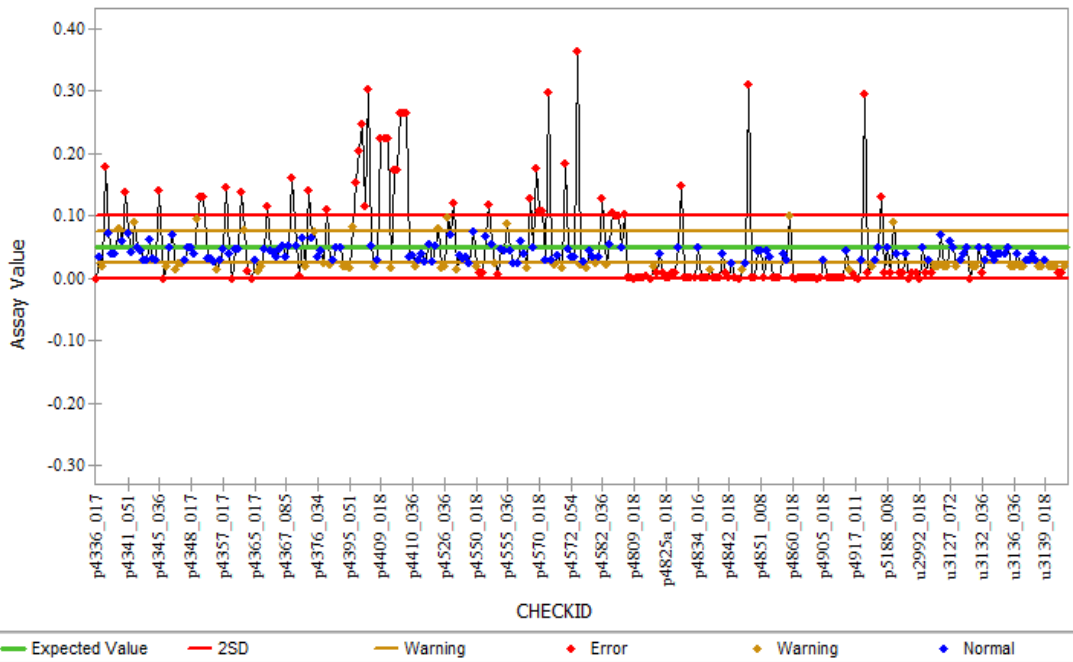
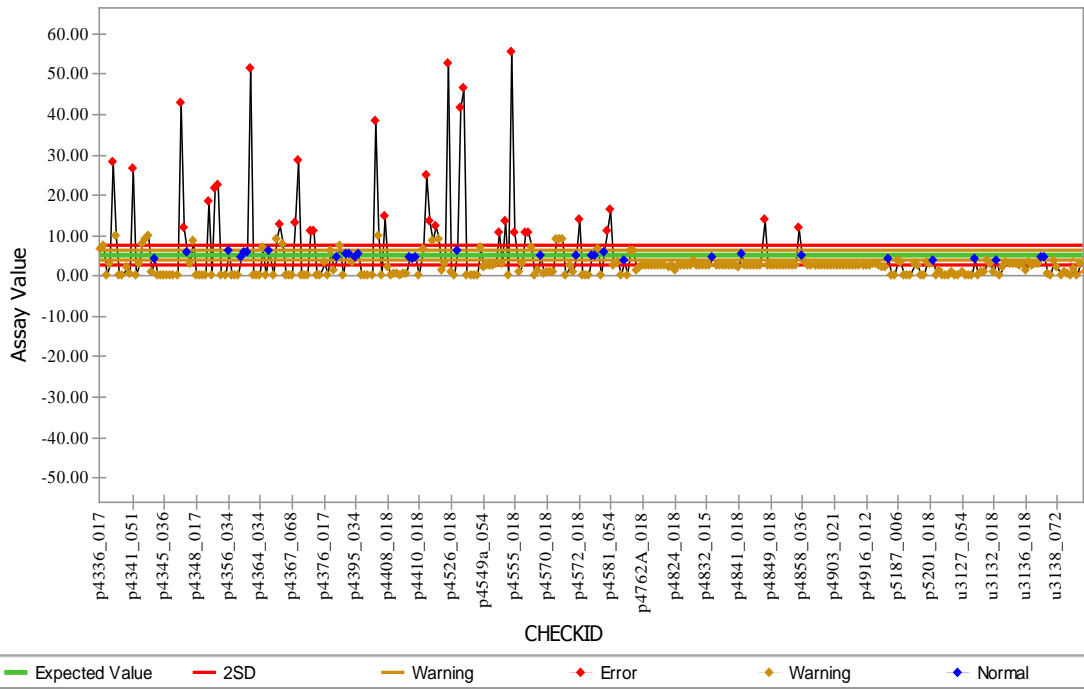


Figure 19 SS\_BLANK Zn Total (%) standard analyses by sequence; zoomed in around the acceptable minimum and maximum value



**Figure 20 SS\_BLANK Ag (ppm) standard analyses by sequence**

#### 4.11 Field Duplicates

A field duplicate is a repeat sample generated by splitting a field sample. At Rosh Pinah Mine, duplicates are taken after the drill core sample is jaw crushed to a size of 5.5 mm, with the purpose of quantifying any possible errors introduced after the crushing stage. Duplicates are used to assess precision or repeatability by comparing the paired (original and duplicate) data (Snowden, 2009).

The pass/fail criterion for duplicates at Rosh Pinah Mine is that the repeat should not vary more than 10% from the original samples. A total of 477 Zn field duplicates (Figure 21) were submitted, of which 135 (28.30%) Zn duplicates varied more than 10% from the original samples. The checks have a positive bias of 0.05 (Appendix N), which implies the checks reported assay values that are slightly higher than the original samples. The slight high bias is also revealed by the check sample mean of 4.59%, which is higher than the original sample mean of 4.37%. The original sample population has a higher variability compared to the check samples due to its higher coefficient of variation of 1.15, compared to that of the check samples of 1.10. However, the check samples vary more from their population mean compared to the original samples, because the check samples have a higher population standard deviation of 5.06% whilst the original is 5.03%. The Zn check and the original samples have a strong positive correlation of 0.96.

About 20 check samples analysed during October 2011 and January 2012 were split from the wrong original samples; these were corrected and the right original samples were assigned in the AcQuire database. Five other sample results (p4362\_007, p4363\_009, p4435\_007, p4549a\_016 and p4554\_034) could not be explained by contamination or wrong original sample split; those need to be reexamined and further investigation is required. About 88 check samples returned assays that vary 10% and more from the original samples due to contamination and poor repeatability/precision, especially at lower concentrations Zn (4%), Pb (2%) and Ag (50ppm), as shown in Figure 21. At higher grades the differences are mostly within a 10% relative difference.

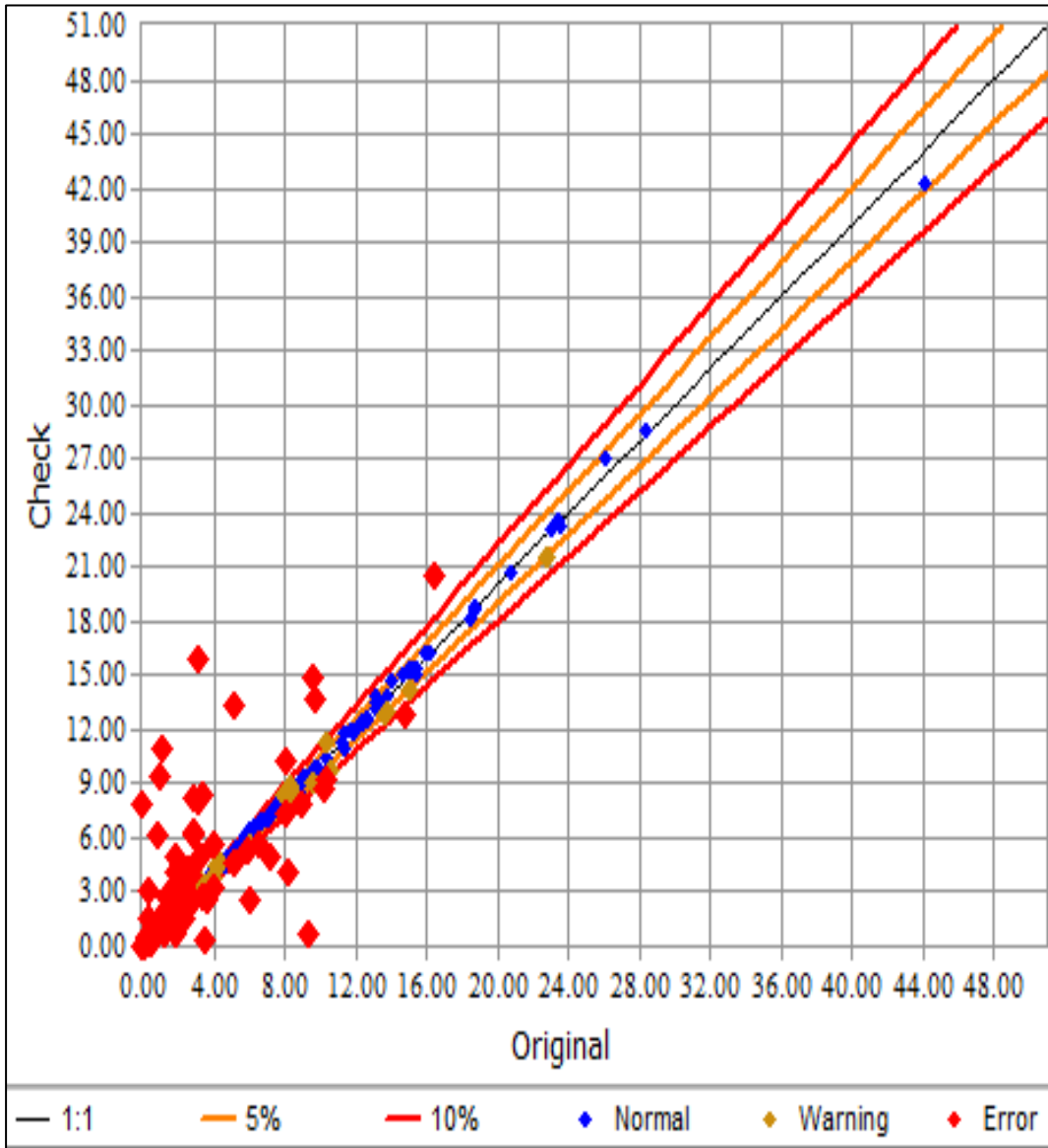


**Figure 21 Original sample versus repeat sample analyses for Zn**

A total of 473 Pb field duplicates were submitted, of which 183 (38.69%) vary more than 10% from the original samples. Appendix N summarizes the descriptive statistics and correlation parameters of the Pb duplicates. The checks have a positive bias of 0.06, which implies the checks reported assay values that are slightly higher than the original samples. The slight high bias is also revealed by the check sample mean of 1.05%, which is higher than the original sample mean of 1.99%. The Pb original sample population has a higher variability compared to the check samples, as shown by its higher coefficient of variation of 1.97

compared to that of the check samples of 1.87. However, the check samples vary more from their population mean compared to the original samples, as check samples have a higher population standard deviation of 1.96%, whilst the original is 1.94%. The Pb check and the original samples have a strong positive correlation of 0.98.

A total of 432 Ag field duplicates were submitted, of which 157 (36.34%) vary more than 10% from the original samples. The Ag checks have a negative bias of -0.03, which implies the checks reported assay values that are slightly lower than those of the original samples. The slight low bias is also supported by the Ag check sample mean of 26.75 ppm, which is lower than the original sample mean of 27.51 ppm. The original sample population has a higher variability compared to the check samples, as shown by its higher coefficient of variation of 1.98 compared to that of the check samples of 1.94. The check samples vary less from its population mean compared to the original samples, as check samples have a lower population standard deviation of 52 ppm, compared to that of the original of the 54.5 ppm. The Ag check and the original samples have a strong positive correlation of 0.94.

#### 4.12 QAQC Summary

The AMIS0147 Pb and Zn standards returned assays outside the acceptable limits due to contamination and dilution at the laboratory. The laboratory staff did not clean their equipment well during October 2011. The Ag analyses returned assays far below the acceptable limits due to an unreliable or inaccurate analytical method.

The AMIS0149 standard reported an unacceptably high bias and four standards were wrongly labelled. The AMIS0149 Ag population has a higher standard error, which implies that Ag is distributed less homogeneously.

No sample swaps occurred during AMIS0153 analyses of Zn and Pb, but samples analysed before November 2011 were highly erratic, which could be due to a poor analytical method or contamination. Pb analyses were less erratic after January 2013. AMIS0153 Ag analyses done before January 2013 were highly erratic; this could be because of a poor Ag analytical method during that period. The laboratory also reported an unacceptably low bias of around 15 ppm during January 2013.

Sample p4395\_033 was wrongly labelled as AMIS0157. AMIS0157 standards analysed between October 2011 and January 2013 returned an unacceptably high bias for Zn. AMIS0157 Ag analyses done before January 2013 were highly erratic, which could be a result of a poor Ag analytical method.

AMIS0158 samples between p4346a\_016 and p4365\_033 analysed during October 2011 returned assay values above acceptable limits for both Pb and Zn. The Zn analyses often reported an unacceptably low bias whilst Pb reported both acceptable and unacceptably high bias. Ag analyses done before sample p4908\_017 (January 2013) were highly erratic and the laboratory reported an unacceptably low bias of 2.5 ppm during 2012, until January 2013.

Blanks analysed indicate that sample swaps occurred, primary samples were occasionally swapped with blanks and it has been confirmed that samples analysed during October 2011 were less reliable.

About 20 check samples analysed during October 2011 and January 2012 were split from the wrong original samples; these were corrected and the right original samples were assigned in the AcQuire database. About 88 check samples returned assays that varied with 10% or more from the original samples due to contamination and poor repeatability/precision at lower Zn (4%), Pb (2%) and Ag (50ppm) concentrations.

## **CHAPTER 5: MODELS**

### **5.1 Introduction**

All geological information is interpreted on section and level plans using all available information on the geological drillhole database and all available mapping information on the Data Security System (DSS – MineSight). Four lithological solids were modelled, namely, the carbonate, microquartzite, breccia and arkose plus the grade model for Zn equivalent above 4%. Three sets of models were created, the MineSight, Leapfrog and a hybrid of MineSight and Leapfrog. The MineSight – Leapfrog hybrid model was created by using borehole information, MS3D sections and level plan interpretations. The tonnes and model outlines of the three solids were compared. The aim was to assess the different models and determine the optimal modelling method that reduces modeling time significantly.

The chapter presents the geometry, sizes, advantages, and limitations of the grade and lithological models and finally presents the method used for modelling EOF deposit. The tonnes of the Leapfrog model build from Minesight sections and level plans compare very well with the traditional Minesight model build using partial linking of the sections and level plans. Both methods had some mineralised intervals of borehole sticking outside the ore solid, especially at the boundary.

### **5.2 Minesight models**

The Minesight models (Figure 22A–F) involve manual interpretations of the sections and level plans. The interpretations are based on drillhole data and mapping done on level maps. The level maps are triangulated to enable viewing in sections. Once the section interpretations are completed, the sections are



triangulated to view them as lines in plan view, which are then used to interpret the level plans.

Three-dimensional solid models are created in MineSight using the partial linking triangulation method, which ensures that the model fits well on the section and level plan interpretations and tunnel mapping. The model is then verified using the surface verification tool in MineSight, which checks for self-intersecting and duplicate faces, openings and non-orientable surfaces.

Grade interpretations follow lithological contacts. In some instances, the grade interpretation does not follow the lithological contacts, but rather the mineralisation (4% Zn equivalent), for example when the footwall breccia is well mineralised (above 4% Zn equivalent). An internal peer review of the geological interpretations of the orebodies was done before and after the solid models were built. This process entails a number of geologists evaluating the interpretations to ensure its integrity regarding geology, structure, mineralisation and digital information standards. In MineSight each model is assigned a respective material code, as listed in Table 6. Based on the EOF ore an average specific density of 3.46 was applied in Minesight to estimate the tonnes. Table 7 gives a summary of the tonnes for the respective wireframes.

**Table 6 Standard material properties for geological modelling**

<b>ORE CLASS</b>	<b>DESCRIPTION</b>	<b>COLOUR</b>	<b>MATERIAL CODE IN MINESIGHT</b>
A	CARBONATE		2
C	ARKOSE		4
	BRECCIA		4
D	MICRO-QUARTZITE		5
ORE ZONE			1

**Table 7 Lithological and grade solid sizes and tonnes (density of 3.46)**

<b>Model</b>	<b>Width (m)</b>	<b>Length (m)</b>	<b>Volume (Million m<sup>3</sup>)</b>	<b>Tonnes (MT)</b>
Carbonate	230	450	1.42	4.82
Microquartzite (slivers)	50	200	0.31	1.06
Breccia	70	200	0.24	0.80
Arkose (slivers)	50 -75	300	0.27	0.90
Ore solid (Zn equivalent above 4%)	250	450	1.79	6.07

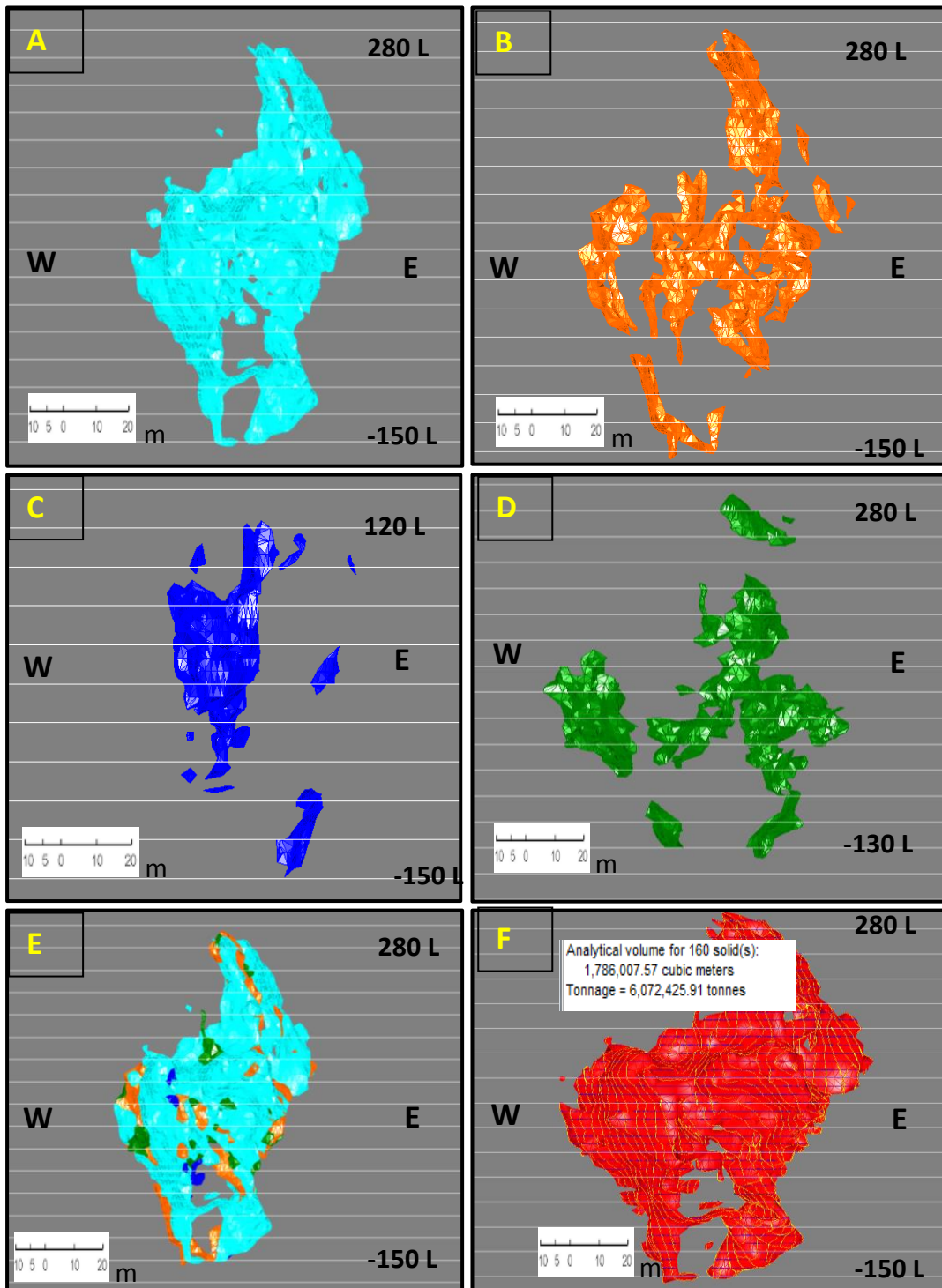


Figure 22 Minesight lithological and grade solids A. Carbonate solid. B. Microquartzite solid. C. Footwall breccia solid. D. Arkose solid. E. All lithological solids. F. Zn Equivalent above 4% grade solid

### **5.2.1 Advantages of Minesight solid (A)**

The Minesight solids take into consideration the geology and mapping information and thus honour the structural complexity of the orebody. The process is easily repeatable and auditable. The method honours the basic foundation of traditional geological interpretations, which is to interpret 2D geological sections and then to connect the sections to create 3D wireframes.

The method gives the geologist full control over the extrapolation of information during interpretations. The standard practice is to extend the interpretation for a distance of half the drillhole spacing from the data limits. With this method, the geologist has the power to extrapolate information that is even further than half the drill spacing. This helps in avoiding the creation of a saw tooth interpretation due to a lack of information on some sections where the mineralisation is continuous. For example, if holes are drilled shorter on the tertiary sections but on the main (secondary) sections the mineralisation is drilled out, then the mineralisation should be extrapolated from the one main section to the next main section. The interpretation should not show saw tooth, whereby the mineralisation extend in depth on the main sections and is shorter on the tertiary sections because the interpretation is limited to the shallow holes drilled to a certain level on the tertiary section. Furthermore, most geologists at Rosh Pinah are well versed in the application of Minesight on section interpretation and extrapolation, with many having more than four years of experience.

### **5.2.2 Limitations of Minesight solid (A)**

In Minesight, the linking is manual and tedious, and at times it is extremely difficult to consider both the sections and level plans, especially at sharp edges and internal waste. To overcome this, one has to fit it to either of the two. This may result in some ore being left out. If the ore was not interpreted on the sections, it might be left out; some holes drilled on the EF2 grid (Figure 25 B) were

not included in the interpretation and those ore lenses were excluded from the ore solid.

There is a fundamental flaw in Minesight section interpretation in the fold hinges, especially if the hinge is thinner than 10m and it is parallel and in between sections, as shown in Figure 23. The drilling and interpretations could miss the fold hinge completely. Thus, it is important for the EOF orebody to be drilled on all three grids.

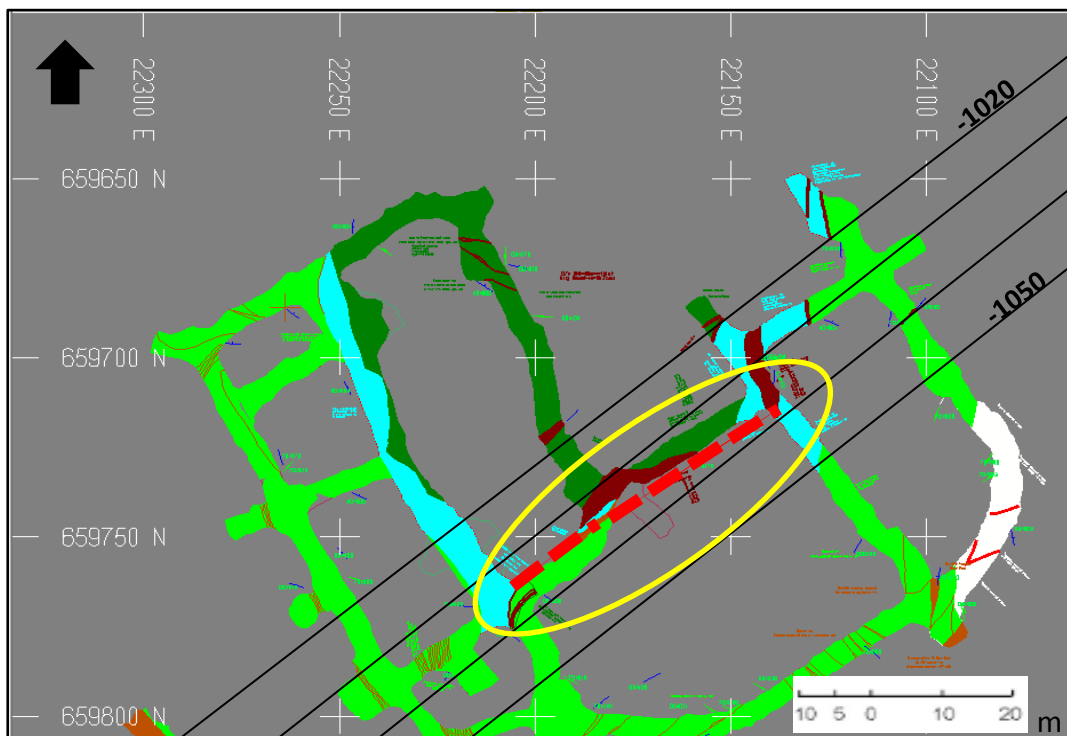


**Figure 23 Plan view of the EOF fold hinge on the -030 level**

At the edges of the ore solids, parts of the mineralised intervals are excluded and some waste intervals get included because the method does not snap to borehole information in 3D space. The models project borehole information onto the 2D planes and do not honour the 3D location of the ore. This may result in some waste being incorporated in the solid and in other cases ore may be excluded. The ore may be 2 m away from the 2D plane being interpreted, but, due to the

projection, it may be indicated as occurring on the plane. One requirement of sectional interpretations is that information must be snapped to the drillholes in 3D space for accurate compositing and sample coding.

### **5.3 Leapfrog model**

Leapfrog is the first software that allows the construction of geological models using 3D interpolation technology, called implicit modelling (Hodkiewics, 2016). It does not require time consuming manual creation and manipulation of polylines and polygons. The software was developed by SRK Consulting and Applied Research Associates of New Zealand (ARANZ). It uses the radial basis function (RBF) interpolation algorithm. Leapfrog has the ability to use wireframe surfaces and polylines as structural trends to guide interpolations in structurally complex or folded units.

Three Leapfrog ore solids were created (Figure 25B–D); the first model was created using the Minesight sections and level plans only. The second was created using a combination of borehole data (composited to 1.5), sections and level plans and the solid was snapped to all data. The third solid was created using borehole information and trend data (Figure 25D) obtained from mapping information. The solid was snapped to all data; a surface resolution of 5 was applied (Figure 24 A).

To minimize dilution, all unspecified intervals were treated as exterior samples (Figure 24C) and exterior samples shorter than 0.5 m flanked by ore were converted to ore. Furthermore, the geology was simplified by filtering out ore segments shorter than 1 m and all exterior segments were ignored (Figure 24B). Table 8 summarizes the width, length, volume and tonnes of the ore solids.

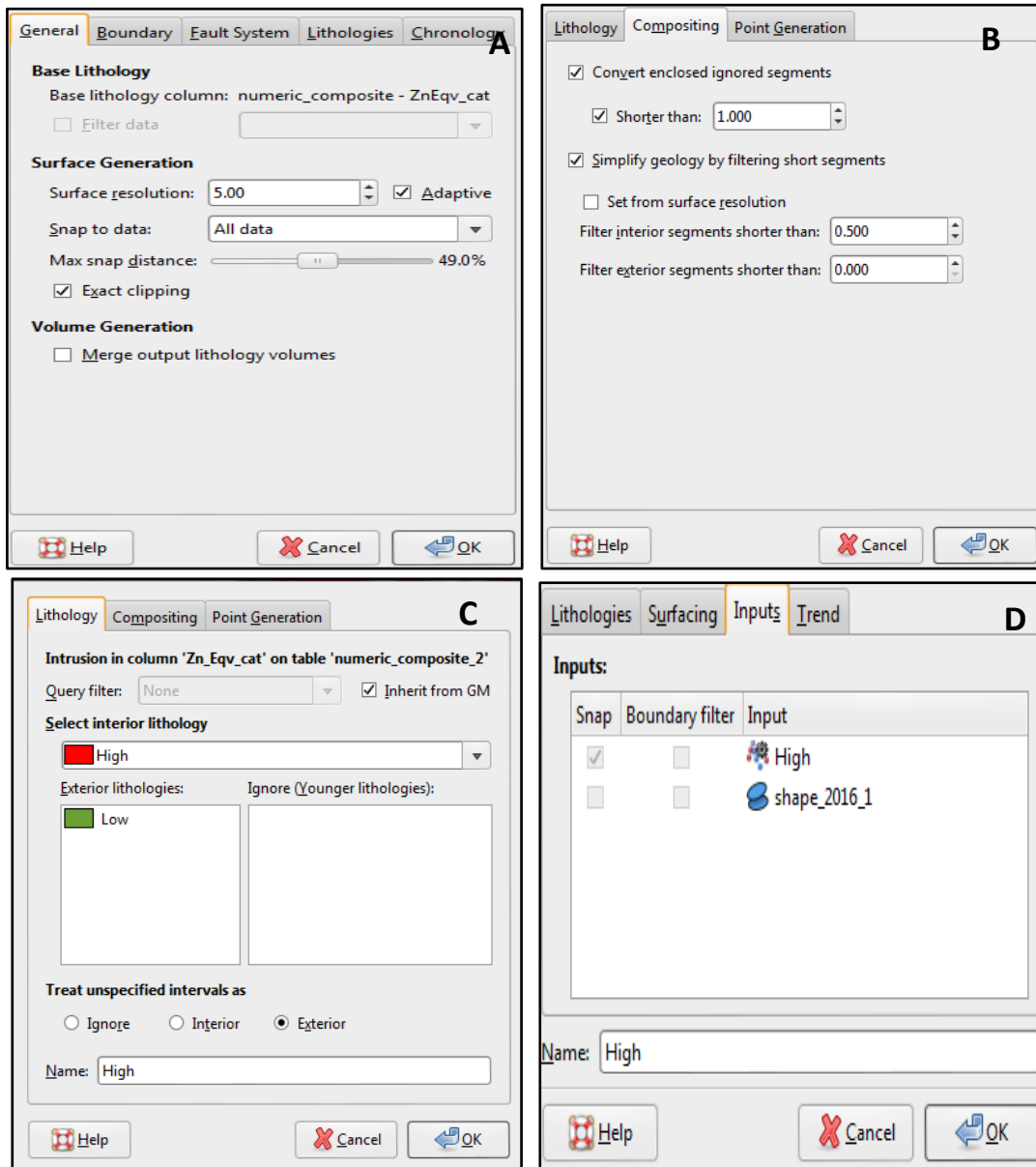
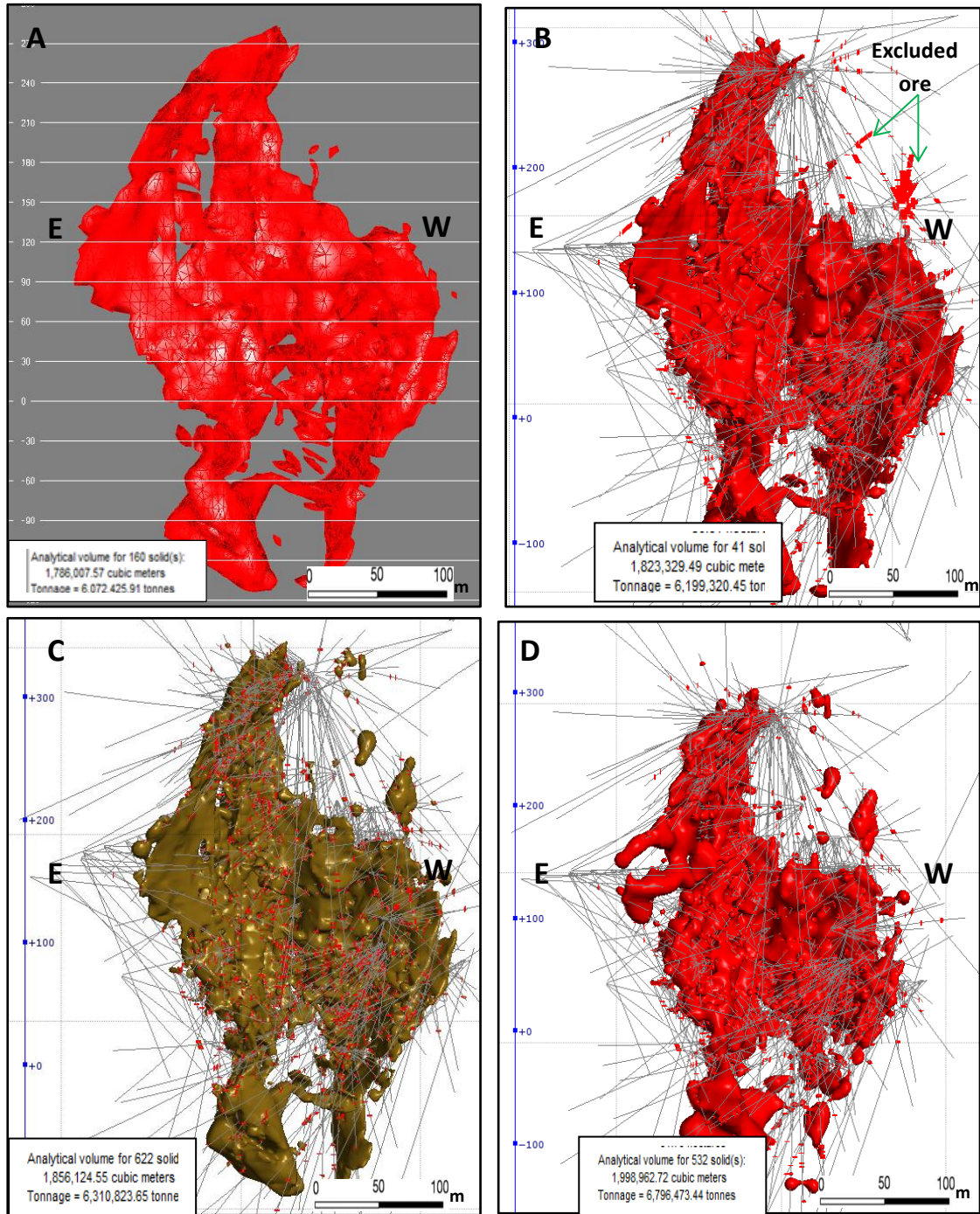


Figure 24 Leapfrog settings. A. Surface resolution of five and wireframe snapped to drilling data only. B. Ignored segments shorter than 0.5 were converted to ore if flagged by ore on either side; interior segments shorter than 1 m were filtered out and all exterior segments were excluded. C. Interior lithology is the high-grade ore above 4% and all other lithologies were treated as exterior. D. Trend data and composites from borehole information



**Figure 25 A. Minesight solid of Zn equivalent grade above 4%. B. Leapfrog model created from Minesight sections and level plans. C. Leapfrog model created from Minesight sections, level plans and borehole data. D. Leapfrog model created from boreholes information only**



**Table 8 The width, length, volume and tonnages of experimental ore solids**

<b>Model</b>	<b>Width</b> (m)	<b>Length</b> (m)	<b>Volume</b> (Million m <sup>3</sup> )	<b>Tonnes</b> (MT)
<b>A.</b> Minesight ore solid	250	450	1.79	6.07
<b>B.</b> Leapfrog polylines only	250	450	1.82	6.20
<b>C.</b> Leapfrog polylines and borehole information	250	450	1.86	6.31
<b>D.</b> Leapfrog holes only and mineralisation trend	250	450	2.00	6.80

The tonnes and volume difference were minimal in Model A to C, but not in model D. Model D is the Leapfrog model from borehole data and the mineralisation trend; it has over 500 000 tonnes more than the others. The shapes of Model A to C are very similar. Model A, the Minesight model, has less tonnes, followed by Model B, Leapfrog solid from Minesight level plans and sections.

### **5.3.1 Advantages of Leapfrog solids (Model B–D)**

Leapfrog software significantly reduces the amount of time required to interpret drillhole data; it is very powerful in identifying mineralisation trends and domains for resource estimation. Leapfrog is easy to learn and use, models are timely updated as new data become available and multiple interpretations can be modelled and tested because Leapfrog is fast. The models are snapped onto

borehole locations in 3D space, thus the models are more accurate, especially at the boundaries.

### **5.3.2 Limitations of Leapfrog solids (Model B –D)**

If borehole information and the mineralisation trend are used (Model D), the solid created does not honour the ore–waste contact obtained from mapping information. Even though Leapfrog has the ability to use structural trends to guide interpolations in structurally complex or folded units, when few or wrong structural data are used it may produce inaccurate models. This may increase dilution and results in tunnels to be developed in waste. Figure 26B indicates that over-extrapolation occurs at the ore–waste boundary when borehole information and trends are used.

Additionally, the Leapfrog solids are discontinuous (Figure 26A) because the interpolation was limited mostly to half the drill spacing (50%), even if the geology was continuous. Opening up the interpolation (snapping window 100%) creates solids that interpolates into waste. The final Leapfrog solid still needs to be edited by a geologist to make the limbs more continuous when the geology supports continuity. The Leapfrog solid that is created from Minesight levels and sections has exactly the same limitations as the Minesight solid created by partial linking, but it is faster and slightly more accurate than the Minesight solid because it honours all level plans and sections.

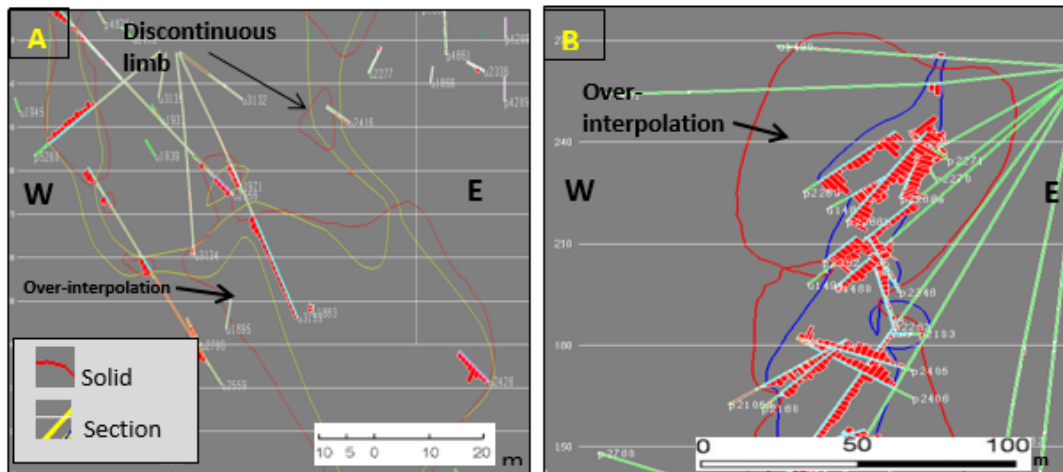


**Figure 26 EF1 Section -1020 interpretation of Leapfrog solid created from borehole information and the mineralisation trend. B. The images display solids that were over-interpolated because of a wide snapping window**

#### **5.4 Modeling EF1 sedimentary exhalative deposit**

The following steps were followed for modelling the EF1 sedimentary exhalative deposit:

- 1) Map all development tunnels on all mining levels on neat maps, ensure that the easting, northing, reference pegs are clearly labelled and ruler scales drawn in for measuring distances. Ensure that during mapping you capture lithological information, mineralisation contacts, veins, alterations, mineralisation, grading, younging directions and structural data (bedding, cleavages, slickensides, lineations, faults and folds).
- 2) Scan, import and georeference the field map (Figure 27). Digitize the level map and triangulate it to enable viewing in section.
- 3) Carry out primary exploration and secondary exploration drilling; ensure that drilling grids are perpendicular to the ore strike directions. In highly folded deposits, establish different grid sets for the fold hinges and fold limbs.



- 10) Under surface chronology, create new intrusion and add base lithology contacts, sections and level plans. The interior lithology should be the ore or the lithology of interest, the exterior lithology is the low grade or the other contacts.
- 11) All other imported unspecified intervals should be treated as exterior intervals. To minimize dilution, exterior samples shorter than 0.5m flanked by ore should be converted to ore. Furthermore, simplify the geology by filtering out ore segments shorter than 1m and all exterior segments must be ignored.
- 12) Export the created ore output volume as dxf and import into MineSight. Verify solid and modify in Minesight to ensure continuity and delete unwanted small lenses.

## **5.5 Summary**

The tonnes and volumes of the Leapfrog Model B built from Minesight sections and level plans compares very well with the Minesight model A built using partial linking of the sections and level plans. This is because both models are created from the same raw data (Minesight sections and levels plans) and use the same principle of creating wireframes. Both methods aim to include all level plans and sectional interpretations.

The Minesight and Leapfrog hybrid model is recommended for modelling complex sedimentary exhalative deposits because it reduces the time spent on building the wireframe from three weeks to two days and it allows manual manipulation where necessary.

## CHAPTER 6: STATISTICAL ANALYSIS OF ASSAY DATA AND COMPOSITES

### 6.1 Introduction

There are two main groups of classical statistics required to be understood for geostatistics. The first is the measure of central tendency (mean, mode and median), which aims to address the typical grade for the domain. The second measure is the measure of spread, which includes the range, inter-quartile range, variance, standard deviation and coefficient of variation. The measures of spread address how different the sample grades are from the typical grade, whether the domain consistently has a high grade and whether the data have a lot of variability and uncertainty.

This section deals with the statistical tools used to describe grade populations. Classical statistical methods treat individual samples as being random and independent. This chapter presents the effect of different composite sizes on classical statistics. It further includes an investigation of the underlying distributions. Statistical investigations are also presented that answer basic questions about the dataset. Firstly, the Z-scores and probability plots are presented with the aim to assess the normality of the dataset. Secondly, the two-parameter Log-normal distribution for  $n > 40$  is presented with the aim to estimate the population mean of the different variables. Thirdly, the principal components analyses (PCA) is presented, which is based on finding which variables are most strongly correlated with each component. Fourthly, the outliers are detected using quantile regression methods. The chapter concludes with a summary.

## 6.2 Compositing data

The objective of compositing data is to obtain an even representation of sample grades and to eliminate any bias due to sample length (Snowden, 2009). Typically, the dominant sample interval is selected as the composite length; Figure 28 indicates that the dominant sample length for EOF datasets is 1.5 m. Thus a fix composite length of 1.5 m was selected. Small intervals at the end of the hole were merged to the composite above. The composites created honour the geology, which implies that a composite is not created across a lithological boundary. Based on the assumption that bigger blocks have lower variances, a composite length of 3m was tested.

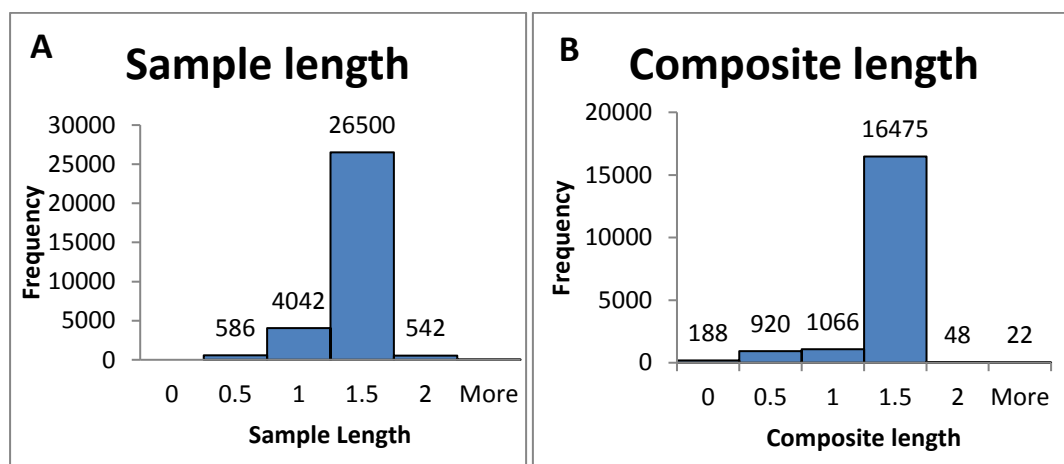


Figure 28 A. Histogram of the sample length. B. Histogram of the composite length

## 6.3 Comparison of assay data and composites

A comparison of assay data to the 1.5 m composites for Zn, Pb, Cu and Fe variables is presented in Table 9. The difference in the mean of the assay data and 1.5 m composite is insignificant because the dominant sample length is also 1.5 m. The Zn mean for Domain 1 of the 3 m composite is 12.43% (Table 11), which is less than the mean of the assay data and the 1.5 m composites. The standard

deviation, variance and numbers of extreme outliers are lower for the 3 m composites compared to the assay data and the 1.5 m composites. The number of extreme outliers for the 3 m composites is 50% less than the assay data and 1.5 m composites. Similar observations were made for all the other variables and also for Domain 2 (Tables 9–11).

The coefficient of variation (COV) is a tool for determining how skewed the data are; near-normal distributions have a COV of less than 1.0. Based on the statistics Pb, Cu, Ag and Mn have a COV above 1.0, which means these elements' distributions are unlikely to be normal distributions. Zn, Fe, Mg and Rd have a COV of less than 1.0.

#### **6.4 Skewness and Kurtosis**

The symmetry or lack of symmetry is measured by the skewness statistics; if negative, then the distribution is negatively skewed; if zero, the distribution is symmetrical, and if positive, the distribution is positively skewed. Positively skewed distributions have many low values and few high values whilst negative skewness implies that there are many high values and few low values. The data are symmetric around the average if each positive deviation has a negative deviation.

Table 12 gives a comparison of assay data and composites skewness and kurtosis for Zn, Pb, Cu, Fe, Ag, Mn, Mg and RD. The RD is the only element with a skewness value close to zero, thus it is the only element with a near symmetrical distribution. All the other elements have a positively skewed distribution, with Cu, Ag and Mn being significantly skewed, as shown in Appendix O. Generally, increasing the composite size reduces the skewness of the data; the only exception was for Domain 1 Mn and Mg.



Kurtosis is the measure of peakedness; it measures the concentration of the values in the centre as opposed to the thickness of the tails. If the kurtosis is above 3, then the data are peaked (leptokurtic) and has long thin tails; if it is less than 3, the distribution is flat (platykurtic) and it has short fat tails. All elements except RD, Domain 1 Zn and Mg have peaked distributions, with Cu, Ag and Mn having the most peaked distributions. Generally, increasing the composite size reduces the peakedness of the distribution.

## **6.5 Histograms**

Generally, increasing the composite size from 1.5 m to 3 m shortens the tails of the histograms. The histograms (Appendices O and P) also confirm that all elements except for RD have positively skewed distributions.

The Ag histogram indicates two sets of Ag data that come from a similar population; the histograms display higher distributions of multiples of 10 compared to 5. There is almost double the amount of assays that returned values of multiples of 10 compared to 5. The shapes of the two histograms are similar; the data are derived from the same population. The observation might be related to the rounding off of assay values during different reporting periods. Increasing the composite size to 3 m minimizes this effect.

The Mg histogram for Domain 2 presented in Appendix P has two populations with a lower sample mean around 1% and a second mean around 7.5%. Increasing the composite sizes to 3 m reduces the effect of two populations.

**Table 9 Comparison of assay data and 1.5 m composites for Zn, Pb, Cu and Fe variables**

Domain	ZN % assay Data								ZN % 1.5 m composites							
	No	Min	Max	Mean	SD	Variance	COV	No. of extreme outliers	No	Min	Max	Mean	SD	Variance	COV	No. of extreme outliers
1	9364	0	60.83	13.05	9.2	84.62	0.71	36	9279	0	60.34	13	9.13	83.3	0.7	38
2	9391	0	66.96	11.15	8.81	77.58	0.79	234	9248	0	66.96	11.21	8.72	76.11	0.78	233
Domain	Pb % assay Data								Pb % 1.5 m composites							
	No	Min	Max	Mean	SD	Variance	COV	No. of extreme outliers	No	Min	Max	Mean	SD	Variance	COV	No. of extreme outliers
1	9364	0	49.26	2.37	3.09	9.53	1.3	220	9279	0	31.1	2.35	3	8.98	1.28	203
2	9391	0	28.64	2.57	2.87	8.24	1.12	239	9247	0	26.36	2.57	2.81	7.91	1.1	238
Domain	Cu % assay Data								Cu % 1.5 m composites							
	No	Min	Max	Mean	SD	Variance	COV	No. of extreme outliers	No	Min	Max	Mean	SD	Variance	COV	No. of extreme outliers
1	9364	0	60.5	0.21	0.76	0.58	3.61	627	9278	0	37.95	0.21	0.63	0.4	3	618
2	9391	0	20.42	0.2	0.38	0.14	1.89	420	9248	0	19.33	0.2	0.36	0.13	1.83	446
Domain	Fe % assay Data								Fe % 1.5 m composites							
	No	Min	Max	Mean	SD	Variance	COV	No. of extreme outliers	No	Min	Max	Mean	SD	Variance	COV	No. of extreme outliers
1	9364	0	38.95	4.05	3.05	9.29	0.75	35	9278	0	38.95	4.02	3	9.02	0.75	36
2	9392	0	44.8	3.52	2.66	7.08	0.76	80	9249	0	44.8	3.52	2.64	6.96	0.75	75

**Table 10 Comparison of assay data and 1.5 m composites for Ag, Mn, Mg and Rd variables**

Domain	Ag ppm assay Data								Ag ppm1.5 m composites							
	No	Min	Max	Mean	SD	Variance	COV	No. of extreme outliers	No	Min	Max	Mean	SD	Variance	COV	No. of extreme outliers
1	9246	0	2247	67.7	112.3	12619	1.7	377	9163	0	2247	67.2	111	12310	1.7	352
2	9263	0	1.75	62.4	75.3	5677	1.2	178	9133	0	1750	62.7	74.7	5576	1.2	166
Domain	Mn % assay Data								Mn % 1.5 m composites							
	No	Min	Max	Mean	SD	Variance	COV	No. of extreme outliers	No	Min	Max	Mean	SD	Variance	COV	No. of extreme outliers
1	2904	0	19.9	1.02	1.22	1.48	1.19	14	2912	0	19.9	1.02	1.22	1.48	1.19	15
2	3485	0	18.6	1.44	1.55	2.39	1.08	30	3433	0	18.6	1.45	1.54	2.39	1.07	31
Domain	Mg % assay Data								Mg % 1.5 m composites							
	No	Min	Max	Mean	SD	Variance	COV	No. of extreme outliers	No	Min	Max	Mean	SD	Variance	COV	No. of extreme outliers
1	2434	0	9.48	1.99	1.98	3.92	0.995	0	2446	0	9.48	1.99	1.97	3.88	0.99	0
2	2807	0	37.1	3.51	3.22	10.39	0.92	8	2762	0	37.1	3.56	3.21	10.32	0.9	8
Domain	RD assay Data								RD 1.5 m composites							
	No	Min	Max	Mean	SD	Variance	COV	No. of extreme outliers	No	Min	Max	Mean	SD	Variance	COV	No. of extreme outliers
1	2517	2.44	5.11	3.42	0.358	0.128	0.104	1	2498	2.44	5.11	3.42	0.35	0.13	0.103	1
2	3308	1.75	4.69	3.24	0.36	1.13	0.11	0	3232	1.75	4.69	3.24	0.36	0.13	0.11	0

**Table 11 Summary statistics of 3 m Composites for Zn, Pb, Cu, Fe, Ag, Mn, Mg and Rd variables**

Domain	Zn % 3 m composites								Ag ppm 3 m composites							
	No	Min	Max	Mean	SD	Variance	COV	No. of extreme outliers	No	Min	Max	Mean	SD	Variance	COV	No. of extreme outliers
1	5397	0	58.30	12.43	8.84	78.12	0.71	17	5339	0	1960	64.5	98	9610	1.5	185
2	5354	0	58.94	10.75	8.34	69.62	0.78	114	5289	0	1750	60.9	67.3	4528	1.1	80
Domain	Pb % 3 m composites								Mn % 3 m composites							
	No	Min	Max	Mean	SD	Variance	COV	No. of extreme outliers	No	Min	Max	Mean	SD	Variance	COV	No. of extreme outliers
1	5397	0	31.10	2.28	2.83	8.06	1.24	116	1656	0	19.90	0.97	1.18	1.38	1.21	10
2	5354	0	24.67	2.50	2.63	6.93	1.05	121	2027	0	18.10	1.34	1.47	2.15	1.09	19
Domain	Cu % 3 m composites								Mg % 3 m composites							
	No	Min	Max	Mean	SD	Variance	COV	No. of extreme outliers	No	Min	Max	Mean	SD	Variance	COV	No. of extreme outliers
1	5397	0	30.41	0.20	0.58	0.33	2.86	356	1388	0	8.78	1.89	1.84	3.40	0.97	0
2	5354	0	9.69	0.19	0.29	0.08	1.50	216	1645	0	30.65	3.31	3.05	9.3	0.92	4
Domain	Fe % 3 m composites								Rd 3 m composites							
	No	Min	Max	Mean	SD	Variance	COV	No. of extreme outliers	No	Min	Max	Mean	SD	Variance	COV	No. of extreme outliers
1	5397	0	23.19	3.83	2.77	7.69	0.71	20	1418	2.44	5.11	3.41	0.35	0.12	0.10	1
2	5354	0	22.86	3.45	2.42	5.84	0.70	45	1921	2.23	4.48	3.22	0.35	0.12	0.11	0

**Table 12 Comparison of Skewness and Kurtosis of Assay, 1.5 m composites and 3 m composites**

Domain	Zn assay		Zn 1.5 m composites		Zn 3 m composites	
	Skewness	Kurtosis	Skewness	Kurtosis	Skewness	Kurtosis
1	1.275	2.140	1.286	2.190	1.261	2.202
2	2.035	5.299	2.062	5.470	2.023	5.411
Domain	Pb assay		Pb 1.5 m composites		Pb 3 m composites	
	Skewness	Kurtosis	Skewness	Kurtosis	Skewness	Kurtosis
1	2.819	13.933	2.549	9.185	2.468	8.645
2	2.782	11.196	2.704	10.526	2.544	9.314
Domain	Cu assay		Cu 1.5 m composites		Cu 3 m composites	
	Skewness	Kurtosis	Skewness	Kurtosis	Skewness	Kurtosis
1	54.739	4205	31.093	1585	30.094	1432
2	23.134	1049	22.731	1012	11.577	279
Domain	Fe assay		Fe 1.5 m composites		Fe 3 m composites	
	Skewness	Kurtosis	Skewness	Kurtosis	Skewness	Kurtosis
1	1.931	8.120	1.870	7.522	1.585	3.751
2	2.593	16.164	2.613	16.741	1.925	5.872
Domain	Ag assay		Ag 1.5 m composites		Ag 3 m composites	
	Skewness	Kurtosis	Skewness	Kurtosis	Skewness	Kurtosis
1	6.6	71.2	6.5	65.1	5.9	60.1
2	6.3	85.4	6.2	83.8	5.7	91.4
Domain	Mn assay		Mn 1.5 m composites		Mn 3 m composites	
	Skewness	Kurtosis	Skewness	Kurtosis	Skewness	Kurtosis
1	4.778	50.354	4.775	49.918	5.086	57.913
2	3.275	21.927	3.293	22.135	3.276	21.565
Domain	Mg assay		Mg 1.5 m composites		Mg 3 m composites	
	Skewness	Kurtosis	Skewness	Kurtosis	Skewness	Kurtosis
1	1.127	0.526	1.125	0.525	1.168	0.676
2	1.968	10.647	1.977	10.888	1.938	9.638
Domain	Rd assay		Rd 1.5 m composites		Rd 3 m composites	
	Skewness	Kurtosis	Skewness	Kurtosis	Skewness	Kurtosis
1	0.289	0.161	0.283	0.145	0.235	0.217
2	0.372	0.082	0.334	0.087	0.375	-0.260

## 6.6 Assessing normality using probability plots

### 6.6.1 Z-Score

Z-scores measure the distance of a data point from the mean in terms of the standard deviation. This is also called standardization of data. The standardized data set has mean 0 and standard deviation 1 and retains the shape properties of the original data set (same skewness and kurtosis). Z-scores can be used to put data on the same scale before further analysis. This allows comparison of two or more data sets with different units.

For a random variable  $X$  with mean  $\mu$  and standard deviation  $\sigma$ , the Z-score of a value  $x$  is

$$z = \frac{(x - \mu)}{\sigma}.$$

(Dohm, 2010)

For sample data with mean  $\bar{X}$  and standard deviation  $S$ , the Z-score of a data point  $x$  is:

$$z = \frac{(x - \bar{X})}{S}.$$

(Dohm, 2010)

The Z-scores were calculated for Zn, Pb and Ag and plotted on a normal probability plot to assess normality of the payable metals.

### 6.6.2 Normal probability plots

Normal probability plots were used to assess graphically whether sample data have a normal distribution and the type of departure from normality. A normal probability plot shows the empirical cumulative distribution of the sample data versus the theoretical cumulative distribution function of a normal distribution.

The horizontal axis plots the sorted sample data. The vertical axis plots the normal order statistic medians, calculated using the uniform order statistic medians and the inverse cumulative distribution function (ICDF) of the normal distribution. If the sample data have a normal distribution, then the plot is linear. Distributions other than normal introduce curvature in the plot. Appendix R and S present the normal probability plots for Zn, Pb and Ag. All three elements display positively skewed distributions.

### 6.7 Population mean of the LN (2), $N > 40$ for Zn, Pb and Ag

In Section 5.4–5.6 the author established that all elements except RD have a positively skewed distribution. The few high values increase the arithmetic mean substantially, thus rendering it to be deceptive as an estimator. To deal with this, the grade values are transformed to the natural log (ln) values. The log-transformed distributions are more symmetrical and the estimates of parameters are less sensitive to outliers.

The arithmetic average was tested to determine if it is acceptable as an estimator. The average is acceptable if the difference between the average of the data and the expected value of the probability density model of the data is negligible. The 2-parameter log-normal LN (2) probability density distribution model was applied. The sample mean, variance and population mean are estimated using the formulas below as summarised in Dohm (2010). Table 13 summarizes the results.

Average of the ln values:

$$\xi = \bar{y} = \frac{1}{n} \sum y_i = \frac{1}{n} \sum \ln(z_i) \quad (6.1)$$

Variance of the ln values:

$$\sigma_L^2 = \frac{1}{n-1} \left[ \sum y_i^2 - \frac{(\sum y_i)^2}{n} \right] \quad (6.2)$$

Population mean:

$$\mu^* = \tau = e^{\xi + \frac{1}{2}\sigma_L^2} = e^{\xi} \times e^{\frac{1}{2}\sigma_L^2} \quad (6.3)$$

**Table 13 Estimating the parameters of the LN (2),  $N > 40$**

	Zn	Pb	Ag
Average of the ln values	2.21	0.24	3.78
Variance of the ln values	0.73	1.79	0.99
population mean	13.15	3.11	71.99
sample mean	12.10	2.46	64.93
% difference	7.98	20.98	9.81

The percentage difference between the average of the data and the expected value of the probability density model of the data is significant, thus the sample mean is a bias estimator for Zn, Pb and Ag.

## 6.8 Principal Component Analysis

Sometimes data containing multiple variables are collected from a single population. The dispersion matrix may be too large to study and difficult to interpret with multiple variables. It is therefore necessary to reduce the number of variables to a few, interpretable linear combinations of the data. Each linear combination will correspond to a principal component. PCA involves a mathematical procedure that transforms a number of (possibly) correlated variables into a number of uncorrelated variables called principal components.



The first principal component accounts for as much of the variability in the data as possible, and each succeeding component accounts for as much of the remaining variability as possible.

Matlab software was used to calculate the principal component value for the EOF data. Table 14 presents the PCA scores for the data. Interpretation of the principal components is based on finding which variables are most strongly correlated with each component. The larger in magnitude the number, the stronger the correlation, the further from zero in either positive or negative direction. A correlation value above 0.05 is deemed important. These larger correlations are presented in boldface in Table 14 below.

**Table 14 Principal component analysis results**

Variable	Principal Component							
	1	2	3	4	5	6	7	8
ZN	<b>0.06</b>	<b>0.98</b>	-0.04	-0.11	-0.12	-0.01	-0.01	-0.02
PB	<b>0.02</b>	<b>0.09</b>	<b>0.07</b>	-0.26	<b>0.96</b>	0.00	0.03	-0.02
AG	<b>1.00</b>	<b>-0.06</b>	-0.01	0.00	-0.02	0.00	0.00	0.00
CU	0.00	0.01	-0.01	0.01	-0.02	-0.03	<b>1.00</b>	0.06
FE	0.01	<b>0.13</b>	0.02	<b>0.96</b>	<b>0.24</b>	-0.10	-0.01	-0.02
MN	0.00	0.03	<b>0.36</b>	<b>0.09</b>	-0.01	<b>0.92</b>	0.04	-0.05
MG	0.00	0.02	<b>0.93</b>	-0.04	-0.08	-0.36	-0.01	-0.01
RD	0.00	0.02	0.03	0.02	0.02	0.04	-0.06	<b>1.00</b>
	1.10	1.22	1.36	0.67	0.97	0.46	0.98	0.94

The first principal component increases with increasing Ag, Zn and Pb. It is primarily a measure of the payable metals or the ore; based on the correlation of 1.00 the higher-grade ore has higher Ag contents at EOF. The second principal component increases with Zn, Fe, and Pb and decreases with Ag. Based on a correlation of 0.98, the second principal is primarily a measure of Zn in the ore. The third principal component increases with Mg and Mn. This suggests that an area with higher-grade ore has high Mg and Mn contents.

## 6.9 Outlier detection using Quantile Regression

“An outlier is an extremely high or extremely low value of a variable which lies outside the range of values expected based on the distribution of the rest of the data”, Snowden (2009). The removal of grades is not recommended unless the outlier is thought to be an error or geologically unrepresentative of the mineralisation. Top cuts are applied to prevent overestimation in small sub-sample sets due to disproportionate high-grade outliers. Snowden further states that top cuts should be considered for positively skewed distributions with COV greater than one.

Histogram and probability plots were used to determine the top cut, the point where the distribution decays or disintegrates. The top cuts are highlighted with a red line in Appendices O to Q; Table 15 summarizes the results. These top cuts were compared to top cuts obtained using the quantile regression methods. The quantile regression method is defined by any observation that is greater than  $F_2$ , where  $F_2$  is defined as

$$F_2 = Q_3 + 1.5IQR \quad (6.4)$$

*IQR* is the inter-quartile range and  $Q_3$  is the third quartile.

**Table 15 Top cut grades used for Domain 1 and Domain 2**

Element	DOM 1	DOM 2	$F_2$
Zn (%)	41.0	43.0	29.9
Pb (%)	12.5	12.4	7.1
Cu (%)	1.5	0.97	0.44
Fe (%)	13.0	12.5	9.88
Ag (ppm)	370.0	262.0	165.0
Mn (%)	3.4	3.8	4.4
Mg (%)	7.0	9.7	9.6
Rd	4.2	4.2	4.3

The outliers calculated using the quantile regression methods are generally lower than the ones obtained from histogram and probability plots. Hence, it is recommended that the outliers used for estimation are obtained from the quantile regression method because they are more conservative. A Majority of the outliers at EF1 are vein mineralisation, massive sulphide ore and high-grade intervals hosted in carbonates, thus they were not excluded from the dataset.

### **6.10 Summary**

The mean of the 3 m composites is generally less than the mean of assay data and the 1.5 m composites. The standard deviation, variances and numbers of extreme outliers are lower for the 3 m composites compared to the assay data and the 1.5 m composites.

Pb, Cu, Ag and Mn have a COV above 1.0; these elements' distributions are unlikely to be normal distributions. Zn, Fe, Mg and RD have a COV of less than 1.0. The RD is the only element with a symmetrical distribution; it has a skewness value of less than 1. All the other elements have a positively skewed distribution, with Cu, Ag and Mn being significantly skewed.

Generally, increasing the composite size reduces the skewness of the data. Skewness was managed by the use of top cuts. EOF Mg distribution has two populations; ideally, it should be estimated with two domains, Domain 1 ranging from 0–4% and Domain 2 in the range of 4–12%.

All elements, except RD, have a peaked distribution, with Cu, Ag and Mn having the most peaked distributions. Generally, increasing the composite size reduces the peakedness of the distribution. The 2-parameter log-normal LN (2) model indicates that the percentage difference between the average of the data and the expected value of the probability density model is significant, thus the sample mean is a biased estimator for Zn, Pb and Ag.

The first principal component increases with increasing Ag, Zn and Pb; it is strongly correlated with these three elements. Based on the correlation of 1.00 the first principal component is primarily a measure of Ag. Based on the correlation of 0.98, the second principal is primarily a measure of Zn in the ore. The third principal component increases with Mg and Mn. An area with higher-grade ore has high Mg and Mn contents.

The high values that look like outliers at EOF are sampled mainly from vein type mineralisation, massive sulphide ore and high-grade intervals hosted mainly in carbonates. It is recommended that the outliers be detected using the quantile regression method because it is more conservative.

## **CHAPTER 7: GEOSTATISTICAL ESTIMATION PARAMETERS**

### **7.1 Introduction**

In the previous chapter, the underlying distribution of the samples was described and the top-cuts for the elements were determined and investigated. This is important because the grade interpolation method to be used is selected based on the underlying sample distribution. The decision on how to deal with outliers during the grade interpolation process is based on the outcome of the investigation of the outliers.

This chapter explains why the Ordinary Kriging (OK) interpolation method was selected; it further explains the preparatory work or estimation parameters required for kriging interpolation. The process involves creating estimation domains, plotting contours to determine rotation or the new north, dip and plunge of the data and modelling variograms in the major, intermediate and minor directions in order to determine the ranges in the respective directions. The spherical model is also defined in this chapter and the chapter concludes by giving a summary of the kriging estimation parameters used to estimate EOF and comparing the range of influence for Domain 1 compared to Domain 2.

### **7.2 Interpolation method**

The OK interpolation method was selected for estimating the block grades. The final block estimate determines if material is ore OR waste. The OK interpolation method is selected for estimation because it relaxes the assumption of global stationarity, implying that the mean is estimated using the local search data. Zn, Pb and Ag have positively skewed distributions, as stated in Chapter 6. Therefore, an interpolation method that uses the local search data is ideal.

### **7.3 Dealing with outliers**

The outlier cut-offs determined in Section 6.9 are used to restrict the spatial influence of high-grade composites during estimation. The high values at EF1 are due to vein mineralisation, massive sulphide ore and high-grade intervals hosted mainly in carbonates. Thus the actual values of composites above the outlier cut-off grade were not capped to the cut-off grades but were accepted and their spatial influence was restricted. The interpolation from these composites is only restricted to the variogram range. The outliers are not used in the block estimate if they are at a distance that exceeds the variogram range from the block to be estimated. For example, if the range of Zn is 50 m, then outliers that are 50 m or more away from the block to be estimated are not included in estimating the grade of the block, although they fall within the search radius. Restricting the spatial influence of composites with assays above the outlier cut-off prevents the estimation algorithm from smearing high outlier grades into lower-grade areas that are further away but allows the high grade to locally influence the block estimate.

With this option, the influence is specified by the design of a search ellipsoid with dimensions smaller than that applied for grade estimation. It is based on the size of the high-grade search ellipsoid which should not extend beyond the high-grade continuity, in this case, the variogram range.

### **7.4 Domaining**

Boyle (2010) and Deutsch et al. (2014) emphasized that subdividing the data into stationary domains is more important than increasing the number of data in the search radius. The EOF data was divided into two domains based on the structural orientation of the two limbs. Domain 1 dominantly consists of EF2 limb data with

a NE–SW strike whilst Domain 2 consists of the EF1 limb data with a NW–SE strike as shown in Figure 29.

The blocks, ore solid and composites were coded accordingly, such that blocks were only estimated from domains with a similar code. During the 2015 estimation, the domains were swapped; in a previous estimation the domains were coded the other way around. The estimation results were not affected because the composites and blocks were coded accordingly, such that Domain 1 composites were used for estimating blocks coded with a similar code.

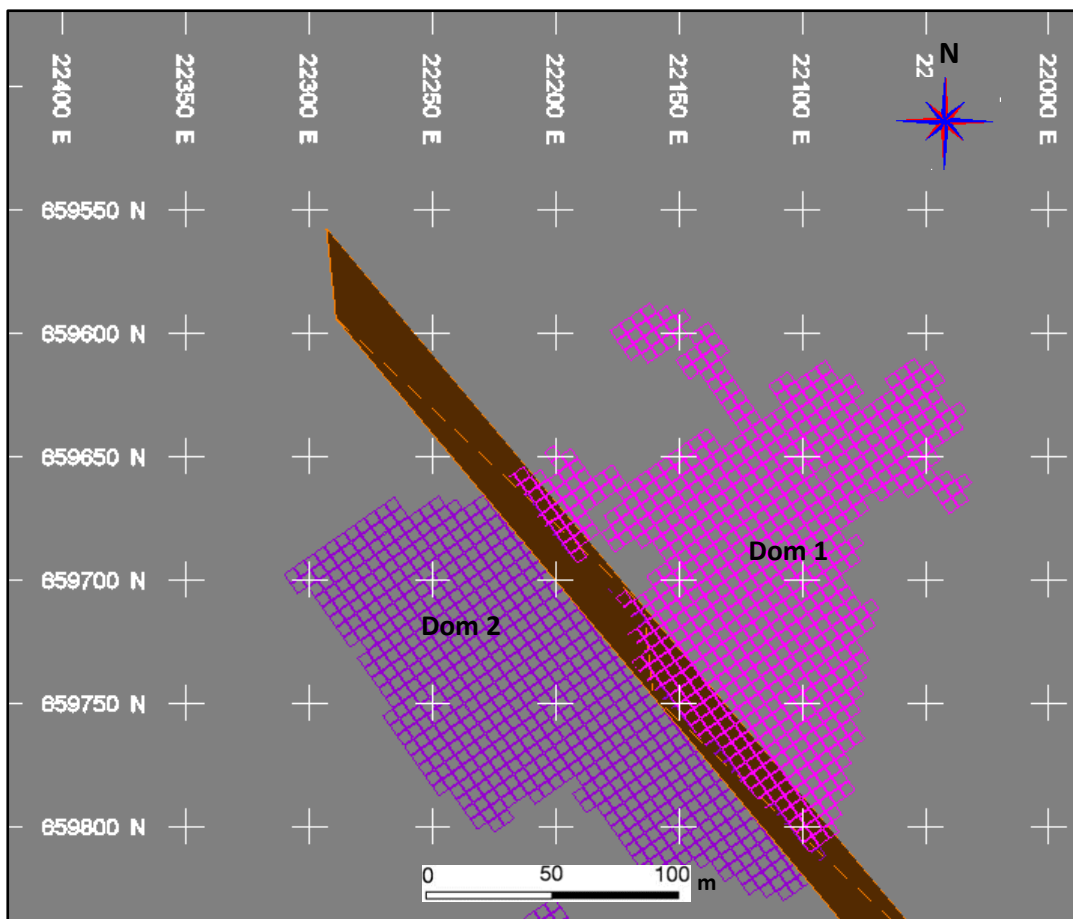


**Figure 29 Plan view of Domain 1 and Domain 2**

## 7.5 Contour plots

In order to use variograms for estimation, they need to be modelled in the three orthogonal directions to define a three-dimensional ellipsoid. If there is no anisotropy and the ranges of continuity are the same in all directions, then an omni-directional variogram can be calculated and the ranges in all three directions will be the same (isotropic). If there is anisotropy in the domain, then directional variograms need to be calculated in the directions of greatest continuity, the intermediate and minor directions.

All elements displayed anisotropy in their respective domains. Figure 30 shows the Domain 1 contour plots for Zn. The Zn rotation in the northern direction is  $47.5^\circ$  (ROTN/New North); the plunge in the northern direction (DIPN) is  $0^\circ$  whilst the dip in the eastern direction (DIPE) is  $-69^\circ$ .

Figure 31 shows the Domain 1 contour plots for Pb. The Pb rotation in the northern direction is  $46^\circ$  (ROTN/New North); the plunge in the northern direction (DIPN) is  $17^\circ$  whilst the dip in the eastern direction (DIPE) is  $-56^\circ$ .

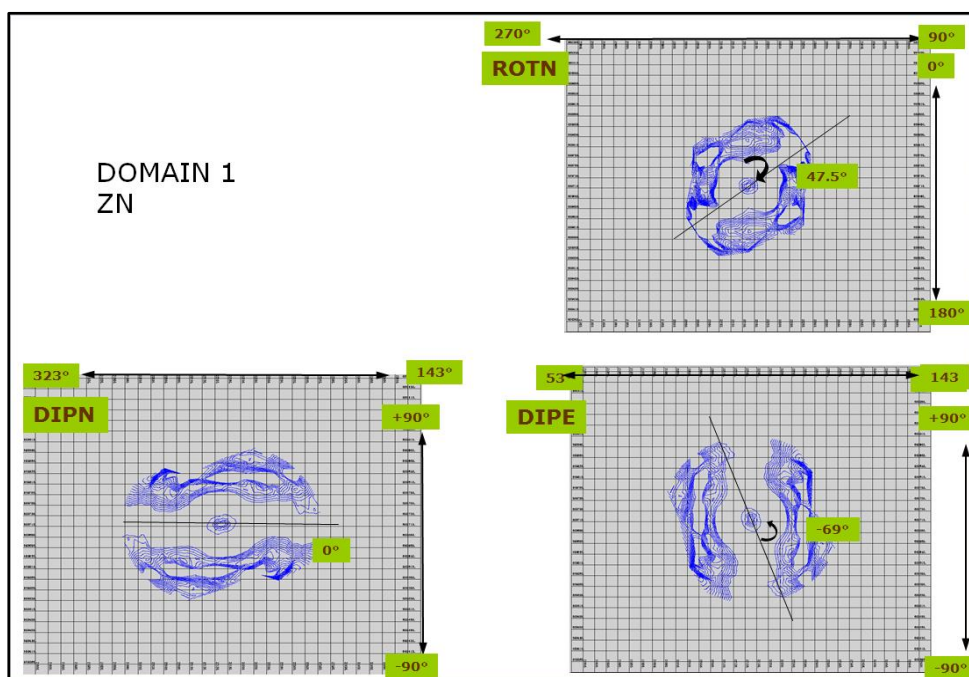
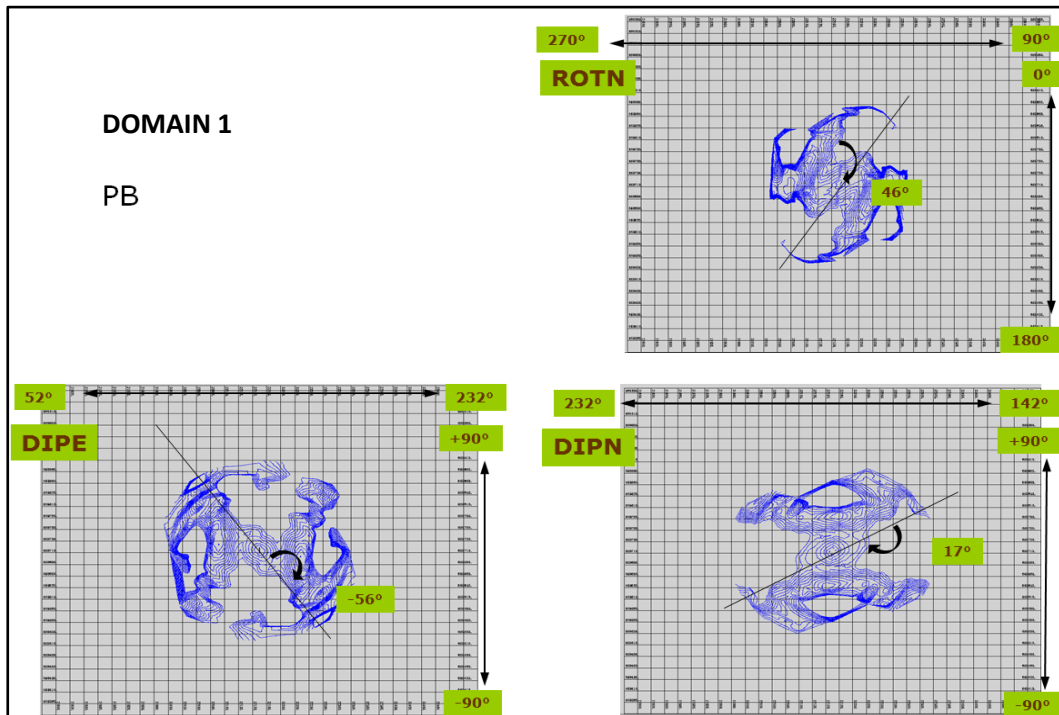


Figure 30 Domain 1 rotation or New North, plunge and dip for Zn





**Figure 31 Domain 1 rotation or New North, plunge and dip for Pb**

As stated earlier, all elements displayed anisotropy, for Domain 1, Pb and Zn show anisotropy in the same direction (about  $47^\circ$ ), with a non-plunging major axis and an average easterly dip of  $-70^\circ$ . Mn, Mg and Cu have similar anisotropy along the direction of the major axis of about  $155^\circ$  but different plunges and dip in the eastern direction. Mn and Mg have a similar dip in the eastern direction of about  $79^\circ$ . Fe and Ag have similar direction of the major axis (about  $155^\circ$ ) and a plunge of  $-23^\circ$  but a different easterly dip. Fe has an easterly dip of  $75.5^\circ$  versus  $-88.5^\circ$  for Ag.

For Domain 2, all elements have a similar direction of the major axis, ranging between  $118^\circ$  to  $167^\circ$ . The plunges are mainly shallow to moderately plunging, mainly around  $35^\circ$ , except for Zn and Ag with a  $-20^\circ$  plunge. The dip in the eastern direction is steeply dipping with  $-55^\circ$ .

The directions of the major axis reflect the directions of the limbs of the EOF anticline. As stated in Section 7.4, Domain 1 dominantly consists of EF2 limb data

with a NE–SW strike whilst Domain 2 consists of the EF1 limb data with a NW–SE strike. The EOF fold is a D2 fold with a steep southerly plunge ( $64^\circ$  towards  $052^\circ$ ); the plunges of the elements in the major axis do not conform to the D2 deformation. The elements have non-plunging to moderate plunges. This is possible because the EOF mineralisation is a reworked classic SEDEX deposit associated with remobilization and sulphides enrichment after the main deformation during the emplacement of the volcanics and mafics. The dip in the easterly direction is mostly steeply dipping ( $-55^\circ$ ), which is in line with the D2 fold axial planes, which are slightly westerly overturned.

## **7.6 Variograms**

The variogram is a tool used to study the spatial continuity; it describes how samples relate to each other in space. The variogram is computed using a discrete number of points. The EOF composites were used for variogram computation. It is assumed that there are  $n$  pairs of samples; each pair is separated by distance  $h$ . In addition, all these samples are assumed to lie on a straight line, along which the variogram computation is being performed.

The analyses of spatial continuity for the omni-directional variogram were first carried out to determine the nugget effect, and the sills. The omni-directional variograms contain more sample pairs than any directional variogram; therefore, they are more likely to show a clearly interpretable structure. Another reason is that they can serve as an early warning for erratic directional variograms.

All elements displayed well behaved omni-directional variograms, thus the various directional variograms were analysed to determine the ranges. The nugget effects and sills for the directional variograms were determined from omni-directional variograms.

Table 16 gives a summary of all the elements' rotations, plunges and directions for both domains as well as the different ranges, nugget effects and sills. The

nugget effect ( $C_0$ ) is the expected difference between samples when the separation distance is almost negligible (Snowden, 2009). The total sill ( $C_1$ ) represents the total variability inherent in the data and the range ( $a$ ) of continuity is the lag or separation distance at which the variability reaches the sill. Appendices U to X show the Zn omni-directional, major, intermediate and minor direction variogram for Domain 1. Variograms for Domain 2 generally have lower nugget effects, except for Zn, which implies that Domain 2 has lower variability compared to Domain 1. Generally, Domain 2 also has longer ranges compared to Domain 1, with the exception of Cu.

The spherical model was used and below are shown the spherical model equations (Isaaks and Srivastava, 1989):

$$\gamma(h) = C_0 + c [1.5 (h/a) - 0.5 (h^3/a^3)] \quad \text{if } h < a \quad (7.1)$$

$$\gamma(h) = C_0 + c \quad \text{if } h > a \quad (7.2)$$

In the equation “ $a$ ” refers to the range of the variogram and  $C_0 + c$  is the sill of the variogram. The spherical model rises rapidly at short lag distances near the origin, but flattens out at larger distances; it reaches the sill at  $a$ , the range of influence (Figure 32).

In mining, drilling occurs on an irregular grid. Therefore, when computing the variogram along a specified direction, one has to accept pairs that are close to the direction of the variogram although they are not laying exactly on the line of the direction. This tolerance is referred to as the vertical or horizontal window, depending on the direction. The tolerance is highlighted in red in Figure 33. Window angles (Figure 34) of  $45^\circ$  along the azimuth and  $60^\circ$  along the dip were used for the EOF estimation. It is important that the directional tolerance is large enough to allow sufficient pairs for a clear variogram, yet small enough that the character of the variograms for separate directions is not blurred.

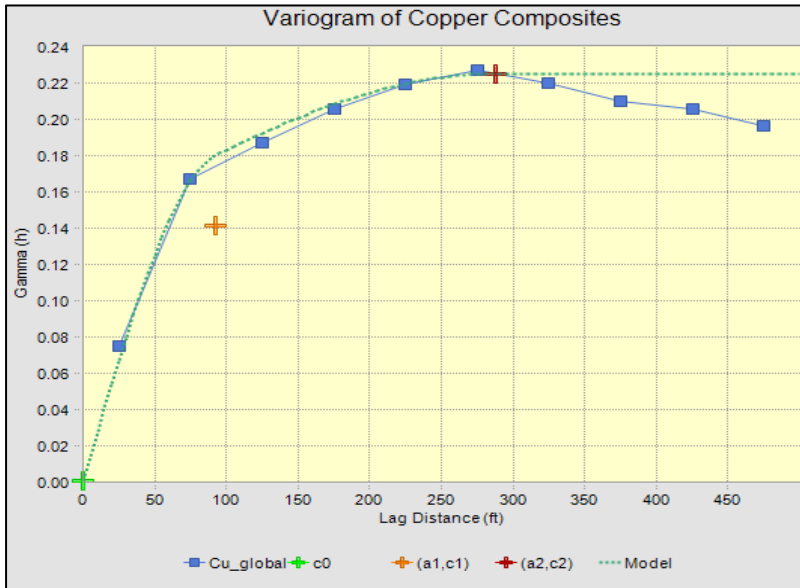


**Figure 32 Two structured spherical model (Anon., n.d.)**

In some situations, the pairs accepted within a tolerance window can be tested if they are within a specified distance from the line of direction of the variogram. This distance is referred to as the band width (Figure 33). Band widths of 30° were used in the horizontal and vertical directions.

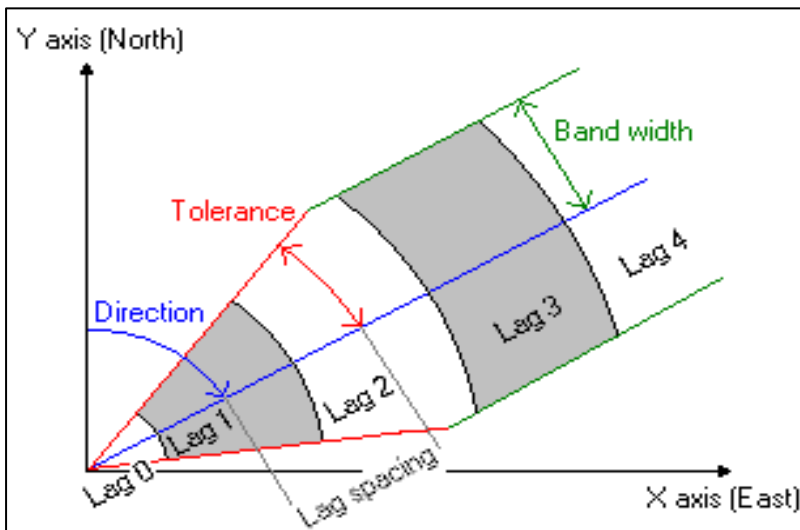


**Figure 33 Lag distance, lag tolerance and band width (Anon., n.d.)**

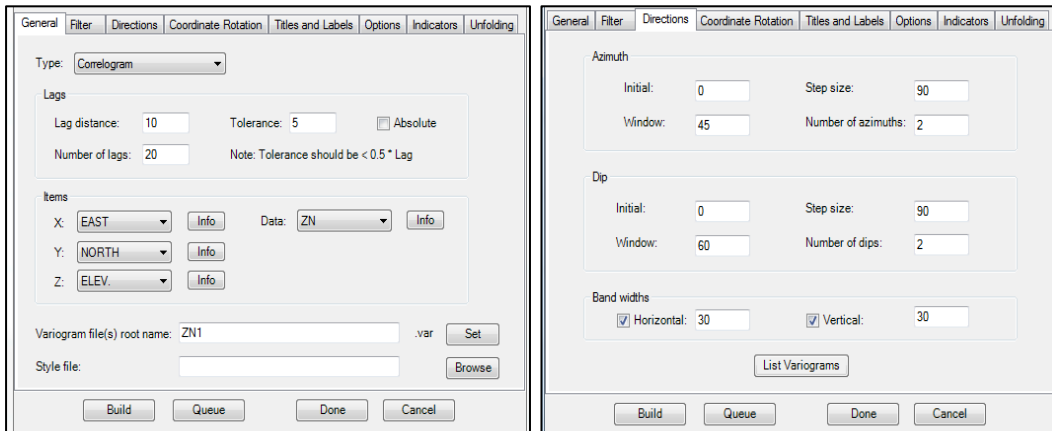


**Figure 34 Lag distance, directions, window angle, and band widths for the EOF estimation**

The lag distance is the separation distance for sample pair selection; normally, the lag distance is equal to the minimum drill spacing. Lags of less than the minimum drill spacing should not be used. A lag distance of 10 m and a lag tolerance of 5 m were used for the EOF grade estimation as shown in Figure 34. Smaller lag distances are recommended to help determine the nugget effect at short lag spacing. Thus, a down-the-hole variography or an omni-directional variogram with a lag distance equal to the dominant sample interval (1.5 m for the EOF estimate) should be used to define the nugget effect. For this estimate, the omni-directional variogram was used.

Samples are rarely spaced at exact distances apart. A tolerance is applied to the lag distance so that sample pairs will be selected if they lie within the lag distance +/- the tolerance. Generally, the lag tolerance is set at half the lag spacing so that samples are not missed.

## 7.7 Ellipsoid validation

Once the three search directions for the search ellipsoid were determined, the ellipsoid was validated by checking the three directions using Minesight modelling software. The Zn ore zone for Domain 1 was viewed at an azimuth of  $47.5^\circ$  and a dip of  $0^\circ$  to see if the directions conform to the solid. This validation was done for both domains and all elements.

Figure 35 displays the Zn search ellipsoids for both domains at EOF. The Zn ellipsoid for Domain 2 is bigger than for Domain 1, which is related to the longer variogram ranges associated with Domain 2. The ellipsoidal search parameters are further discussed in Section 8.2.1.

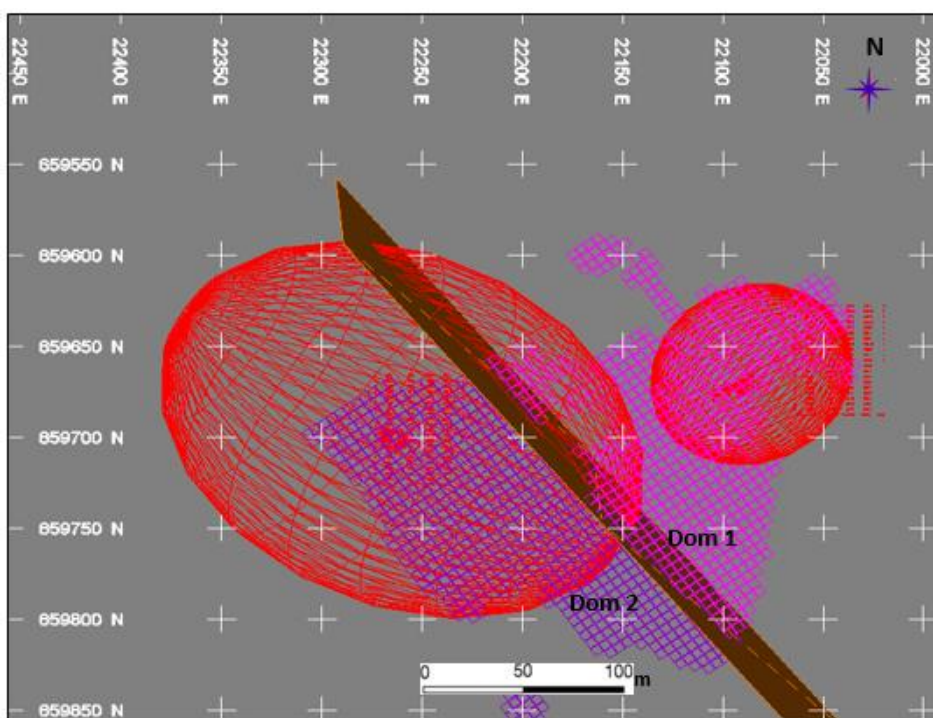


Figure 35 Zn search ellipsoid for Domains 1 and 2

## 7.8 Interpreting variograms

The nugget effect defines the variability at very short distances, so it is ideal if the nugget is interpreted using the closest spaced data available. The closest spaced

data are typically in the downhole direction where samples are adjacent. For EOF the closest spaced sample is equivalent to the composite length of 1.5 m and hence a very small lag can be used to give an indication of the behaviour of the variability at short distances.

Table 16 indicates that most elements at EOF have an average nugget effect of 0.45, as calculated from the omni-directional variogram. This shows that the elements have higher variability even at closer separation distances. Alternatively, the omni-directional variograms used to determine the nugget effect may not provide the best information for interpretation due to the sample spacing. Thus it is recommended that the nugget effects be determined using the downhole variograms.

All elements estimated at EOF displayed geometric anisotropy, implying that each direction has different ranges of continuity, but they typically level out at the same total sill in all directions. For all elements the spherical model best fits the data. Domain 2 generally has lower nuggets, except for Zn, which implies that Domain 2 has a lower variability compared to Domain 1. Generally, Domain 2 also has longer ranges compared to Domain 1, with the exception of Cu. Most elements have ranges along the major axis above 70 m, given that the inferred drilling is done at 60 m; this implies that geostatistics can be used to estimate block grade with confidence even for the inferred drilling.

**Table 16 Summary of rotations, plunge and directions for both Domain 1 and 2 as well as the different ranges, nugget effects and sills**

Directions	Zn		Pb		Cu		FE		Ag		Mn		Mg		RD	
	Dom 1	Dom 2	Dom 1	Dom 2	Dom 1	Dom 2	Dom 1	Dom 2	Dom 1	Dom 2	Dom 1	Dom 2	Dom 1	Dom 2	Dom 1	Dom 2
Direction Major axis	47.5	121	46	151	151.5	160	9	118	15	139	159	117	167	111	179.5	110
Plunge Major axis	0	-17	17	1	8	32	-21	38	-24	-41.5	60	36	-19.5	35	1	43
Dip easterly	-69	-50	-56	-72	-53	54	75.5	-64.5	-88.5	-20	78.5	-51	80	-55	-64	-63
Nugget Effect	0.45	0.49	0.5	0.20	0.77	0.66	0.46	0.13	0.65	0.26	0.51	0.36	0.45	0.37	0.57	0.35
C1	0.38	0.39	0.20	0.64	0.10	0.23	0.32	0.34	0.30	0.56	0.31	0.2	0.28	0.07	0.27	0.34
a1 - Range along major axis	11	14.5	9.3	10.5	26.2	8.8	12.5	9.3	14.6	11	28	70	10.3	45	21.2	62.5
a1 - Range along minor axis (Interm)	11.6	24	9	11	40.4	10.5	15	9	29	10	10.5	28	4.5	50	29.4	48.3
a1 - Range along minor axis	9.8	24	9	10	30.4	9.9	15.2	11	27	11.5	14	55	10.7	38	31	54
C2	0.17	0.12	0.30	0.06	0.15	0.1	0.22	0.44	0.05	0.18	0.18	0.31	0.27	0.4	0.17	0.1
a2 - Range along major axis	60	98	70	129	71.6	58.9	100	145	60	64.8	90	93	78	72	75.7	117.5
a2 - Range along minor axis (Interm)	60	95	62	120	57.9	57	100	115	60	52	60	72	32	68	56.2	56.9
a2 - Range along minor axis	47	95	50	92	45.7	37.8	55	90	40	51.5	37.5	68	20.1	42	48.1	54



## **CHAPTER 8: GEOSTATISTICAL ESTIMATION**

The focus of the first six chapters has been purely descriptive, with the main focus on describing the sample data; this chapter deals with the geostatistical estimation of block grades. It uses the sample information to predict values in areas that are not sampled. The aim of this chapter is to determine the EF1 in-situ resources estimated from 1.5 m composites and 3 m composites into the blockmodel as on 31 December 2016. The chapter summarizes and compares the estimation statistics of the model derived from 1.5 m composites to the model derived from 3 m composites.

Firstly, this chapter defines the block sizes used, and compares the model statistics. Thereafter, the resource classification is presented followed by the resource estimation and grade distribution summary. The chapter further presents the grade tonnage curves, model validation and Quantified Kriging Neighbourhood Analysis (QKNA). The chapter concludes with a summary.

### **8.1 Block size and statistical grade estimation**

A standard block size of 5 x 5 x 5 m was used based on half the minimum drill spacing. Grades were estimated into the blocks from 1.5 m composites and compared to grades obtained from blocks estimated from 3 m composites. Figure 36 shows the blocks and the Zn values estimated from the 1.5 m composite (top) and 3 m composites (bottom) on section -1020 between level -020 and -030, plotted with the borehole assays. This gives a quick validation of the block estimates versus the borehole assays.

Tables 18 and 19 summarize Domain 1 and Domain 2 model statistics estimated from the 1.5 m and 3 m composites. The model estimates obtained from 3 m composites have lower means, standard deviations and variances for all

elements. This finding is also supported by the Zn and Pb histograms shown in Figure 39, which shows that for Domain 1 the estimates from the 1.5 m composites have a higher spread and longer tails to the right compared to the estimates calculated from the 3 m composites. Generally, Domain 2 has lower means compared to Domain 1 for all elements.

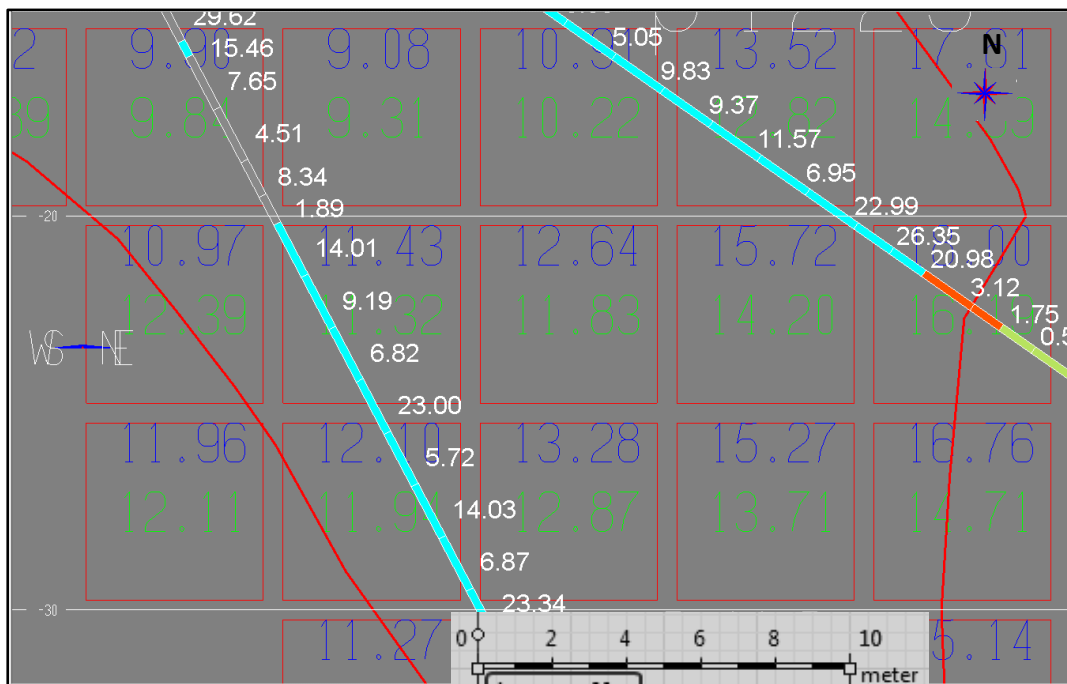


**Figure 36 A vertical section (-1020) displaying the model estimates assays (blue – model estimates from 1.5 m composites; green–model estimates from 3 m composites) and borehole assays (shown in white)**

## 8.2 EOF resource classification

By December 2016, Mineral Resources above the -030 level were mined out, thus only resources below the -030 level was reported as in-situ resources. The resources are calculated in MineSight using a density of 3.46 to calculate the in-situ resource tonnes. Mineral Resources were classified based on the drill spacing and confidence of the available information. Areas drilled out on a 30 x 30 m drill spacing are classified as 'Indicated' and those drilled out on a 10 x 10 m spacing as 'Measured'. Based on this, the -030 to the -060 levels are classified as Measured

Resource whilst all Resources below the -060 level are Indicated Resources. The classification was verified using the PRED system, which is discussed in the subsection below, as well as the QKNA presented in Section 8.5.

### 8.2.1 The PRED system

The structural complexity and varying grades of the Rosh Pinah Mine ore bodies required the development of a method of estimating the reliability of grade predictions from the block model (Crowther, 2014). Grade predictions in a block model are dependent on the following three geostatistical parameters:

- The number of samples within close proximity of the estimated block.
- The distance of the samples to the estimated block.
- The variance between the samples close to the estimated block.

The PRED system was developed to give an objective view of the resource classification and is based on a second '3 pass' grade estimation for Zn and Pb, using a different set of estimation parameters. The inputs to the estimation parameters are identical to the estimation parameters, with a modification to the ranges. The three passes are defined below.

**The 1st pass** attempts to fill the *RZN* and *RPB* values of the blocks at 0.667 times the semi-variogram ranges, with a minimum of 6 samples and a maximum of 20 samples, and flagging the *resource classification indicator (PREDZ and PREDP)* with the value 1.

**The 2nd pass** attempts to fill the *RZN* and *RPB* values of the blocks at 1 times the semi-variogram ranges, with a minimum of 6 samples and a maximum of 25 samples, and flagging the *resource classification indicator (PREDZ and PREDP)* with the value 2.

The **3rd pass** attempts to fill the *RZN* and *RPB* values of the blocks at 3 times the semi-variogram ranges, with a minimum of 6 samples and a maximum of 30 samples, and flagging the *resource classification indicator* (*PREDZ* and *PREDP*) with the value 3.

It should be noted that this method assumes that:

- An estimation based on 2/3 of the semi-variogram range would classify a resource in the measured category.
- An estimation based on 1 times the semi-variogram range would classify a resource in the indicated category.
- An estimation based on 3 times semi-variogram range would classify a resource in the inferred category.

The ellipsoidal search parameters for the resources classification of the main elements for both domains are presented in Figure 37.

DOMAIN 1					DOMAIN 2						
<b>ZN</b>	SEARCH STAGE				<b>ZN</b>	SEARCH STAGE					
	ELLIPS	1	2	3		ELLIPS	1	2	3		
	1	98.0	65	98		490	1	60.0	40	60	300
	2	95.0	63	95		285	2	60.0	40	60	180
	3	95.0	63	95		285	3	47.0	31	47	141
MIN SAMPLES		6	6	6	MIN SAMPLES		6	6	6		
MAX SAMPLES		20	25	30	MAX SAMPLES		20	25	30		
<b>PB</b>	SEARCH STAGE				<b>PB</b>	SEARCH STAGE					
	ELLIPS	1	2	3		ELLIPS	1	2	3		
	1	129.00	86	129		387	1	70.0	47	70	210
	2	120.00	80	120		360	2	62.0	41	62	186
	3	92.00	61	92		276	3	50.0	33	50	150
MIN SAMPLES		6	6	6	MIN SAMPLES		6	6	6		
MAX SAMPLES		20	25	30	MAX SAMPLES		20	25	30		

**Figure 37 Ellipsoidal search parameters for resource classification of Zn and Pb for Domains 1 and 2**

The *PREDZ* and *PREDP* are then combined using equation 8.1 to define the *PRED* value in the block model:

$$PRED = (PREDZ)^3 + (PREDP)^2 \quad (8.1)$$

The PRED values can then be used to indicate the reliability of the estimation for one block relative to another based on the number of samples and the distance of samples from the estimated block. The PRED values will give a preliminary indication of which resource category a block should be classified into and they are reported from the block model as a weighted average of all the blocks on a particular bench.

Thus, the weighted average of the PRED values for a bench must indicate that the complete bench is of a certain classification. Table 17 shows the boundaries of the PRED values for division into resource classes.

**Table 17 Classification criteria according to the PRED system**

	Measured Resource	Indicated Resource	Inferred Resource
Minimum PRED value	1	7	22
Maximum PRED value	7	22	36

### 8.2.2 Results PRED system

The PRED value for all blocks estimated is 2, except for two blocks, which were not populated. The unpopulated blocks were set to 3, as shown in Figure 38B. Most blocks were populated during the first pass for the main elements (Figure 38A), with the exception of two unpopulated blocks. The unpopulated blocks contain less than 2% ore and 98% waste.

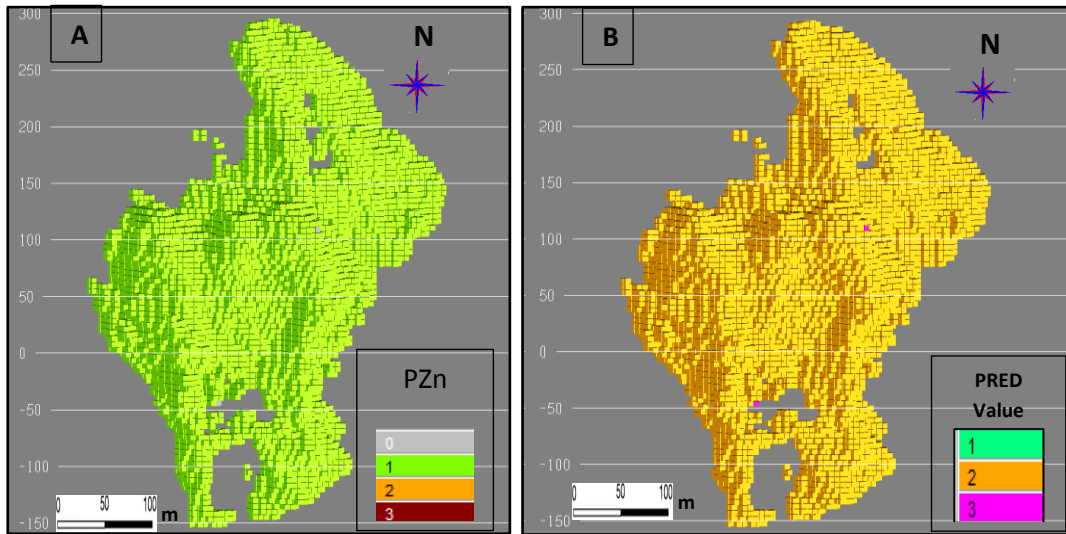


**Figure 38 A. Number pass for blocks to be populated with Zn values (PZn). B. PRED value for resource classification**

Given that the EOF has been drilled out on a 30 x 30 m spacing and the long variogram ranges are more than 60 m, most blocks were populated during the first pass. This implies that, based on the PRED classification system summarised in Table 17, all blocks can be classified as Measured Resources. However, the orebody geometry is very complex and the EOF ore outline swells and pinches over shorter distances. Thus, only levels drilled out on a 10 x 10 m spacing may be classified as measured. Therefore, although all blocks have a PRED value of 2, they may not all be classified as Measured Resources because of the complex nature of the mineralisation.

### **8.2.3 Results of Mineral Resource estimation**

Based on the 1.5 m composites, the global EF1 resource as on 31 December 2016 is estimated to contain 5.51 MT at 12.42% Zn, 2.63% Pb, 3.56% Fe, 0.22% Cu and 68.4ppm Ag. Based on the 3 m composites, the global EF1 resource as on 31 December 2016 is estimated to contain 5.52 MT at 12.18% Zn, 2.56% Pb, 3.54% Fe, 0.21% Cu and 66.9ppm Ag. At the time of writing a total of 4.7 MT has been

mined out. The global grade averages estimated from the 3 m composites are marginally lower than the ones calculated from 1.5 m composites for all elements, mainly due to the volume variance effect; the greater the volume, the greater the dilution of grades and the lower the variance.

A summary of the EF1 in-situ Measured Resources calculated from the 1.5 m composites is given in Table 21. The EF1 in-situ Measured Resources calculated from the 1.5 m composites is 156,200 tonnes at 9.7% Zn, 2.4% Pb and 68.4 ppm Ag versus 155,300 tonnes at 9.2% Zn and 2.3% Pb calculated from the 3 m composites (Table 23). The tonnage difference between the two estimates is insignificant (0.6%) and the global means of the measured resources models obtained from 3 m composites are also lower than those calculated from the 1.5 m composites. The EF1 Indicated Resource obtained from the 1.5 m composites has 666,900 tonnes (Table 22) at 8.71% Zn, 3.58% Pb and 87.39 ppm versus 658,800 tonnes (Table 24) at 8.44% Zn, 3.40% Pb and 82.08 ppm Ag calculated from the 3 m composites. The tonnage difference (0.01%) between the two models is insignificant. The Indicated Resources estimates obtained from the 3 m composites are also conservative compared to those estimated from 1.5 m composites.

The total in-situ tonnes estimated from the 3 m composites as on 31 December 2017 is presented in Table 18. The total EF1 in-situ resources are estimated 814,100 tonnes at 8.58% Zn, 3.19% Pb and 79.22 ppm Ag is.

**Table 18 EF1 insitu Mineral Resource estimate as at December 31, 2016**

BENCH	IN-SITU	ROM Grades						
		ZN1	PB1	FE1	CU1	AG1	MN1	MG1
TOE	ORE (TONNES)	%	%	%	%	(ppm)	%	%
Total								
Measured	155,300	9.2	2.3	2	0.2	67.1	1	3.4
Total								
Indicated	658,800	8.44	3.4	1.88	0.19	82.08	0.76	3.04
Total								
Resources	814,100	8.58	3.19	1.90	0.19	79.22	0.81	3.11

Mineral Resources are estimated at a cut-off grade of 4% Zn equivalent.

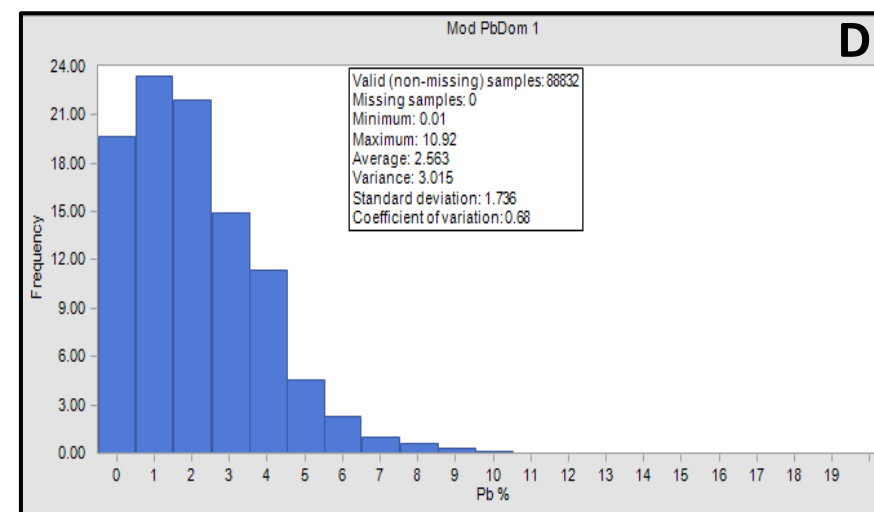
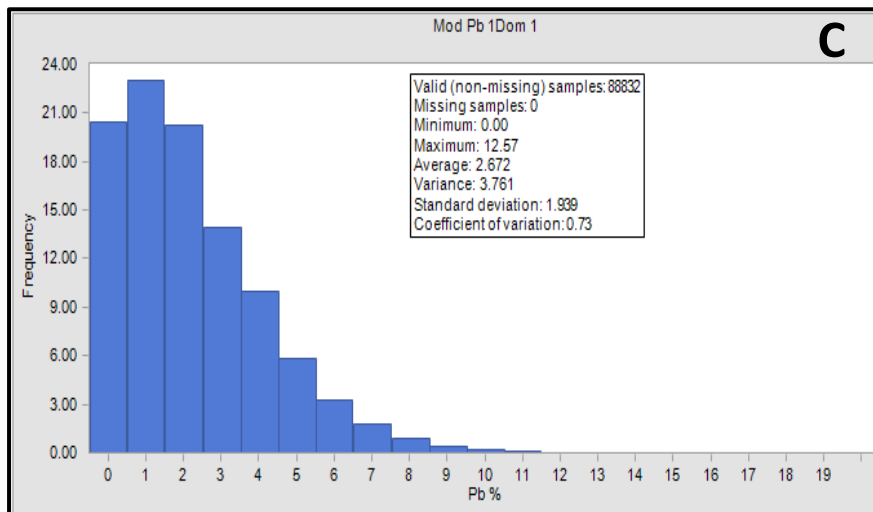
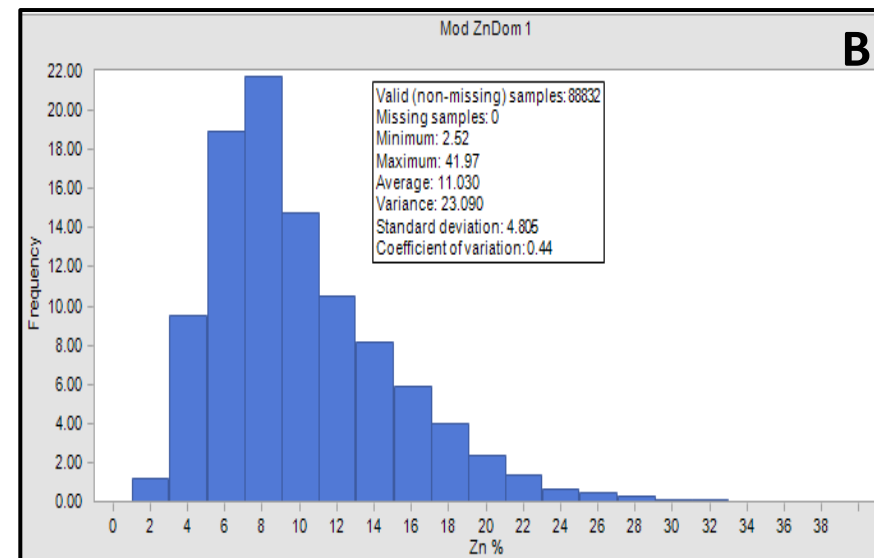
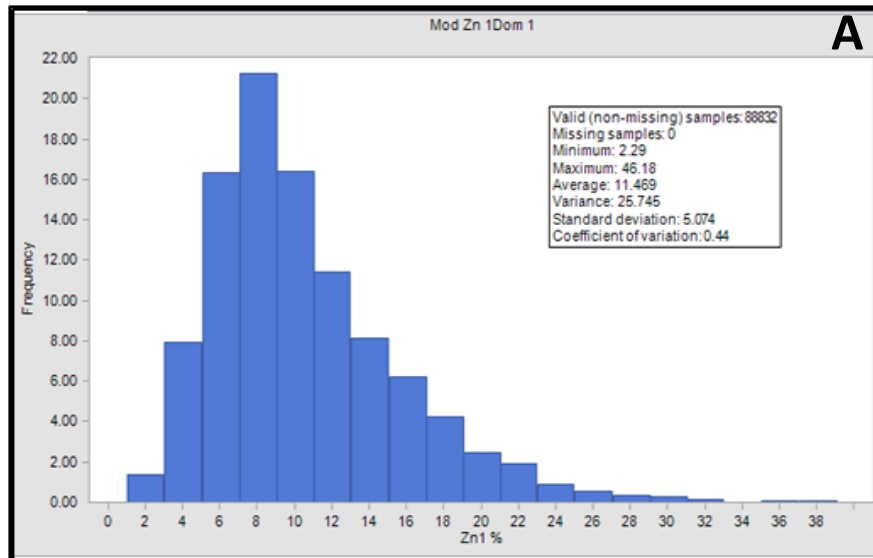


**Figure 39 Zn histogram of the model estimate (Domain 1) calculated from 1.5 m composites. B. Zn histogram of the model estimate (Domain 1) calculated from 3 m composites. C. Pb histogram of the model estimate (Domain 1) calculated from 1.5 m composites. D. Pb histogram of the model estimate (Domain 1) calculated from 3 m composites**



**Table 19 Domain 1 model statistics estimated from 1.5 m and 3 m composites**

STATS	Model 1.5m	Model 3m	Model 1.5m	Model 3m	Model 1.5m	Model 3m	Model 1.5m	Model 3m	Model 1.5m	Model 3m	Model 1.5m	Model 3m	Model 1.5m	Model 3m	Model 1.5m	Model 3m
	Zn	Zn	Pb	Pb	Cu	Cu	Fe	Fe	Ag	Ag	Mn	Mn	Mg	Mg	Rd	Rd
Num samples	11104	174120	11104	174120	11104	174120	11104	174120	11089	174120	11041	172320	9329	163920	10402	165432
Min	2.29	2.52	0	0.01	0	0.2	0.26	0.3	1	1	0.01	0.03	0.04	0.08	2.78	2.63
Max	46.18	41.97	12.57	10.92	4.22	3.12	10.93	13.21	718	614	8.14	10.29	7.78	6.91	4.2	3.96
Mean	11.47	11.03	2.67	2.56	0.22	0.2	3.43	3.31	74.5	65.8	1.29	1.57	2.49	2.44	3.35	3.29
SD	5.07	4.81	1.94	1.74	0.25	0.17	1.78	1.64	64.9	45.9	0.98	1.41	1.42	1.26	0.23	0.24
Variance	25.75	23.09	3.76	3.02	0.06	0.3	3.16	2.69	4212	2103	0.96	1.31	2.02	1.58	0.05	0.06
CV	0.44	0.44	0.73	0.68	1.14	0.85	0.52	0.5	0.9	0.7	0.76	0.73	0.57	0.51	0.07	0.07
Extreme outliers	30	144	5	8	309	2352	0	0	177	624	50	264	0	0	0	0

**Table 20 Domain 2 model statistics estimated from 1.5 m and 3 m composites**

STATS	Model 1.5m	Model 3m	Model 1.5m	Model 3m	Model 1.5m	Model 3m	Model 1.5m	Model 3m	Model 1.5m	Model 3m	Model 1.5m	Model 3m	Model 1.5m	Model 3m	Model 1.5m	Model 3m
	Zn	Zn	Pb	Pb	Cu	Cu	Fe	Fe	Ag	Ag	Mn	Mn	Mg	Mg	Rd	Rd
Num samples	10661	88288	10661	85288	10661	85288	10661	85288	10661	85288	10661	84256	10661	81384	10229	81264
Min	3.4	3.44	0.17	0.23	0.02	0.02	0.49	0.7	2	3	0.06	0.14	0.29	0.44	2.53	2.63
Max	48.72	43.43	12.01	10.74	2.27	1.66	15.35	13.21	299	249	11.7	10.29	24.96	23.01	4.11	3.94
Mean	10.86	10.61	2.57	2.49	0.19	0.19	3.25	3.23	61.1	59.8	1.9	1.86	4.39	4.47	3.24	3.24
SD	5.48	5.11	1.68	1.52	0.14	0.12	1.71	1.62	38.1	34.2	1.43	1.31	2.98	2.85	0.27	0.26
Variance	29.98	26.16	2.81	2.32	0.02	0.01	2.93	2.63	1451	1167	2.03	1.73	8.87	8.12	0.07	0.07
CV	0.5	0.482	0.65	0.61	0.7	0.61	0.53	0.5	0.6	0.6	0.75	0.7	0.68	0.64	0.08	0.08
Extreme outliers	173	816	47	400	254	1584	61	496	18	56	27	128	45	320	0	0

**Table 21 EF1 Measured Resources estimated from 1.5 m composites**

BENCH	RUN	GRADE						
TOE	ORE (TONNES)	Zn1 %	Pb1%	Fe1 %	Cu1 %	Ag1 (ppm)	Mn1 %	Mg1%
-35	30,660	10.697	2.919	2.065	0.241	79.2	1.019	3.136
-40	29,274	10.182	2.577	2.095	0.241	73	0.955	3.073
-45	25,588	10.253	2.194	1.965	0.263	67.8	0.961	3.27
-50	23,569	9.65	2.023	1.855	0.282	64.7	1.02	3.725
-55	22,813	8.719	2.015	1.865	0.25	60.3	1.145	4.351
-60	24,336	8.525	2.491	2.051	0.264	61.3	1.159	4.319
<b>Total Measured</b>	<b>156,200</b>	<b>9.7</b>	<b>2.4</b>	<b>2.0</b>	<b>0.3</b>	<b>68.4</b>	<b>1.0</b>	<b>3.6</b>

**Table 22 EF1 Indicated Resources estimated from 1.5 m composites**

BENCH	RUN	GRADES						
TOE	ORE (TONNES)	Zn1 %	Pb1%	Fe1 %	Cu1 %	Ag1 (ppm)	Mn1 %	Mg1%
-65	25,979	8.32	3.133	2.144	0.284	60.2	1.016	3.47
-70	24,652	8.768	4.206	2.337	0.267	66.4	0.855	2.776
-75	30,811	9.73	4.896	2.172	0.216	71.4	0.729	2.748
-80	40,739	10.392	5.014	2.37	0.21	78.9	0.824	3.039
-85	57,687	10.746	4.799	2.398	0.211	93.1	0.798	2.923
-90	57,975	10.66	4.467	2.224	0.208	90.6	0.797	2.83
-95	53,364	9.761	3.736	2.009	0.176	72.6	0.841	3.022
-100	50,428	8.559	3.093	1.735	0.159	54.4	0.866	3.232
-105	48,313	7.858	2.853	1.572	0.153	53.7	0.833	3.287
-110	47,218	7.575	2.987	1.501	0.177	85.5	0.781	3.085
-115	47,515	7.653	2.887	1.488	0.22	106	0.753	2.874
-120	45,202	7.479	2.803	1.498	0.246	106	0.724	3.042
-125	39,973	7.137	2.905	1.642	0.241	108.3	0.688	3.339
-130	33,361	7.448	3.02	1.759	0.226	122.7	0.645	3.424
-135	24,757	7.087	3.063	1.819	0.205	120.5	0.676	3.692
-140	17,801	7.112	3.036	1.948	0.176	121.2	0.678	3.9
-145	8,811	7.79	3.032	1.972	0.157	130	0.684	4.457
-150	7,486	8.963	3.007	1.993	0.129	107.8	0.519	2.948
-155	4,688	11.066	3.2	2.193	0.104	92.1	0.354	1.705
-160	117	18.769	4.258	2.931	0.09	129.3	0.185	0.451
<b>Total Indicated</b>	<b>666,900</b>	<b>8.71</b>	<b>3.58</b>	<b>1.91</b>	<b>0.20</b>	<b>87.39</b>	<b>0.78</b>	<b>3.12</b>

**Table 23 Measured Resources estimated from 3 m composites**

BENCH TOE	IN-SITU ORE (TONNES)	ROM Zn1 %	GRADES					
			Pb1%	Fe1 %	Cu1 %	Ag1 (ppm)	Mn1 %	Mg1%
-35	30,580	10.21	2.72	2.062	0.237	76.8	0.974	2.97
-40	29,024	9.814	2.554	2.053	0.239	72.8	0.911	2.966
-45	25,437	9.527	2.13	1.936	0.253	66.3	0.917	3.152
-50	23,454	8.885	1.995	1.853	0.251	64.3	0.969	3.519
-55	22,673	8.231	2.057	1.901	0.233	61.1	1.067	4.054
-60	24,130	7.814	2.309	2.024	0.227	57.4	1.066	3.919
<b>Total Measured</b>	<b>155,300</b>	<b>9.2</b>	<b>2.3</b>	<b>2.0</b>	<b>0.2</b>	<b>67.1</b>	<b>1.0</b>	<b>3.4</b>

**Table 24 EF1 Indicated Resources estimated from 3 m composites**

BENCH TOE	IN-SITU ORE (TONNES)	ROM Zn1 %	GRADES					
			Pb1%	Fe1 %	Cu1 %	Ag1 (ppm)	Mn1 %	Mg1%
-65	25,803	7.59	2.8	2.117	0.236	53.8	0.905	3.096
-70	24,470	8.271	3.443	2.31	0.265	58	0.8	2.6
-75	30,593	9.181	4.093	2.22	0.229	64.1	0.765	2.704
-80	40,319	9.806	4.371	2.285	0.197	73.5	0.815	3.029
-85	56,910	10.304	4.412	2.268	0.194	84.3	0.788	2.931
-90	57,161	10.421	4.293	2.173	0.199	84.6	0.795	2.868
-95	52,801	9.576	3.786	1.984	0.18	73.1	0.822	2.986
-100	49,806	8.672	3.275	1.77	0.162	65.8	0.828	3.173
-105	47,632	7.833	3.04	1.596	0.158	72.1	0.811	3.161
-110	46,638	7.47	2.996	1.523	0.166	82.1	0.783	3.056
-115	46,778	7.381	2.842	1.492	0.195	90.5	0.737	2.962
-120	44,552	7.186	2.7	1.507	0.215	94.1	0.697	3.018
-125	39,424	7.19	2.722	1.609	0.213	95.4	0.646	3.135
-130	32,936	7.138	2.836	1.692	0.206	102.5	0.628	3.205
-135	24,410	6.915	2.915	1.775	0.199	112.7	0.654	3.493
-140	17,536	6.833	2.884	1.892	0.175	110.8	0.664	3.687
-145	8,819	7.194	2.841	1.977	0.143	107.4	0.65	3.931
-150	7,465	7.96	2.784	2.049	0.122	93.4	0.503	2.969
-155	4,676	9.564	2.867	2.235	0.105	85.5	0.374	1.79
-160	117	15.655	3.652	2.883	0.095	116.5	0.224	0.601
<b>Total Indicated</b>	<b>658,800</b>	<b>8.44</b>	<b>3.40</b>	<b>1.88</b>	<b>0.19</b>	<b>82.08</b>	<b>0.76</b>	<b>3.04</b>

## 8.2.4 Grade distribution

The EOF orebody has high-grade “pockets” which occur mainly in the fold hinge and in close proximity to major faults. These pockets have Zn grades above 12% and Pb grades above 3.5%. Figure 40A–B show the Zn and Pb grade distribution at EOF. From west to east (Figure 41), the major structures associated with the mineralisation are the AE fault, the Martina fault and the Dennis fault, respectively.

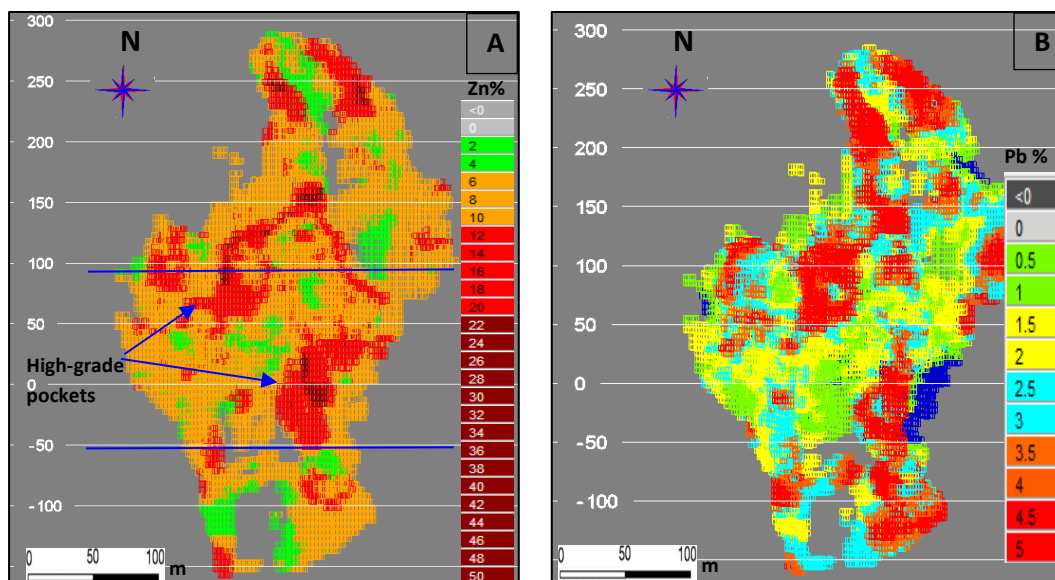


**Figure 40 A. Zn grade distribution. B. Pb grade distribution**

The Rosh Pinah Mine deposits are a reworked classic SEDEX deposit comprising a primary banded sulphide exhalite, part of which was carbonatised with associated remobilization and enrichment of sulphides (Alchin and Moore, 2005). The emplacement of the volcanics and mafics drove hydrothermal fluids along the faults system, leaching base metals from the basin-fill siliciclastics and exhaling base-metal bearing brines onto the sea floor. Hence, the occurrence high-grade mineralisation in close proximity to faults (Figure 41). A similar observation of

anomalous enrichment of Ag and Pb is described by Alchin and Moore (2005), and they explain it as being related to hydrothermal fissure zones along which simultaneous metal-bearing brine expulsions took place.

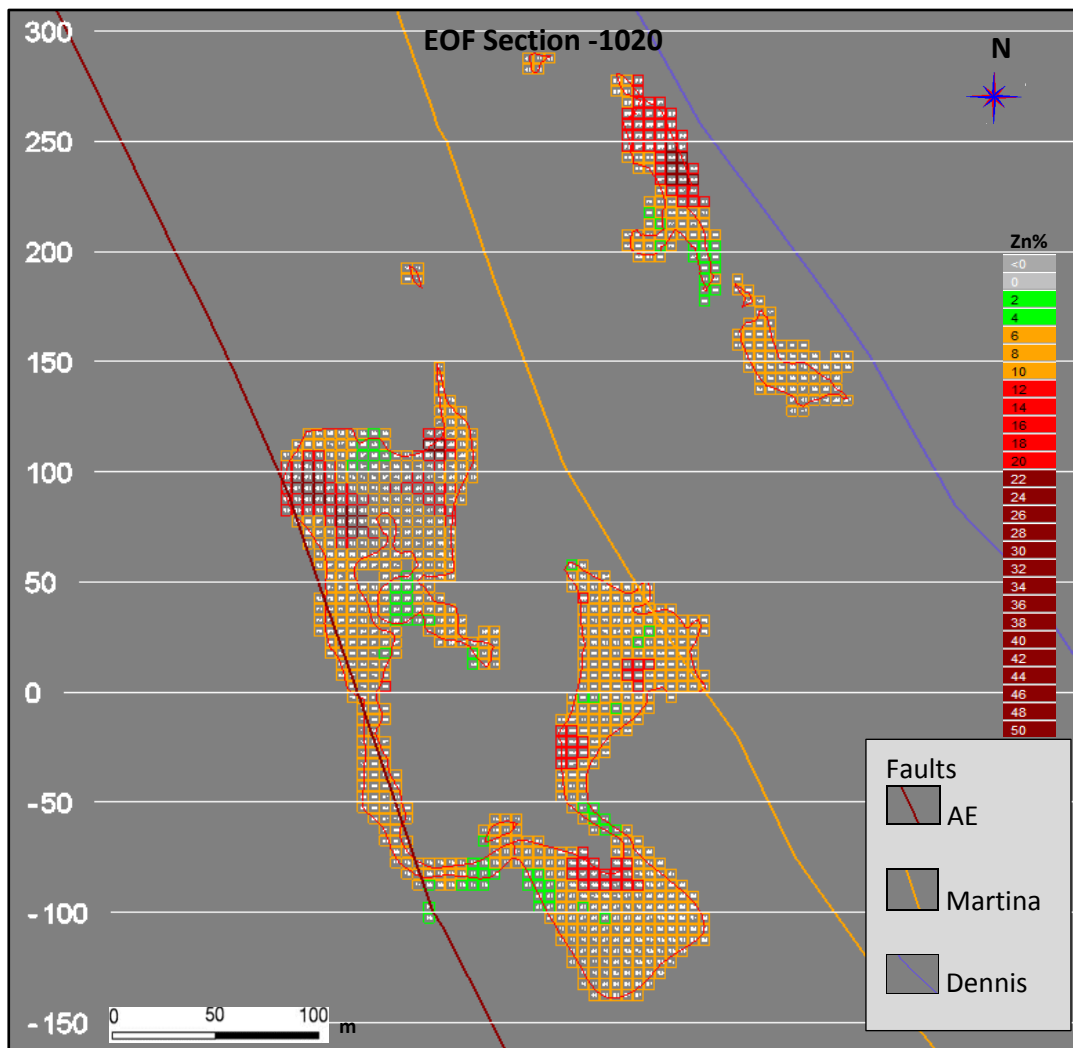


**Figure 41 EOF faults and their association with high-grade mineralisation**

The Rosh Pinah ore deposit has been classified as a SEDEX deposit with volcanogenic massive sulphide (VMS) and Broken Hill-type (BHT) depositional and deformational characteristics (Alchin and Moore, 2005). It was further stated that most of the sulphides were highly recrystallized and remobilized during multiple

events of veining and brecciation. The metal zonation is a common feature of SEDEX deposits; Cu and Fe sulphides are deposited in a more proximal setting relative to the fluid source, whilst Pb and Zn sulphides generally occur more distally to the hydrothermal vent and Fe, Mn and Ba occur on the peripheral zone. The EOF ore body occurs more distal to the hydrothermal vent based on the Pb and Zn sulphide mineralisation. Another chemical zonation pattern that characterizes the EOF mineralisation is the Pb/Ag ratio, which is higher, indicating that the mineralisation is distant from the vent. The understanding of the relationship between the mineralization of interest and the likely related geological processes that govern its emplacement and geometry within the geological framework is essential to the establishment of the geological controls for mineralisation.

### **8.3 Grade tonnage curves**

Grade tonnage curves provide a summary of the estimated tonnes and grade of materials relative to a given cut-off. Grade tonnage curves were plotted for the 1.5 m and 3 m composites and for the model estimates obtained with the 1.5 m and 3 m composites.

The grade tonnage curves (Figures 42–44) indicate that the composites for all elements have higher-grade estimates and tonnes above the cut-offs compared to the block models. The 3 m composites have lower grade estimates and tonnes above the cut-offs compared to the 1.5 m composites. Similarly, the model estimated from the 3 m composites have lower tonnages above cut-off and grades compared to the models estimated from the 1.5 m composites.

The above-mentioned observations are in line with the volume variance effect and block size. The greater the volume used for selection, the greater the dilution of grades. Bigger blocks report less tonnes at lower grades. Similarly, the longer composites have lower variances and lower grades than the shorter ones.

Rosh Pinah Mine applies an economic cut-off grade of 8% Zn equivalent, which equates to actual cut-offs of 6% Zn and 0.7% Pb. At this cut-off grade, about 75% tonnage at an average grade of 11% Zn and 2.5% Pb is above the cut-off. The grade and tonnage differences between the two models are insignificant, but the financial impact is considerable. Considering the Measured Resources only, the Zn metal tonnes of the model estimated from the 1.5 m composites are 11,366 MT versus 10,716 Mt estimated from the 3 m composites. At a selling price of \$2,200, the Zn metal estimated from 1.5 m composites is worth \$25 million, compared to \$23.6 million for the estimate from the 3 m composites; a difference of \$1.4 million. This revenue would be spread over the life of the mine and this is a clear indication that the composite with a support that is closer to the mining block size or SMU should be used for the evaluation. The SMU applied at Rosh Pinah is 4.5m x 5 m, thus a 3 m composite is more preferable.

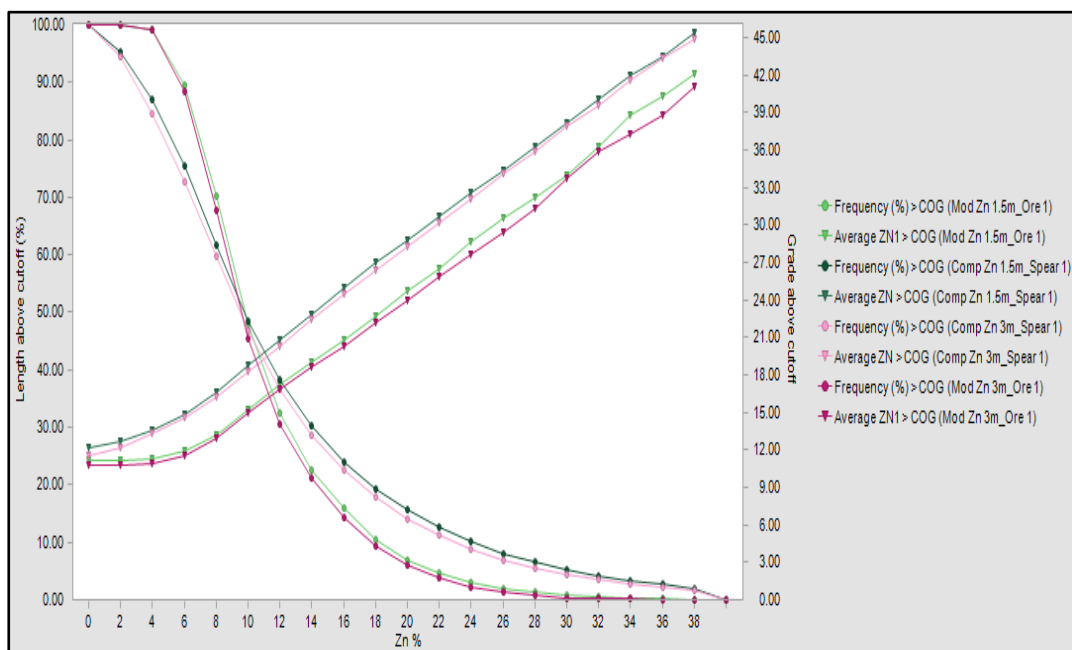


**Figure 42 Zn grade tonnage curves for models obtained from 1.5 m and 3 m composites**

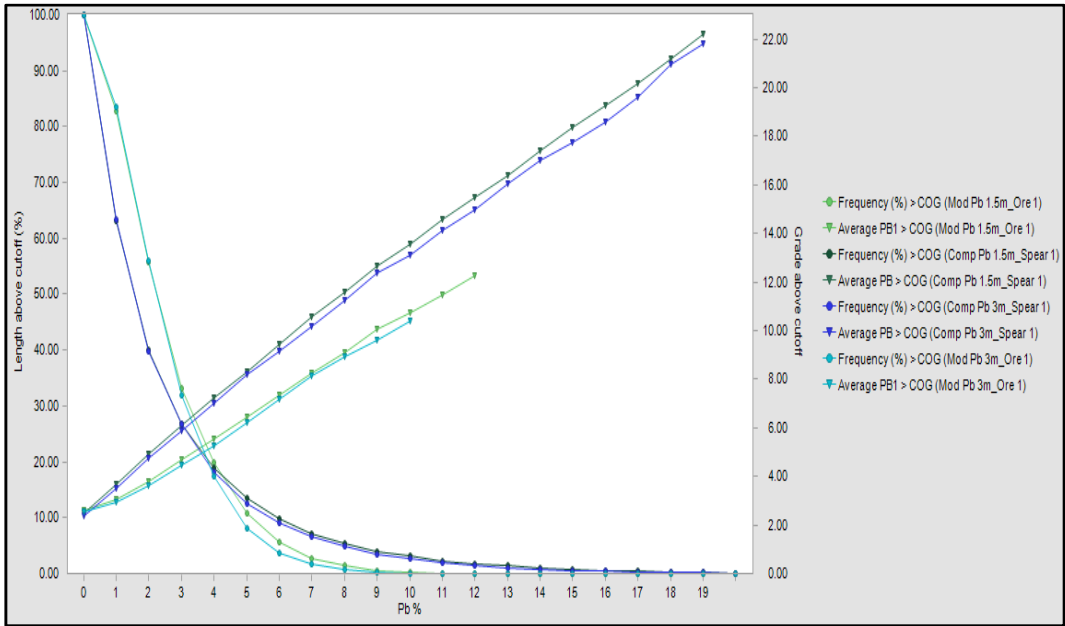


**Figure 43 Pb grade tonnage curves for models obtained from 1.5 m and 3 m composites**

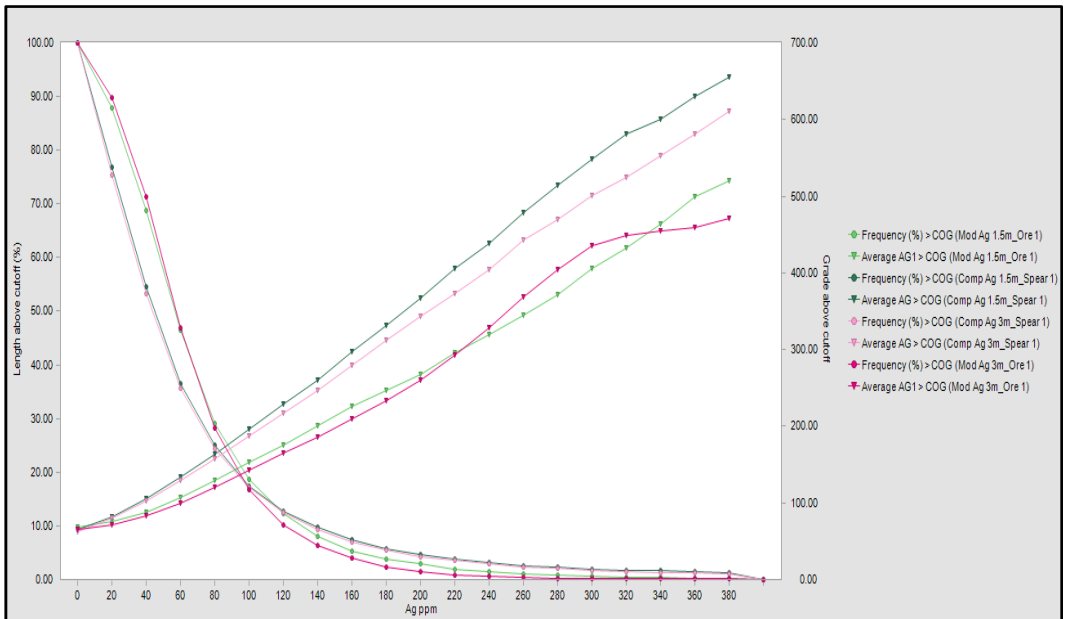


**Figure 44 Ag grade tonnage curves for models obtained from 1.5 m and 3 m composites**



## 8.4 Model validation

The models were first validated by comparing the borehole assays and the model estimates on sections, as shown in Figure 36. The model estimates are generally acceptable, but the model calculated from the 1.5 m composites is more variable whilst the one calculated from 3 m composites is less variable. Secondly, the models were validated by plotting Swath plots and analyzing them. Swath plots are graphs that compare the model mean to the mean of the composites within a series of slices/swaths. The total number of composites is also plotted on the secondary axis of the graph to give an indication of the support for each swath. The swath plots in the eastern direction for Zn, Pb and Ag are presented in Appendices Y and Z.

The swath plots indicate that the means of both models are generally lower than the means of the composites. This is in line with the volume variance effect, which states that the higher the support size, the higher the dilution and the lower the grades. Figure 45 shows the swath plot for EOF along the elevation.

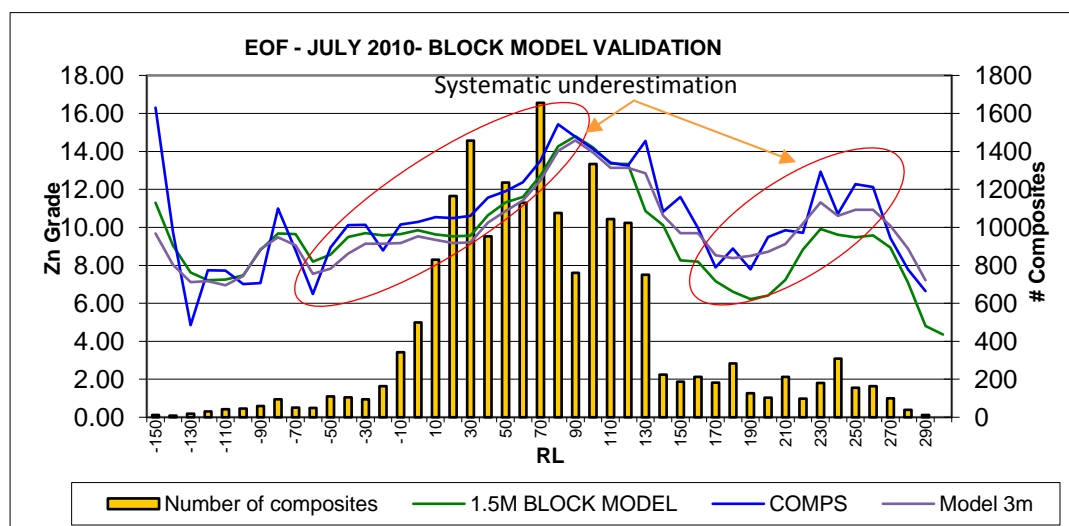


Figure 45 Zn swath plot along the elevation

A significant systematic underestimation is reported between the -50 to the 90 and 120 to 260 levels, as shown in Figure 45. The underestimation is more pronounced in poorly informed areas. From the 90 to the 290 level the estimate from 3 m composites is closer to the composite mean than the estimate from 1.5 m composites. For the easting and northing direction, where there are less data available, the mean of the model estimated from 3 m composites is closer to the mean of the input composites (Appendices Y and Z).

The area that displays significant systematic underestimation is a well-informed area with the highest number of composites. The systematic under estimation is due to the volume variance effect and change in support size. The composite of 3 m has lower volume compared to blocks of 5 m x 5 m, thus the composite will have a higher grade compared to the estimate due to less dilution. It is observed that the area is associated with high-grade zones or high-grade pockets (Figure 40A). The underestimation result is typical, especially if the OK estimation method was applied, because of the smoothing of the estimate.

Pb and Ag swath plots indicate overestimation in the easting direction between the 22,110 and 22,140 swaths; the mean of the model is higher than the mean of the composites (Figure 46). This is an early warning sign that the unusual higher-grade composites have potentially positively influenced the overall estimate. The presence of the higher-grade composites (Figure 47) pulled the overall estimate higher. These elements could be further sub-divided in high- and low-grade zones to improve the estimation; alternatively, capping may be applied to reduce the influence from very high-grade composites.

The models estimated from the 3 m composites have lower means compared to the means of the models estimated from 1.5 m composites for the well-informed blocks. For poorly informed blocks, the model estimated from 3 m composites is closer to the mean of the input composites (Appendices Y and Z).

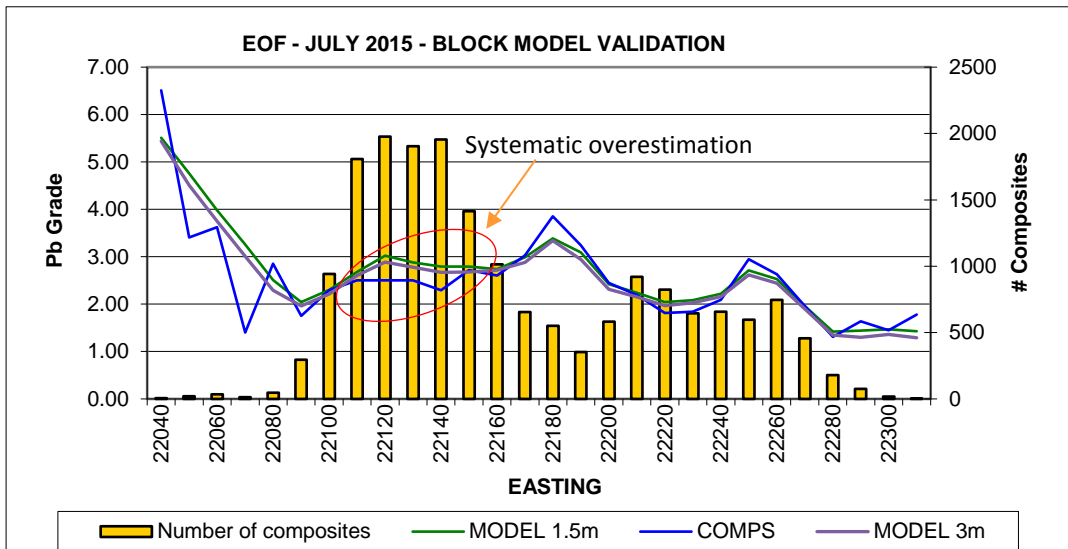


Figure 46 Pb swath plot in the easting direction

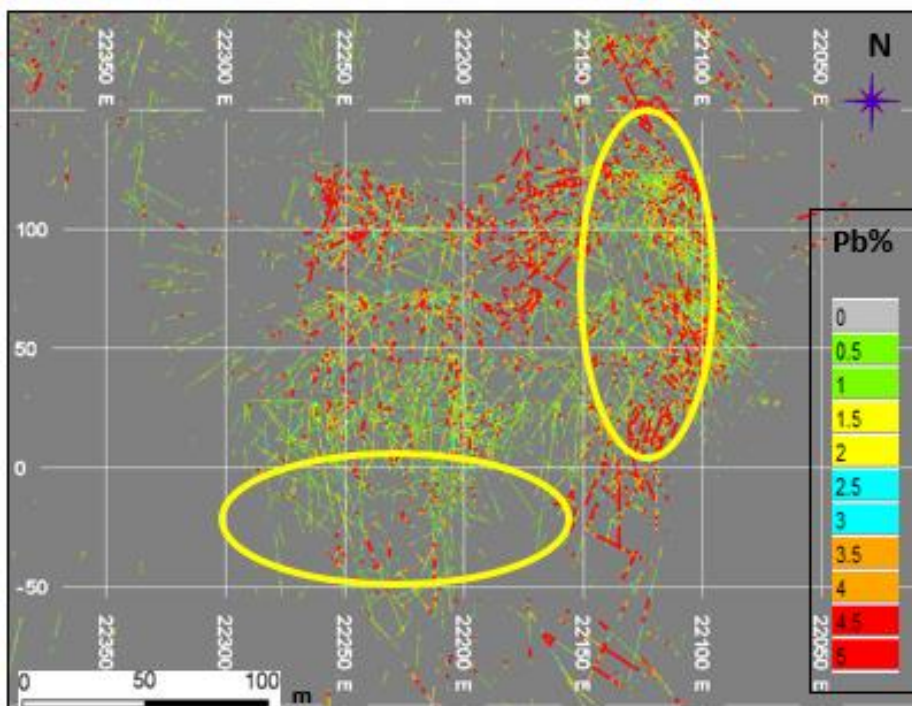
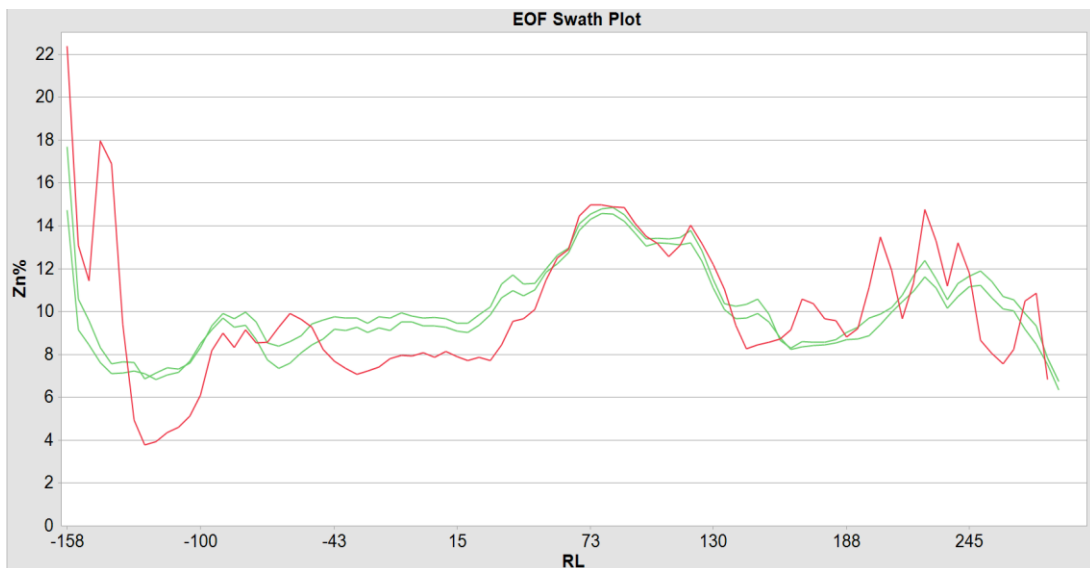


Figure 47 Pb composites showing many lower-grade composites

Although swath plots are often used for model validations, the composite distribution, volume variance effect, smoothing of estimates, higher drilling density in high-grade zones and presence of few higher-grade composites can result in the validation method being less effective. Finally, an inverse distance weighting to the power of 2 ( $IDW^2$ ) was estimated in Zn2 columns and plotted on a swath plot with the OK model estimates from the 1.5 m model and 3 m model (Figure 48). The IDW model displays more variations and between the -50 and 60 levels the IDW estimate is significantly lower than the OK estimate. The third validation method has the same challenges; the mean of the IDW estimate is also influenced by the underlying composite distribution, volume variance effect, presence of many lower-grade composites and drilling density.



**Figure 48 IDW estimate (red) compared to the OK estimates (green) from the 1.5 m model and 3 m model**

## 8.5 Evaluating Kriging

The kriging estimates were evaluated using the QKNA. The QKNA was applied to validate the resource categories, mainly to determine if blocks are well informed or poorly informed. The criteria that were applied for evaluating the EF1 kriging neighbourhood are:

- The slope of regression of the 'true' block grade on the 'estimated block grade.
- The kriging standard deviation.
- Minesight software was used to calculate the kriging variance, standard deviation and the slope of regression.

### 8.5.1 Slope of regression

Vann et al. (2003) state that, under the assumption that the variogram is valid and the regression between the true block grades and estimated block grades is linear, the covariance between estimated and true block grades can be calculated. The slope is given in terms of the covariance and the variance of the estimated blocks by the expression:

$$a = \frac{Cov(Z_v, Z_v^*)}{Var(Z_v^*)}$$

(Vann et al., 2003)

Where:

$a$  is the slope of regression

$Z_v$  is the true block grade

$Z_v^*$  is the estimated block grade

The blocks are conditionally unbiased if the slope of regression is very close to 1.0.

### 8.5.2 Kriging standard deviation

The kriging standard deviation is the square root of the kriging variance. The kriging variance was calculated using Minesight software; the square root of the kriging variance was calculated in Excel from the Minesight model dump. The blocks are conditionally unbiased if the kriging standard deviation is lower, which implies that well-informed blocks have lower standard deviation than poorly informed blocks.

### 8.5.3 Results of the QKNA

The results of the QKNA for the model estimated from 1.5 m composites are presented in Table 25. The Indicated Resources have a higher standard deviation and variance and a lower slope of regression compared to the Measured Resource. Based on the value of the slope of regression and kriging standard deviation, the Measured Resources are well informed with a slope of regression closer to 1 and a standard deviation of 0.3. The Indicated Resources are reasonably informed.

**Table 25 QKNA statistics for EF1**

<b>BENCH TOE</b>	<b>IN-SITU ORE (BCMS)</b>	<b>IN-SITU ORE (TONNES)</b>	<b>KVZN</b>	<b>Slope of regression</b>	<b>Kriging standard deviation</b>
Total Measured (Above -60 Level)	1,451,000	4,847,000	0.1	0.9	0.3
Total Indicated (Below -60 Level)	201,000	667,000	0.4	0.8	0.6

## 8.6 Summary

As on 31 December 2016 the EF1 measured in-situ resources calculated from the 1.5 m composites is 156,200 tonnes at 9.7% Zn and 2.4% Pb versus 155,300 tonnes at 9.2% Zn, 2.3% Pb and 67.1 ppm Ag calculated from the 3 m composites. The model estimated from 3 m composites gives lower grades and less tonnes, Table 24 and 22, the indicated resources, mostly highlight this. This is in line with the volume variance effect and support size as well as the smoothing of high grades during the OK estimation process. The blocks estimated from the 3 m composites have lower means, standard deviations and variances compared to blocks estimated from the 1.5 m composites. This finding is in line with the volume-variance effect, which states that the variance decreases with increasing support or volumes. Based on this, it is recommended that the EF1 model estimates should be calculated from 3 m composites. In line with this recommendation is the fact that 3 m is closer to the SMU at Rosh Pinah Mine, which is 4.5 m x 5 m.

Areas in which the estimates are too high due to the presence of few high-grade composite require further investigations. Elements that are overestimated could be further sub-divided in high- and low-grade zones to improve the estimation; alternatively, capping may be applied to reduce the influence from very high-grade composites. Further work is recommended to investigate sub-domaining of the Pb and Ag as well as capping.

A simplified resource classification method was applied which relied fully on the drill spacing. All resources above the -60 level were classified as Measured whilst those below are classified as Indicated. The QKNA supports the resource classification; the Indicated Resources have a higher standard deviation and variance and a lower slope of regression compared to the Measured Resource. Based on the value of the slope of regression and the kriging standard deviation, the measured resources are well informed and the indicated are reasonably informed.

## CHAPTER 9: CONCLUSIONS

### 9.1 Research questions and main findings

The dissertation had the aim of finding the best method for modelling complex sedimentary exhalative deposits. It was found that using 2D sections and level plan interpretations and combining them with 3D implicit modelling reduces the wireframe building process from three weeks to two days. The 2D sections and level plans help in avoiding the creation of saw tooth interpretations due to a lack of information where the mineralisation is continuous. These are interpretations where continuous lenses are modelled as discontinuous lenses because no drilling was carried out on the in-between sections. The dissertation was also aimed at determining the principal components of the EF1 multivariate orebody. The first principal component is primarily a measure of Ag; higher-grade ore has higher Ag contents. The second principal component is primarily a measure of Zn in the ore.

Furthermore, the dissertation investigated the significance of increasing the composite size from 1.5 m to 3 m on grade estimation. It was found that the mean, standard deviation and variances of the 3 m composites and their respective models are lower than the assay data, the 1.5 m composites and their respective models. Ordinary Kriging is preferred over inverse distance estimation because it is the best linear unbiased estimator with zero mean residual errors and minimum estimation variance. Thus, the model estimated from the 3 m composites yields better estimates than the model estimated from 1.5 m composites; the estimate from the 3 m composites has minimum estimation variance and standard deviations. In mining, it is often better to underestimate than to overestimate, thus an estimate with lower mean is preferred because it is more conservative. The composite size of 3 m is also closer to the SMU at Rosh Pinah, and thus produces a better estimate than the estimate from 1.5 m composites, which will state higher tonnages and grades due to the volume variance effect, which ultimately leads to overestimation of the mineral deposit.



The last objective of the dissertation was to estimate the tonnes and grades of the in-situ EF1 resources as on 31 December 2016. The EF1 in-situ Measured Resources calculated from the 1.5 m composites is 156,200 tonnes at 9.7% Zn, 2.4% Pb and 68.4 ppm Ag versus 155,300 tonnes at 9.2% Zn, 2.3% Pb and 67.1 ppm Ag calculated from the 3 m composites. The total in-situ Indicated Resource calculated from the 1.5 m composite is 666,900 tonnes at 8.71% Zn, 3.58% Pb and 87.39 ppm Ag versus 658,800 tonnes at 8.44% Zn, 3.40% Pb and 82.08 ppm Ag calculated from 3 m composites. The total accepted EF1 in-situ tonnes amounts to 814,100 tonnes of 8.58% Zn, 3.19% Pb and 79.22 ppm, based on the 3 m composite estimate. A greater support size reduces the variability in the ore body and as a result affects the grade tonnage curves and accounts for the differences in the resource estimates.

The QKNA supports the idea that the Measured Resources are well informed, whilst the Indicated are reasonably informed. The PRED classification system results are too optimistic, indicating that all resources can be converted into Measured. The orebody geometry is very complex and the EOF ore outline swells and pinches over shorter distances. Thus, only levels drilled out on a 10 x 10 m spacing may be converted into Measured.

## **9.2 Relationship to previous research**

The modelling method recommended by Wang (2013, p.86) was also used here, especially the process of constructing 3D models from 2D sections. The processes they presented in the schematic flow-chart for 3D modelling by integration of multiple types of geoscience data were also applied in this dissertation, but they did not use implicit modelling software for constructing the models. The findings on the support size are consistent with the volume-variance effect, which states that the variance decreases with increasing support. Comparing the estimated EF1 in-situ resources to those done prior to 2014 (Table 1) at Rosh Pinah Mine, the Zn estimate is much lower, Pb is similar and Ag is higher than previous

estimates. The findings on QKNA are consistent with findings by Vann et al. (2003) on less informed and poorly informed blocks of a case study on well-informed Au estimates and ash content. They found that Indicated Resources have higher standard deviation and variance and a lower slope of regression compared to the Measured Resource. Based on the value of the slope of regression and kriging standard deviation, the Measured Resources are well informed with a slope of regression closer to 1 and a standard deviation of 0.3. The Indicated Resources are reasonably informed with a slope of regression of 0.8 and a standard deviation of 0.6.

### **9.3 Limitations of the study**

It should be borne in mind that the study has a number of limitations:

- Section and level plan interpretation is a manual process that requires the geologist to digitized polylines. It is difficult for the model to honour both the sections and the level plans and as a result, some ore may be left behind.
- The boreholes are projected on sections and the model may exclude part of the mineralised intersections and include unmineralised intersections in 3D space. This may result in waste being incorporated in the solid and ore being excluded.
- The final wireframes created with implicit modelling software still requires manual tweaking because of geological understanding and insight that the modelling software does not accommodate.
- The EF1 resource classification was based on drill spacing only, and this may cause resources to be placed in the wrong resource categories. Although it was backed up with the QKNA, the PRED system was less effective in classifying the resources correctly.
- Domaining is based on the position and location of the fold hinge, but some elements' distribution may not be related to the direction of the

limbs. The search ellipsoid in the direction of maximum, intermediate and minor continuity of the elements may not be similar to the strike and dip of the fold limbs. This may cause conditional unbiasedness of the estimate.

- This study has been primarily concerned with the estimation of Mineral Resources in a structurally complex sedimentary hosted deposits.

#### **9.4 Recommendations**

The following is recommended:

- For wireframe modelling of structurally complex sedimentary deposits, 2D sections and level plan interpretations combined with 3D implicit modelling should be used. The 2D sections and level plans help in the extrapolation of mineralisation where the mineralisation is continuous but no drilling was carried out on the in-between sections. Thus, the geologist will provide better estimates of resource tonnages and better delineation of the ore-waste contact and subsequently minimize dilution and ore losses. Correct delineation of the ore-waste contact will prevent waste to be loaded as ore and ore losses. The 3D implicit modelling reduces the amount of time required to interpret drillhole data, thus allowing timely update of models.
- The final wireframe model should include all mineralised intersections; no mineralised intersections should be excluded during modelling. This will prevent ore loss and optimise mine designs, thus ultimately increasing the value of the mineral deposit.
- The quantile regression method is the chosen method for outlier detection. The outliers detected using the quantile regression method are mostly between 90 to 95 percentile whilst those detected using histograms and CPP plots are around 98 percentiles. The quantile

regression method for outlier detection is repeatable and auditable; all resource geologists would get the same outliers, but the other methods are based on the assessment of the geologist and the outliers may be different. The correct identification of outliers reduces overestimation caused by the presence of few high-grade composites, thus ultimately reducing the chance of the mineral deposit to be overvalued.

- The EF1 block estimates should be calculated from 3 m composites. These give a better estimate than the point-model estimated using 1.5 m composites. The block-model estimates using 3 m composites are more conservative and give less tonnes and lower grades. The standard deviations and variances are also lower than the block-model estimate from the 1.5 m composites because of the volume variance effect and support sizes, and smoothing of grades during Ordinary Kriging estimation. The 3 m composite size is closer to the SMU at Rosh Pinah, and produces a better estimate than 1.5 m composites, which will give more tonnes and higher grade due to the volume-variance effect, which ultimately leads to overestimation of the mineral deposit.
- Pb and Ag need to be sub-domained based on high- and low-grade zones. This reduces the effect of overestimating low-grade blocks due to the smearing of few high-grade composites and underestimating high-grade blocks due to smoothing during Ordinary Kriging estimation.
- The nugget effects should be determined using omni-directional variograms with a lag distance of 1.5 m because it is ideal that the nugget is interpreted using the closest spaced data available, which is the sample size. The closest spaced data are typically found in the downhole direction, where samples are adjacent, which is equivalent to the composite length of 1.5 m. Hence, a very small lag can be used to give an indication of the behaviour of the variability at short distances. The omni-directional variogram with a lag distance of 10 m was used to determine the nugget effects as shown in Appendix T.

## CHAPTER 10: REFERENCES

Abedini, M.J., Nasser, M. & Burn, D.H. 2012. The use of a genetic algorithm-based search strategy in geostatistics: application to a set of anisotropic piezometric head data, *Computers & Geosciences* 41, pp 136 -146.

Alchin, D.J., Frimmel, H.E. & Jacobs, L.E. 2005. Stratigraphic setting of the metalliferous Rosh Pinah Formation and the Spitzkop and Koivib Suites in the Pan-African Gariep Belt, southwestern Namibia. *South African Journal of Geology*, 108, pp. 19 – 34.

Alchin, D.J. and Moore, J.M. 2005. A review of the Pan-African, Neoproterozoic Rosh Pinah Zn-Pb deposit, southwestern Namibia. *South African Journal of Geology*, 108 (1), pp71-86.

Boyle, C. 2010. Kriging neighbourhood analysis by slope of regression and weight of mean; evaluation with the Jura data set. *Mining Technology*, 119, pp. 49 - 58.

Calcagno, P., Chiles, J., Courrioux, G. & Guillen, A. 2008. Geological modeling from field data and geological knowledge: part I. Modelling method coupling 3D potential-field interpolation and geological rules. *Physics of the Earth and Planetary Interiors*, 171 (1 -4), pp. 147 - 157.

Cornah, A., Vann, J. & Driver, I. 2013. Comparison of three geostatistical approaches to quantify the impact of drill spacing on resource confidence for a coal seam (with a case example from Moranbah North, Queensland, Australia), *International Journal of Coal Geology*, 112, pp. 114 – 124.

Corrans, R. D., Gewalt, H., Whyte, R. M. and Land, B. N. 1993. The Skorpion SZ secondary zinc deposits - South Western Namibia. *Conference on Mining Investment in Namibia, Abstract Volume, Windhoek.*

Crowther, P. 2014. Mineral resources and ore reserves statement, Rosh Pinah Zinc Corporation, Namibia.

Daya, A.A., 2012, Reserve estimation of central part of Choghart north anomaly iron ore deposit through Ordinary Kriging method, *International Journal of Mining Science and Technology*, 22, pp. 573 – 577.

Deutsch, J.L., Szymanski, J., and Deutsch, C.V. 2014. Checks and measures of performance for kriging estimates, University of Alberta, Alberta, Canada.

de Souza, L.G. & Costa, J.F.C.L. 2013. Sample weighted variograms on the sequential indicator simulation of coal deposits, *International Journal of Coal Geology*, 112, pp. 153 – 163.

Dohm, C. 2010. Geostatistical Methods in Mineral Resource Evaluation, University of the Witwatersrand, July 12 – 23, pp. 7.

Ertunç, G., Tercan, A.E., Hindistan, M.A., Ünver, B., Ünal, S., & Killioğlu, S.Y. 2013. Geostatistical estimation of coal quality variables by using covariance matching constrained kriging. *International Journal of Coal Geology*, 112, pp. 14 – 25.

Falivene, O., Cabrere, L., Tolosana – Delgado, R., and Sáez, A. 2010. Interpolation algorithm ranking using cross-validation and the role of smoothing effect. A coal zone example. *Computers & Geosciences*, 36, pp. 512 -519.

Fallara, F., Lequalt, M., Rabeau, O. 2006. 3-D Integrated geological modeling in the Abitibi subprovince (Québec, Canada): techniques and applications. *Exploration and Mining Geology* 15, pp. 27 - 41.

Frimmel, H.E., and Frank, W. (1998). Neoproterozoic tectono-thermal evolution of the Gariiep Belt and its basement. *Namibia/South Africa Precambrian Research*, 90, pp. 1 - 28.

Glencore International plc, 2012, Glencore completes acquisition of controlling interest in Rosh Pinah.

<http://www.glencorexstrata.com/assets/Uploads/201206110800-Glencore-completes-acquisition-of-controlling-interest-in-Rosh-Pinah.pdf>

Heriawan, M.N. & Koike, K. 2008. Identifying spatial heterogeneity of coal resource quality in a multilayer coal deposit by multivariate geostatistics, *International Journal of Coal Geology*, 73, pp. 307 – 330.

Hodkiewics, P. 2016. Leapfrog: new software for faster 3D geological modelling. SRK Consulting, West Perth, Australia.

[https://www.leapfrog3d.com/\\_data/assets/pdf\\_file/0017/539/new-software-for-faster-and-better-3d-geological-modelling.pdf](https://www.leapfrog3d.com/_data/assets/pdf_file/0017/539/new-software-for-faster-and-better-3d-geological-modelling.pdf)

Hoffman, D. R. 2003. *Effective Database Designs for Geosciences Professionals*, PenWell Corporation, USA, pp. 191 – 204.

Hohn, M.E. & Britton, J.Q. 2013. A geostatistical case study in West Virginia: All coals are not the same, *International Journal of Coal Geology*, 112, pp. 125 – 133.

Isaaks, E.H., and Srivastava, R.M. 1989. *An introduction to applied geostatistics*, Oxford, New York, pp. 561.

Jiménez-Espinosa, R., and Chica-Olmo, M. 1999. Application of geostatistics to identify gold-rich areas in the Finisterre-Ferrenza region, NW Spain, *Applied Geochemistry*, 14, pp. 133 – 145.

Kaufman, O., and Martin, T. 2008. 3D geological modelling from boreholes, cross-sections and geological maps, application over former natural gas storages in coal mines. *Computers & Geosciences*, 34 (3), pp. 278 – 290.

Krige, D.G. 1951. A statistical approach to some basic mine valuation problems on the Witwatersrand, *J. Chem. Met. Min. Soc. S. Afr.*, 52, pp. 119 – 139.

Krige, D.G. 1952. A statistical analysis of some of the borehole values in the Orange Free State goldfield, *J. Chem. Met. Min. Soc. S.Afr.* Sept, 1952, pp. 47 – 64.

Krige, D.G. 1996a. 'A basic perspective on the roles of classical statistics, data search routines, conditional biases and information and smoothing effects in ore block valuations', *Proceedings of the conference on Mining Geostatistics*, held at Bergen – Dal conference centre, Kruger National Park, South Africa, pp. 1 – 10.

Krige, D.G. 2000. Essential basic concepts in mining geostatistics and their links with geology and classical statistics. *South African Journal of Geology*, 102, pp. 147 -152.

Lemon, A.M., and Jones, N.L. 2003. Building solid models from boreholes and user- defined cross-sections. *Computers & Geosciences* 29, 547–555.

Leuangthong, O. Khan, K.D. Deutsch, C. V. 2008. *Solved problems in geostatistics*. Jon Willy & Sons Inc., Hoboken, New Jersey.

Maleki, M., Madani, N. & Emery, X. 2013. Capping and kriging grades with long-tailed distributions, Department of Mining Engineering & Advanced Mining Technology Center, University of Chile, University of Chile, Santiago, Chile.



Mallet, J.L. 2002. Geomodeling. Applied Geostatistics. Oxford University Press, New York, pp. 1–10.

Marinoni, O., 2003, Improving geological models using a combined ordinary – indicator kriging approach, Engineering geology, 69, pp. 37 – 45.

Monteiro, R.N., Fyfe, W.S. & Chemale Jr, F. 2004. The impact of the linkage between grade distribution and petrofabric on the understanding of structurally controlled mineral deposition: Ouro Fino Gold Mine, Brazil, Journal of Structural Geology, 26, pp. 1196 – 1214.

Mouton, E.L. 2006. Depositional Style of the Rift-Related Rosh Pinah Formation, Namibia. 17<sup>th</sup> International Sedimentological Congress, Fukuoka, Japan.

Mukumbi, A. '2014. PPI/G.002 QAQC pass/fail criteria and resubmission'. Rosh Pinah Mine, Namibia.

Oliver, M.A. & Webster, R. 2014. A tutorial guide to geostatistics. Computing and modelling variograms and kriging, Catena, 113, pp. 1246 – 1266.

Pardo-Igúzquiza, E., Chica-Olmo, M., Garcia-Soldado, M. J. & Luque-Espinar, J. A. 2008. Using semevariogram parameter uncertainty in hydrogeological applications. Ground Water, 47 (1), pp. 25 – 34.

Richard, J.M. & Martin, G.J. 2003. 'Mineralogical investigation of borehole core samples and screened samples from the Eastern Ore Body, Rosh Pinah Mine. Namibia,' Lakefield Research, Johannesburg, South Africa.

Saikia, K. & Sarkar, B.C. 2013. Coal exploration modelling using geostatistics in Jharia coalfield, India. International Journal of Coal Geology, 112, pp. 36 – 52.

Snowden, V. 2009. Professional development Courses: Resource estimation. Snowden Mining Industry Consultants. Australia

Srivastava, R.M., 2013. Geostatistics: A toolkit for data analysis, spatial prediction and risk management in the coal industry, *International Journal of Coal Geology*, 112, pp. 2 -13.

Tercan, A.E., Hindistan, M.A., & Ünver, B. (2012), " Resource Estimation of a Coal Deposit Using NETPRO/Mine ", 21st International Symposium on Mine Planning and Equipment Selection (MPES 2012), November, New Delhi, India, 861-870

van Vuuren, C. J. J. 1986. Regional setting and structure of the Rosh Pinah zinc-lead deposit, South West Africa/Namibia, 1593-1607. In: Annhaeusser, C. R. and Maske, S. (eds) *Mineral Deposits of Southern Africa*. *Geol. Soc. S. Afr.*, 2, pp. 2335.

Vann, J., Jackson, S., and Bertoli, O. 2003. Quantitative Kriging Neighbourhood Analysis for the Mining Geologist – A description of the method with worked case examples. Bendigo, Victoria, Australia, pp. 1 – 9.

Wang, G., Zhang, S., Yan, C., Song, Y., Sun, Y., Li, D. & Xu, F. 2011. Mineral potential targeting and resource assessment based on 3D geological modeling in Luanchuan region, China, *Computers & Geosciences*, 37, pp. 1976 – 1988.

Wang, G. & Huang, L. 2012. 3D geological modeling for mineral resource assessment of the Tongshan Cu deposit, Heilongjiang Province, China, *Geoscience Frontiers*, 3(4), pp. 483 – 491.

Wang, G., Pang, Z., Boisvert, J.B., Hao, V., Cao. Y. & Qu, J. 2013. Quantitative assessment of mineral resources by assessment of mineral resources by

combining geostatistics and fractal methods in the Tongshan porphyry Cu deposit (China), *Journal of Geochemical Exploration*, 134, pp. 85 – 98.

Watkeys, M.K. 2001. 'A preliminary report on the structural geology of the Eastern Orefield, Rosh Pinah'. School of Geological and Computer Sciences, University of Natal, Durban, South Africa.

Watson, M.D. 1980. The geology, mineralogy and origin of the Zn-Pb-Cu deposit at Rosh Pinah, South West Africa. Unpublished PhD thesis, University of Pretoria, South Africa, pp. 250.

Webster, R., and McBratney, A.B. 1987. Mapping soil fertility at Broom's Barn by simple kriging. *J. Sci. Food Agric.* 38, pp. 97–115.

Webber, T., Costa, J.F.C.L. & Savadoretti, P. 2013. Using borehole geophysical data as soft information in indicator kriging for coal quality estimation. *International Journal of Coal Geology*, 112, pp. 67 – 75.

Zawadzki, J., Fabijańczyk, P. & Badura, H. 2013. Estimation of methane content in coal mines using supplementary physical measurements and multivariable geostatistics, *International Journal of Coal Geology*, 118, pp. 33 – 44.

**APPENDIX A****COLLARS WITHOUT COORDINATES**

<b>BHID</b>	<b>Comment</b>
p4400	Remove from database, missing coordinates
p4401	Remove from database, missing coordinates
p4402	Remove from database, missing coordinates
p4403	Remove from database, missing coordinates
p4404	Remove from database, missing coordinates
p4405	Remove from database, missing coordinates
p4406	Remove from database, missing coordinates
p4343	Remove from database, missing coordinates
p4206a	Remove from database, missing coordinates

APPENDIX B

HOLES SAMPLED BUT MISSING ASSAY RESULTS

<b>BOREHOLE NUMBER</b>	<b>SECTION</b>	<b>OREFIELD</b>	<b>SAMPLES</b>	<b>ANHALYSIS</b>
p2427	-1050	EF1	√	x
p2499	-1040	EF1	√	x
p2629	-1100	EF1	√	x
p2650A	-1070	EF1	√	x
p2730A	-1100	EF1	√	x
p2781	-1090	EF1	√	x
p2856	EOF2_40	EF2	√	x
p2879	-1010	EF1	√	x
p2886	-1030	EF1	√	x
p4208	90MG 930	EF1	√	x
p4354	-960	EF1	√	x
u1667	-960	EF1	√	x
u1679	-990	EF1	√	x
p4343	-970	EF1	√	x
p2899a	-1010	EF1	√	x
p2629	-1100	EF1	√	x
p3563	EOF2 70	EF2	x	x

**APPENDIX C**

**HOLES WITH WRONG ORIENTATIONS OR CONFLICTING GEOLOGY AND GRADE**

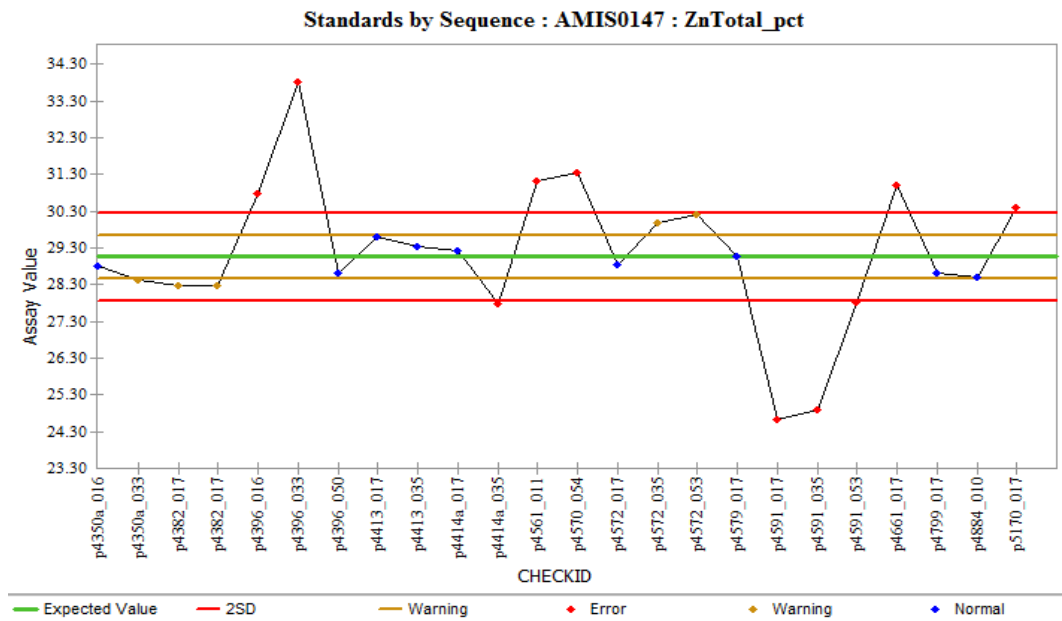
BHID	Section
p4389	-930
p4374a	-940
p4367	-950
p4358	-960
p4535	-970
p4351	-970
p4344	-980
p4573	-980
p3605	-980
p4792	-990
p4330	-1000
p3611	-1000
p3565	-1020
p4914	-1020
p4826	-1030
p2886	-1030
p4815	-1030
p4221	-1030

BHID	Section
p2786	-1040
p2787	-1040
p4227	-1040
p4308	-1040
p3684	-1050
p2427	-1050
p3188	-1050
p3189	-1050
p2387	-1060
p2388	-1060
p2447a	-1090
p4295	EOF2 0
p3577	EOF2 0
p4880	EOF2 0
p4300	EOF2 10
p4239	EOF2 10
p4237	EOF2 20
p4308	EOF2 30

BHID	Section
p4221	EOF2 50
p3189	EOF2 50
p3188	EOF2 50
p3650	EOF2 80
p4274	EOF2 80
p3929	EOF2 120
u1774	-930
u2627	-990
u1679	-990
u1696	-990
u2627	-1000
u2567	-1000
u2627	-1010
u1663	-1020
u2412	-1030
u1520	-1030
u2264	-1030
u1468	-1040

BHID	Section
u2588	-1040
u2412	-1040
u1695	-1050
u1697	-1050
u1693	-1050
u1650	-1050
u1512	-1110
u1527	-1110
u1544	-1120
u1323	EOF2 120
u1508	EOF2 0
u1895	EOF2 0
u1504	EOF2 0
u1916	EOF2 80
u2125	EOF2 90
u1841	EOF2 60

AMISO147 Zn ANALYSES & SUMMARY STATISTICS



AMISO147 – Zn standard descriptive statistics

# of Analyses above Threshold	# Outside Error Limit	% Outside Error Limit	Mean	Median	Min	Max	Standard Deviation	Standard Error	Total Bias
24	10	41.67	29.25	28.95	24.64	33.81	1.89	0.39	0.003

**APPENDIX E**

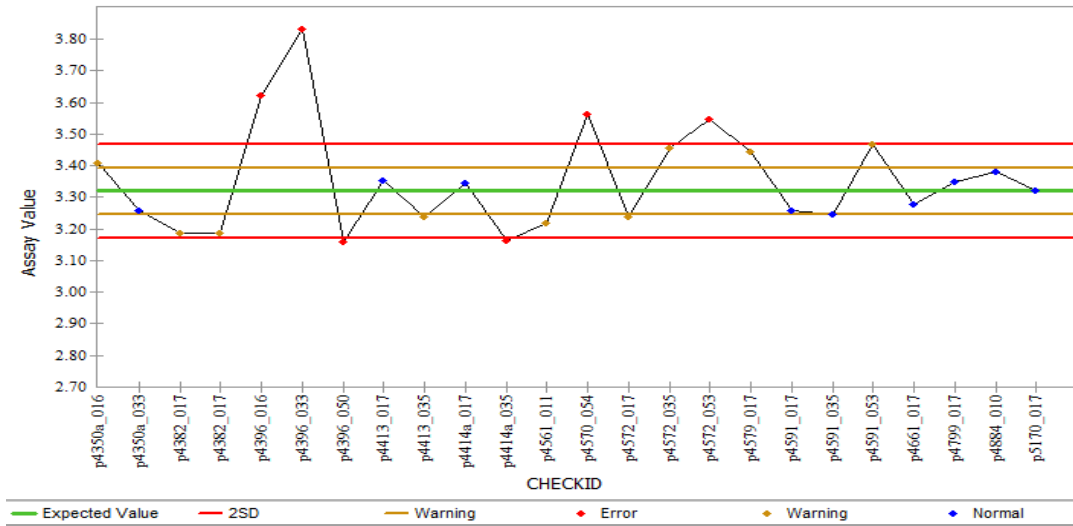
**AMISO147 RETURNING ASSAYS THAT PLOT OUTSIDE ACCEPTABLE LIMITS**

CHECKID	STANDARD VALUE	ASSAY VALUE	ACCEPTABLE MIN	ACCEPTABLE MAX	RETURN DATE	ANALYSIS
p4396_016	29.05	30.76	27.85	30.25	10-Oct-11	Zn
p4396_033	29.05	33.81	27.85	30.25	10-Oct-11	Zn
p4414a_035	29.05	27.79	27.85	30.25	05-Dec-11	Zn
p4561_011	29.05	31.10	27.85	30.25	10-Oct-11	Zn
p4570_054	29.05	31.35	27.85	30.25	10-Oct-11	Zn
p4591_017	29.05	24.64	27.85	30.25	10-Oct-11	Zn
p4591_035	29.05	24.88	27.85	30.25	10-Oct-11	Zn
p4591_053	29.05	27.80	27.85	30.25	10-Oct-11	Zn
p4661_017	29.05	31.00	27.85	30.25	10-Oct-11	Zn
p5170_017	29.05	30.38	27.85	30.25	15-Sep-13	Zn
p4396_016	3.32	3.62	3.17	3.47	10-Oct-11	Pb
p4396_033	3.32	3.83	3.17	3.47	10-Oct-11	Pb
p4396_050	3.32	3.16	3.17	3.47	10-Oct-11	Pb
p4414a_035	3.32	3.17	3.17	3.47	05-Dec-11	Pb
p4570_054	3.32	3.56	3.17	3.47	10-Oct-11	Pb
p4572_053	3.32	3.55	3.17	3.47	10-Oct-11	Pb
p4396_050	62.8	0	57.8	67.8	10-Oct-11	Ag
p4570_054	62.8	6.631	57.8	67.8	10-Oct-11	Ag



APPENDIX F

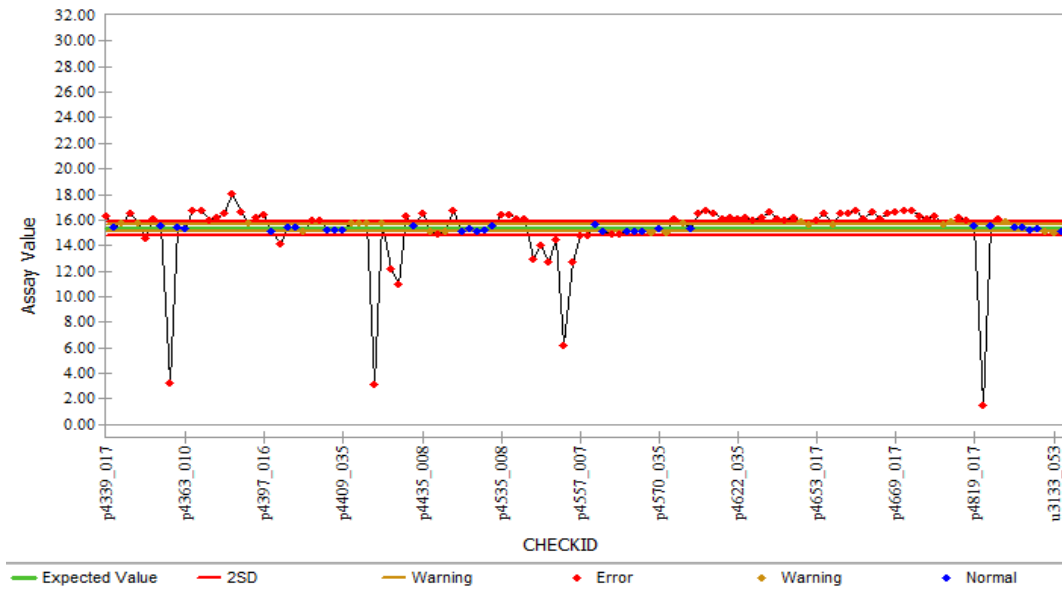
AMISO147 Pb ANALYSES & SUMMARY STATISTICS



AMISO147 – Pb standard descriptive statistics

# of Analyses above Threshold	# Outside Error Limit	% Outside Error Limit	Mean	Median	Min	Max	Standard Dev.	Standard Error	Total Bias
24	6	25	3.34	3.33	3.16	3.83	0.16	0.03	0.011

AMISO149 Zn ANALYSES & SUMMARY STATISTICS

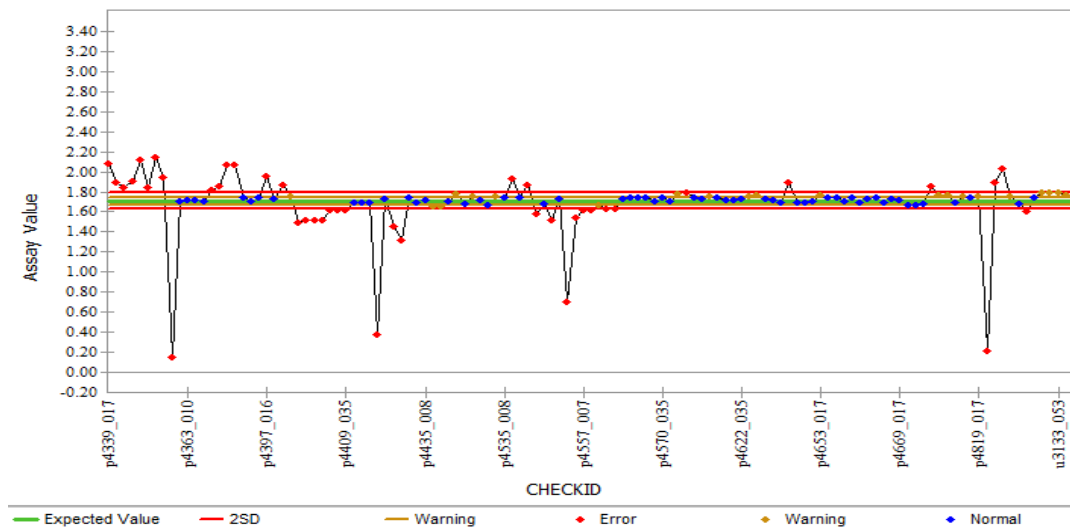


AMISO149 Zn Total (%) standard analyses by sequence.

AMISO149 – Zn standard descriptive statistics

# of Analyses above Threshold	# Outside Error Limit	% Outside Error Limit	Mean	Median	Min	Max	Standard Dev.	Standard Error	Total Bias
122	71	58.20	15.70	15.74	1.53	18.05	2.42	0.22	-0.008

AMISO149 Pb ANALYSES & SUMMARY STATISTICS



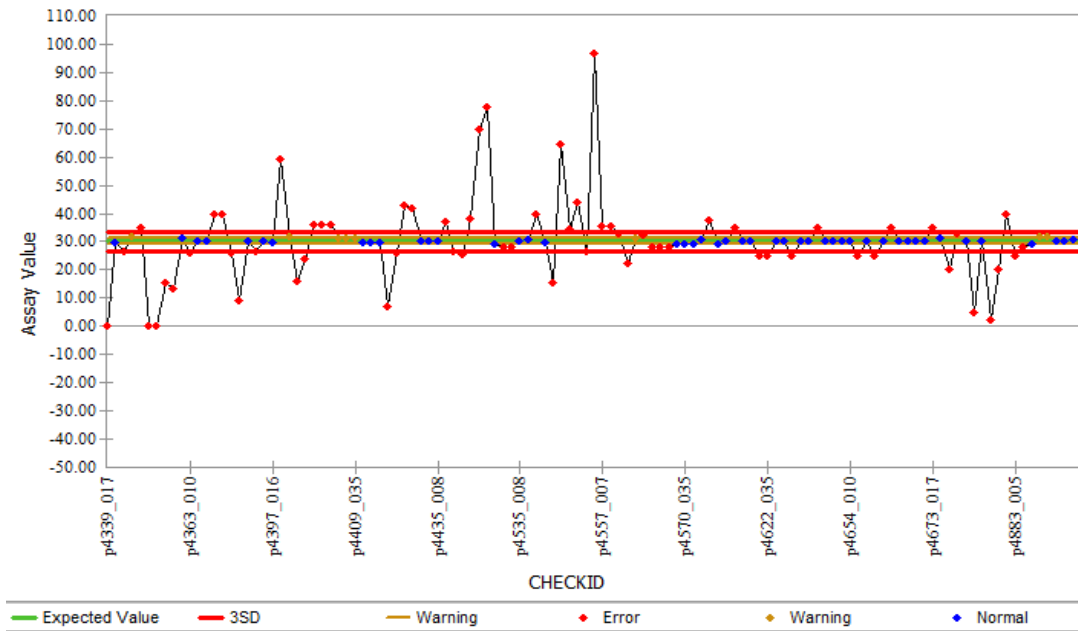
AMISO149 Pb Total (%) standard analyses by sequence.

AMISO149 – Pb standard descriptive statistics

# of Analyses above Threshold	# Outside Error Limit	% Outside Error Limit	Mean	Median	Min	Max	Standard Dev.	Standard Error	Total Bias
122	42	34.43	1.73	1.73	0.15	2.14	0.28	0.03	-0.009

APPENDIX I

AMISO149 Ag ANALYSES & SUMMARY STATISTICS

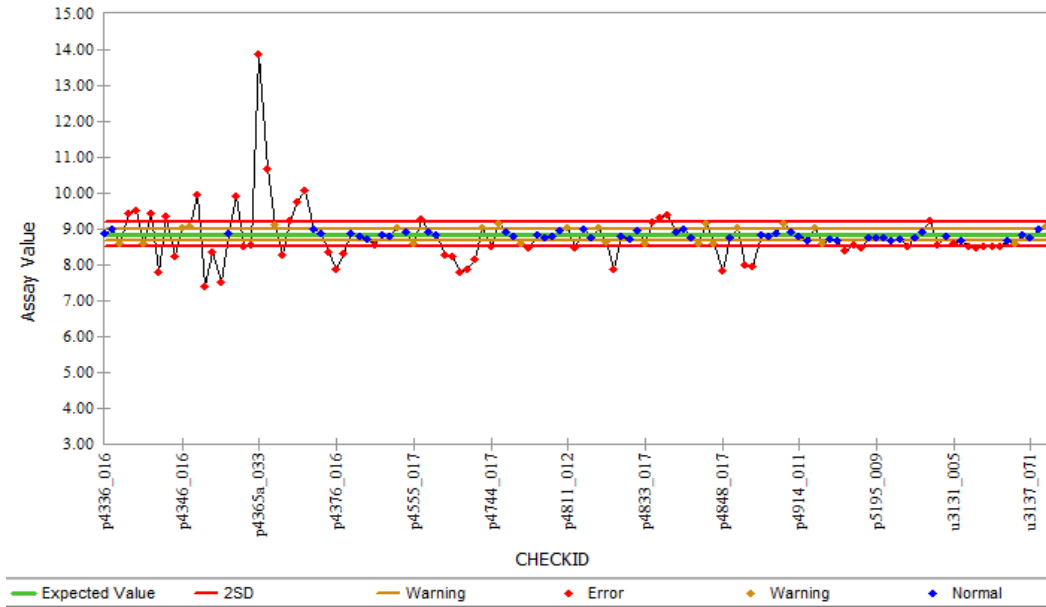


AMISO149 Ag Total (ppm) standard analyses by sequence.

AMISO149 – Ag standard descriptive statistics

# of Analyses above Threshold	# Outside Error Limit	% Outside Error Limit	Mean	Median	Min	Max	Standard Dev.	Standard Error	Total Bias
118	64	54.24	29.98	30	0	97.05	12.48	1.15	0.009

AMISO153 Zn ANALYSES & SUMMARY STATISTICS



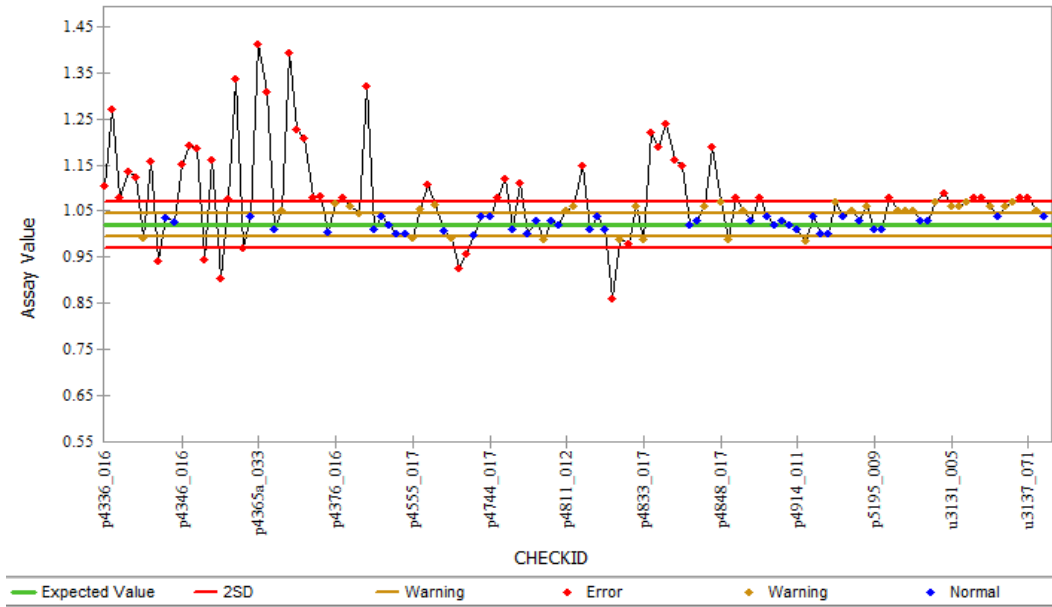
AMISO153 Zn Total (%) standard analyses by sequence.

AMISO153 – Zn standard descriptive statistics

# of Analyses above Threshold	# Outside Error Limit	% Outside Error Limit	Mean	Median	Min	Max	Standard Dev.	Standard Error	Total Bias
123	51	41.46	8.77	8.77	7.39	13.88	0.66	0.06	-0.004

APPENDIX K

AMISO153 Pb ANALYSES & SUMMARY STATISTICS



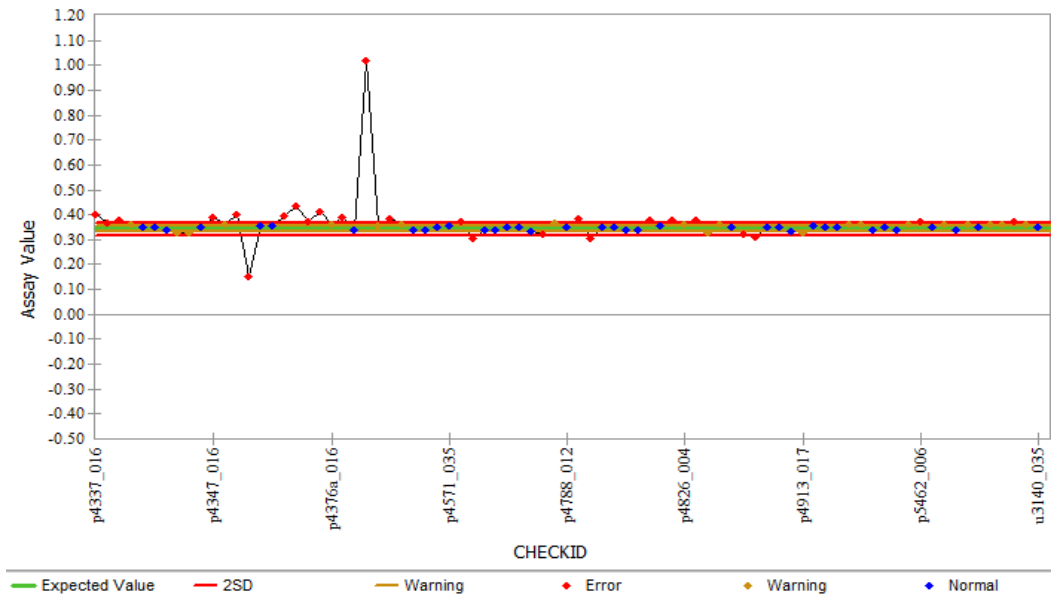
AMISO153 Pb Total (%) standard analyses by sequence.

AMISO153 – Pb standard descriptive statistics

# of Analyses above Threshold	# Outside Error Limit	% Outside Error Limit	Mean	Median	Min	Max	Standard Dev.	Standard Error	Total Bias
123	48	39.0244	1.05	1.05	0.86	1.4129	0.09	0.01	0.046

APPENDIX L

AMISO157 Pb ANALYSES & SUMMARY STATISTICS



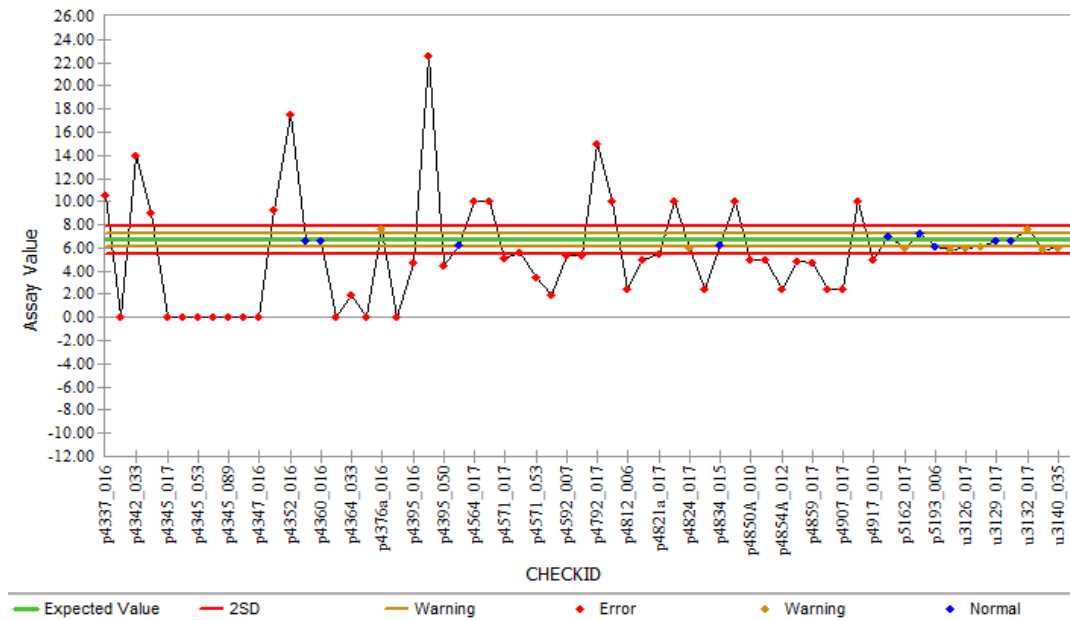
AMISO157 Pb Total (%) standard analyses by sequence.

AMISO157 – Pb standard descriptive statistics

# of Analyses above Threshold	# Outside Error Limit	% Outside Error Limit	Mean	Median	Min	Max	Standard Dev.	Standard Error	Total Bias
72	22	30.56	0.35	0.35	0.30	1.02	0.08	0.01	0.06

APPENDIX M

AMISO157 Ag ANALYSES & SUMMARY STATISTICS



AMISO157 Ag Total (ppm) standard analyses by sequence.

AMISO157 – Ag standard descriptive statistics

# of Analyses above Threshold	# Outside Error Limit	% Outside Error Limit	Mean	Median	Min	Max	Standard Dev.	Standard Error	Total Bias
63	45	71.43	5.14	5.62	0	22.54	4.40	0.55	-0.15



APPENDIX N

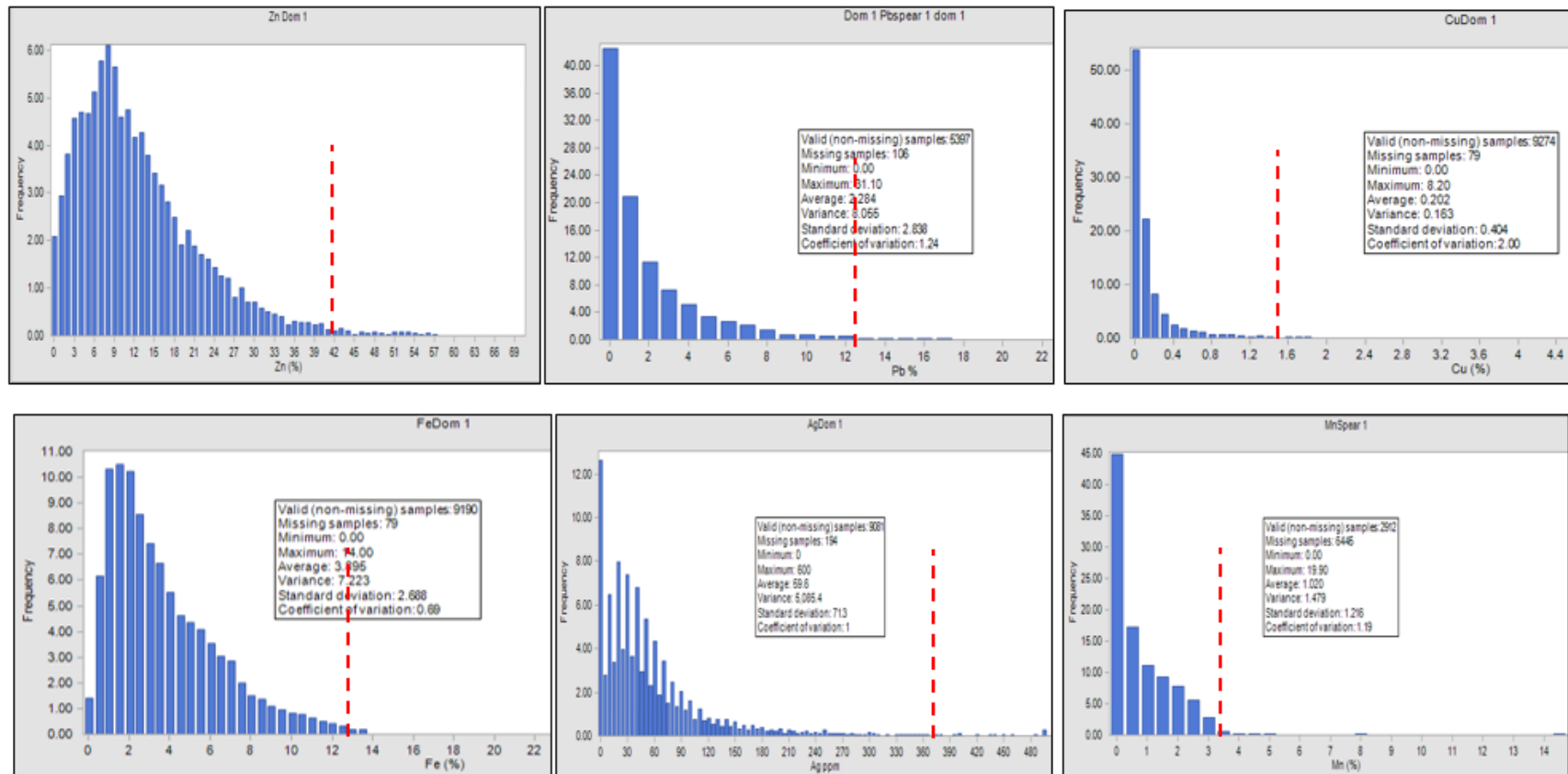
DUPLICATES DESCRIPTIVE STATISTICS

<b>Zn Field duplicates</b>	<b>Original</b>	<b>Check</b>
Count	477	
# Outside Error Limit	135	
Mean	4.3663	4.5903
Median	2.86	3.22
Min	0.01	0.01
Max	44.1	42.2
Range	44.09	42.19
Variance	25.3228	25.6514
Coefficient of Variation	1.1525	1.1034
Pop. Std. Dev.	5.0322	5.0647
Bias	0.0513	
Correlation Coefficient	0.9614	
Error	1.9862	
% of Population with AMPRD > 10%	28.7212	

<b>Pb Field duplicate</b>	<b>Original</b>	<b>Repeat</b>
Count	473	
# Outside Error Limit	183	
Mean	0.9854	1.0455
Median	0.38	0.3924
Min	0	0
Max	21.08	20.89
Range	21.08	20.89
Variance	3.7687	3.8296
Coefficient of Variation	1.97	1.8718
Pop. Std. Dev.	1.9413	1.9569
Bias	0.0609	
Correlation Coefficient	0.9805	
Error	0.5476	
% of Population with AMPRD > 10%	38.6892	

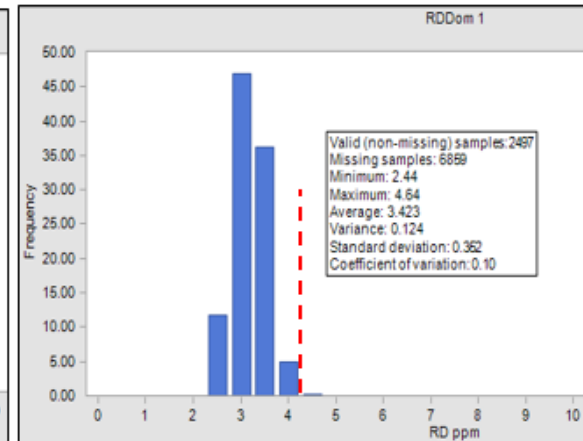
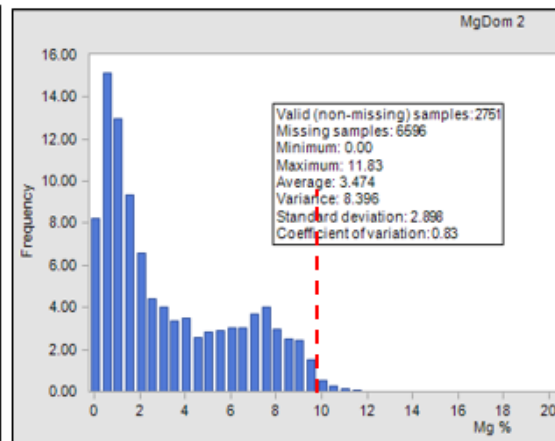
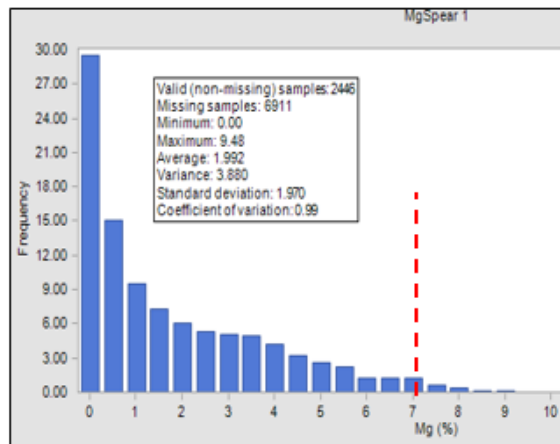
APPENDIX O

Zn, Pb, Cu, Fe, Ag, Mn histograms of 1.5m composites for Domain 1

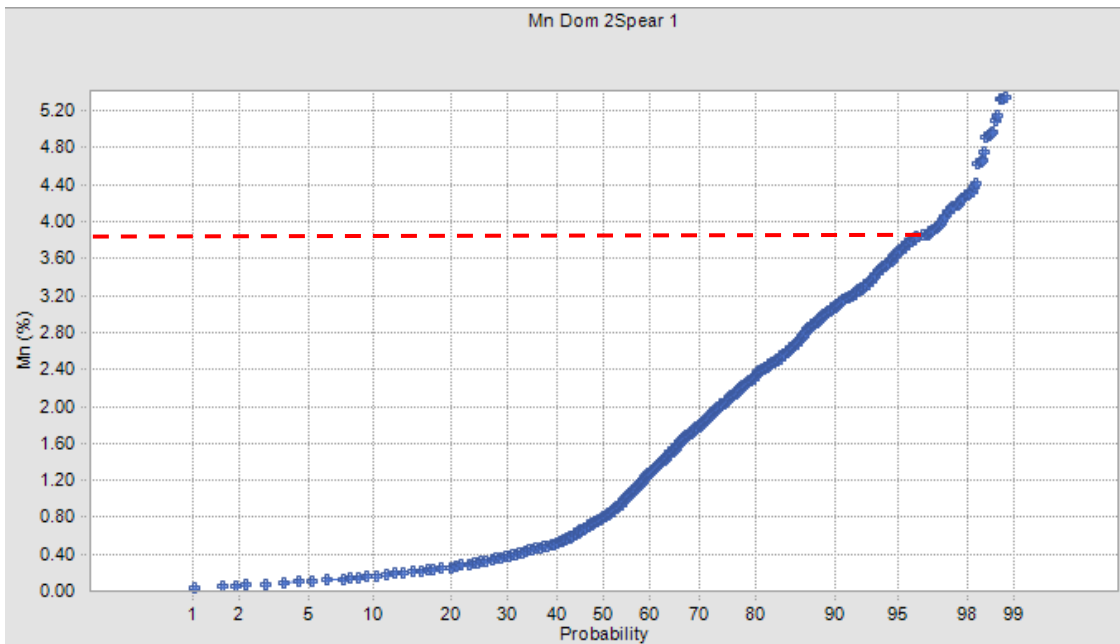
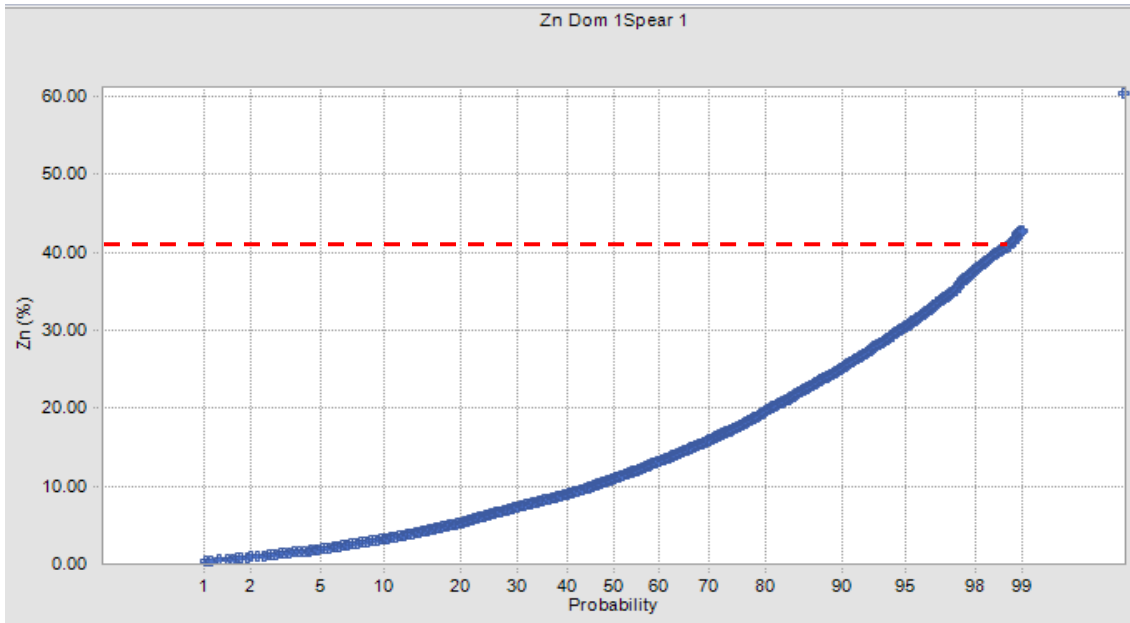


APPENDIX P

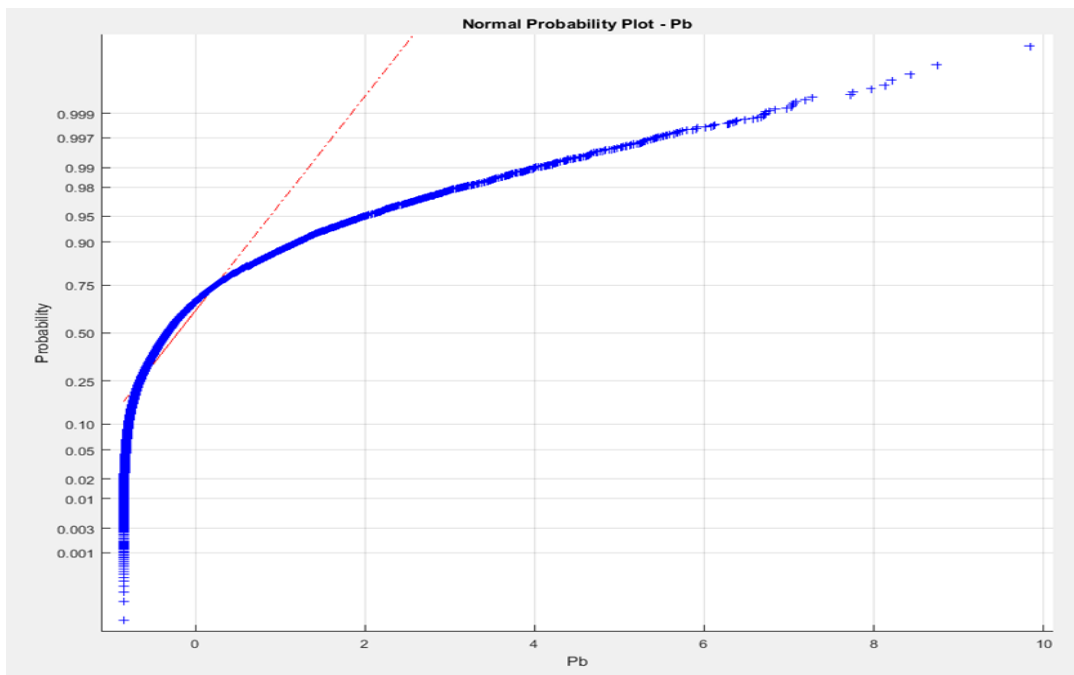
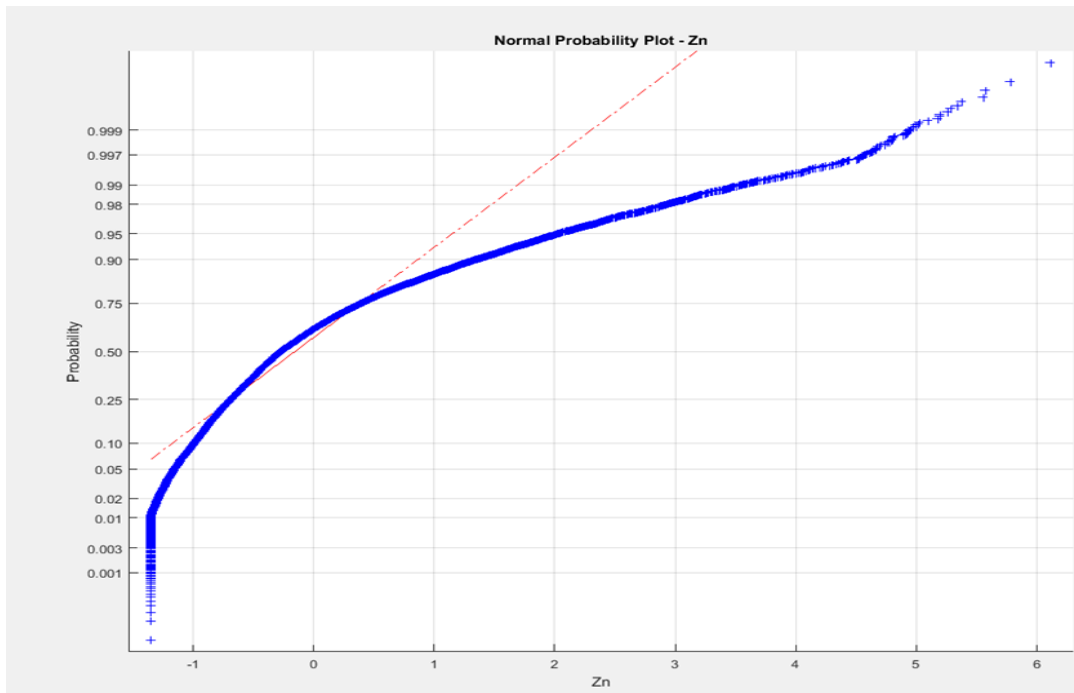
Domain 1 Mg, Domain 2 Mg and Domain 1 Rd histograms of 1.5m composites



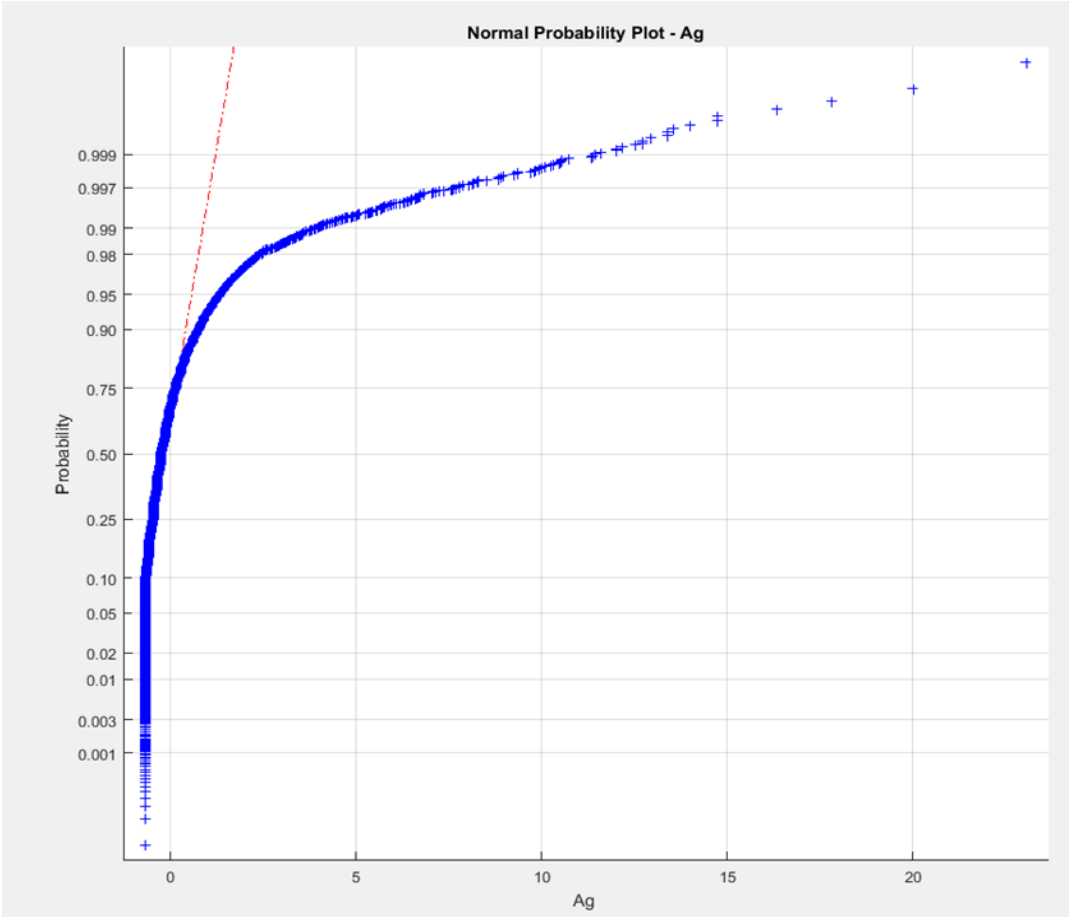
Cumulative Probability Plot for Domain 1 Zn and Domain 2 Mn



Z-scores Normal Probability Plot for Zn and Pb



Z-scores Normal Probability Plot for Ag

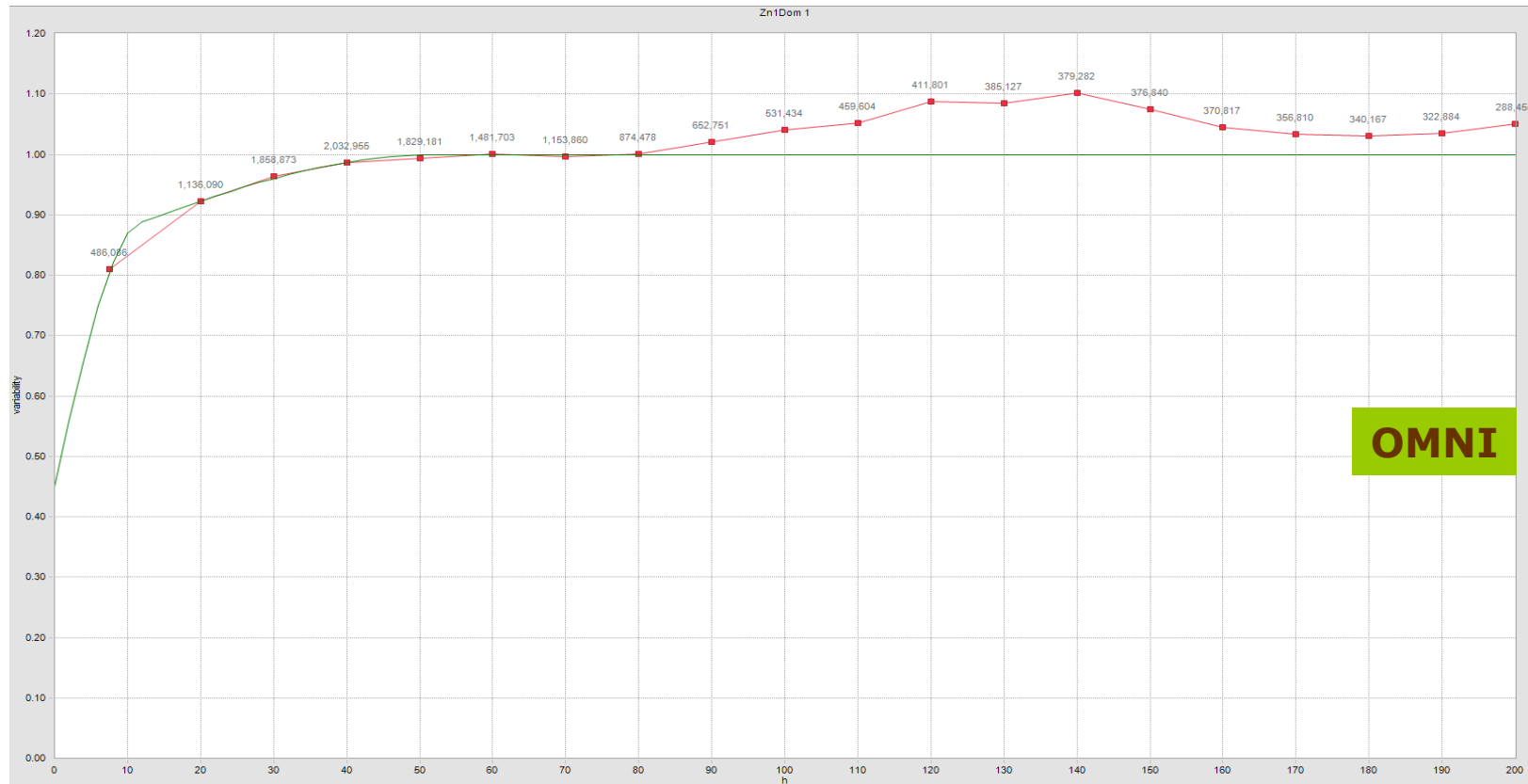


Zn Omni-Directional Variogram for Domain 1

OMNI-DIRECTIONAL VARIOGRAM, LAG 10M TO DETERMINE NUGGET  
(IN PLACE OF DOWNHOLE VARIOGRAM)

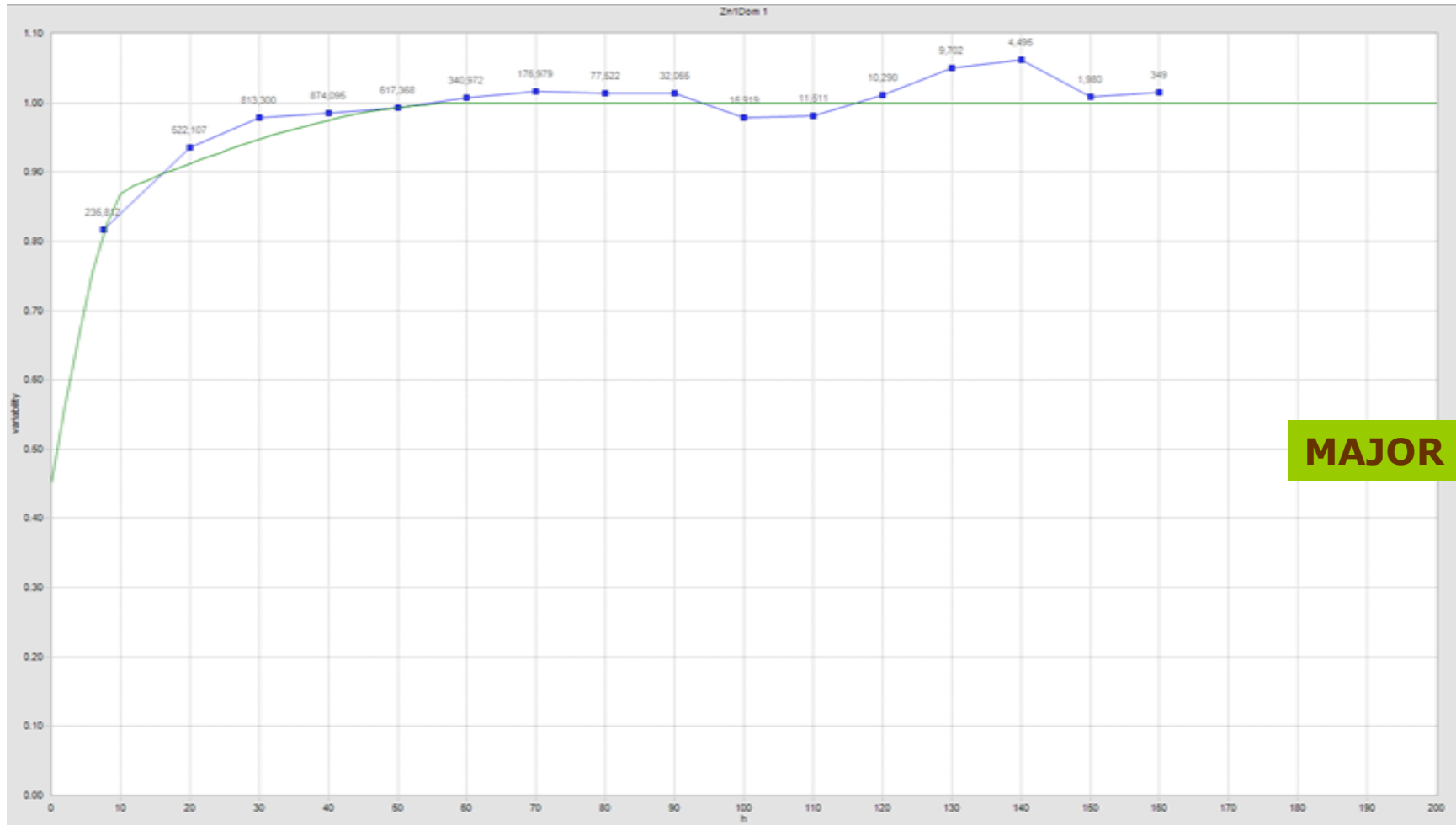
ROT = 47.5  
DIPN = 0  
DIPE = -69

FROM CONTOURED  
VARIOGRAPHY



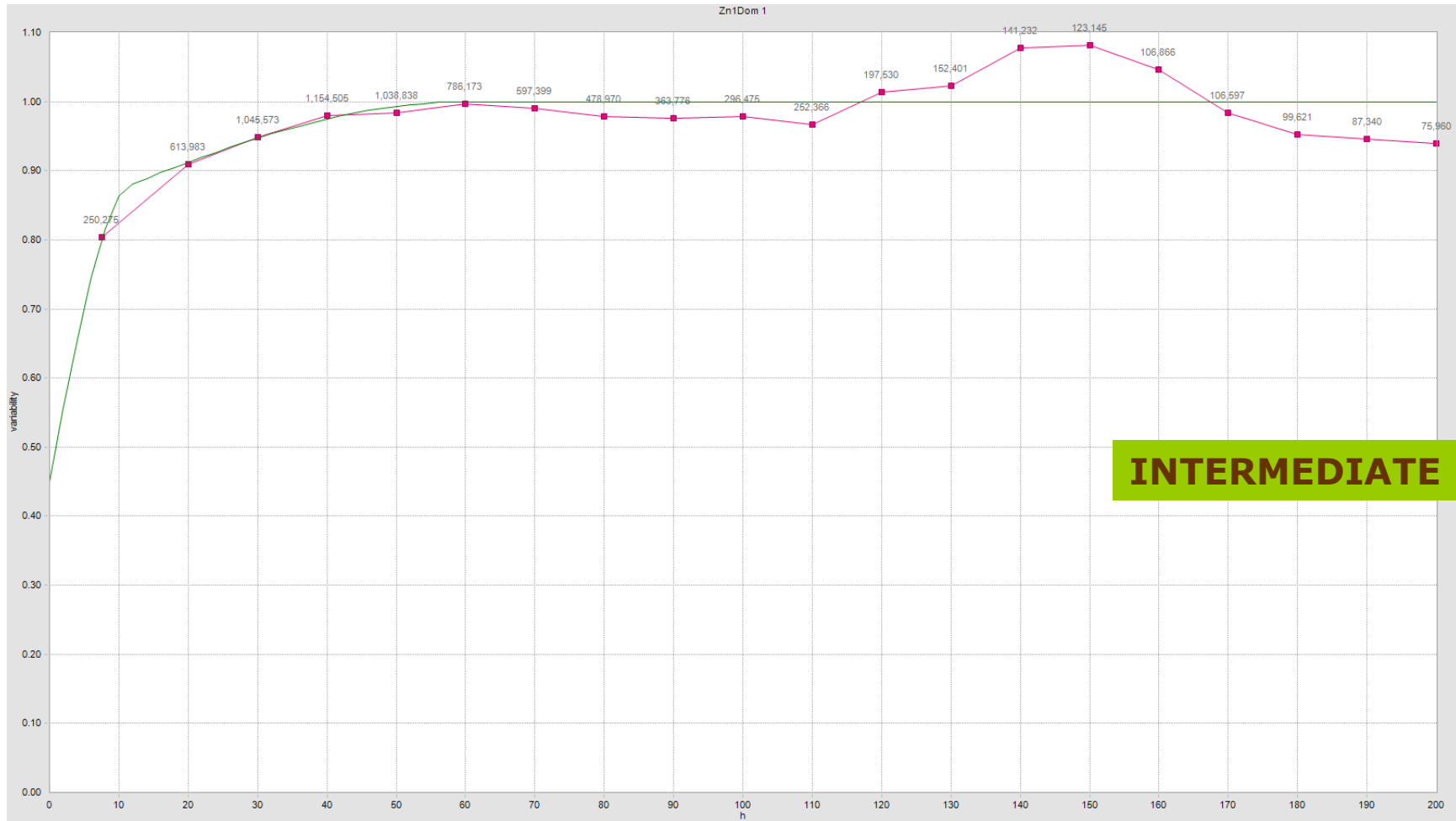
CUT-OFF OF 0.01 % Zn (Bottom cut) and 41% (Top Cut)  
45° Windowing angle  
10m Lag distance  
30m band width

Zn Variogram for Domain 1 in the major direction

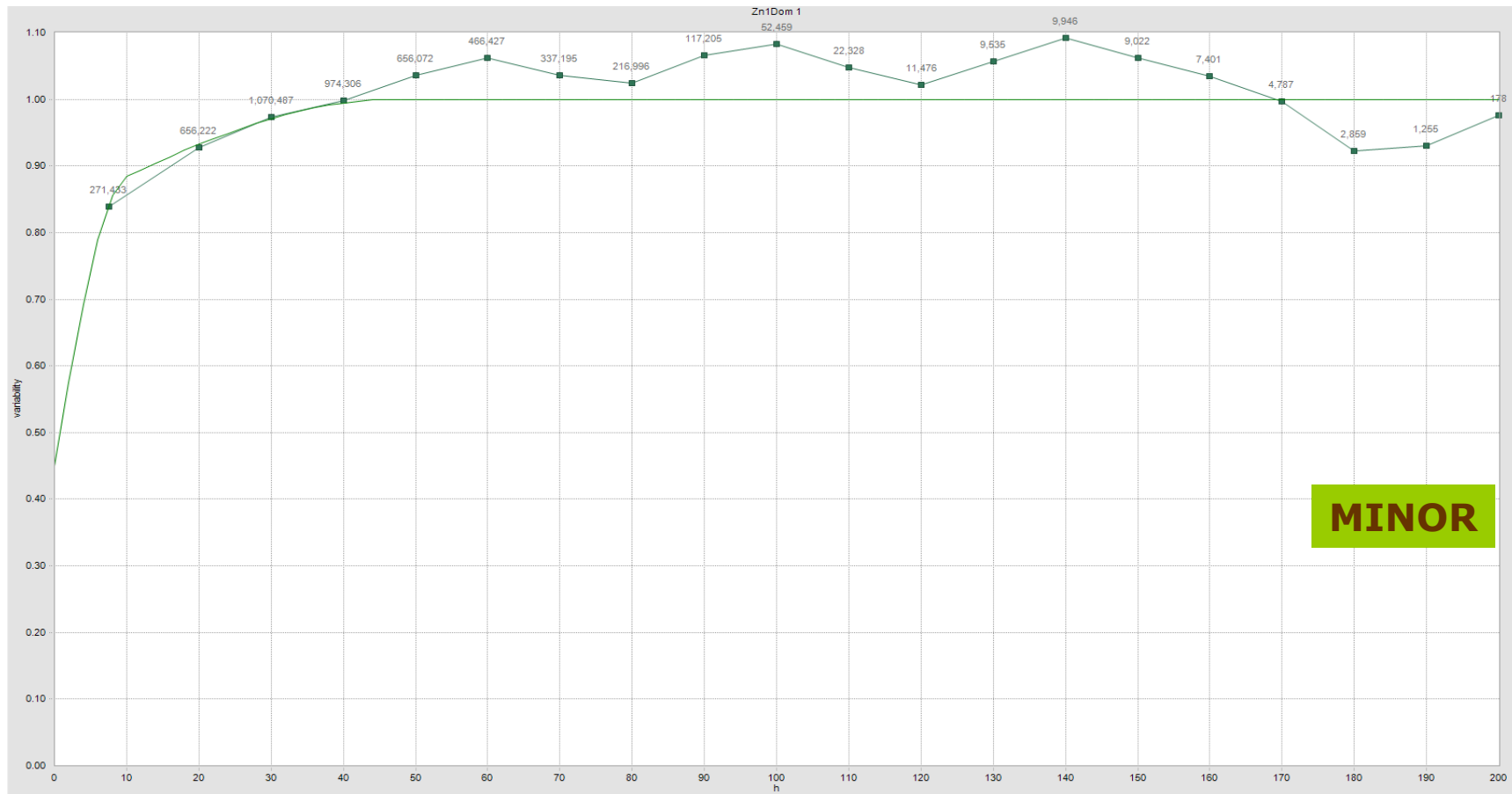




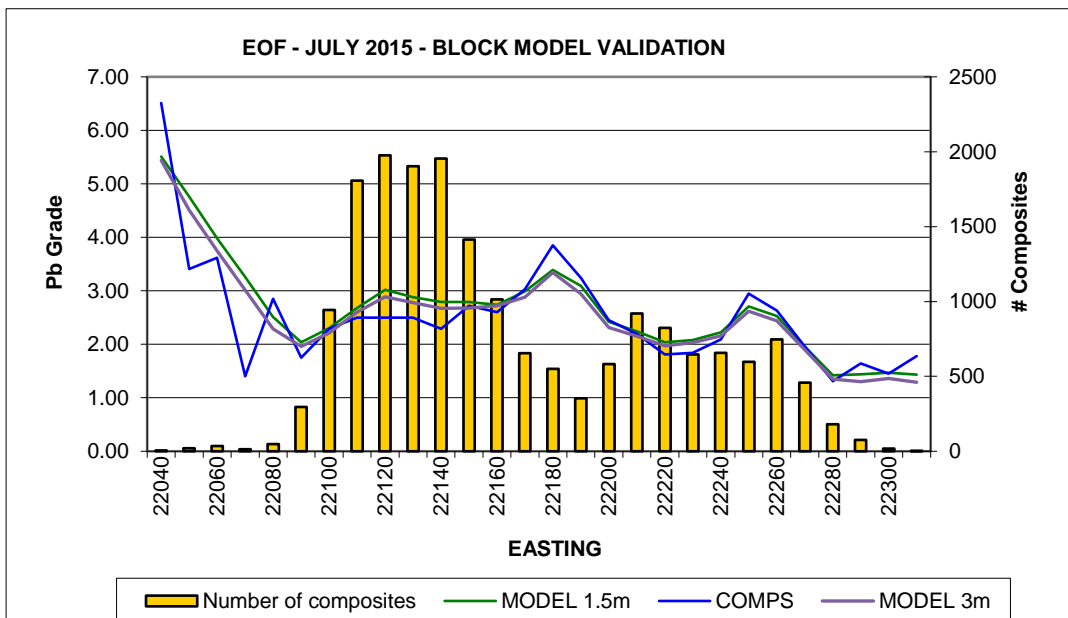
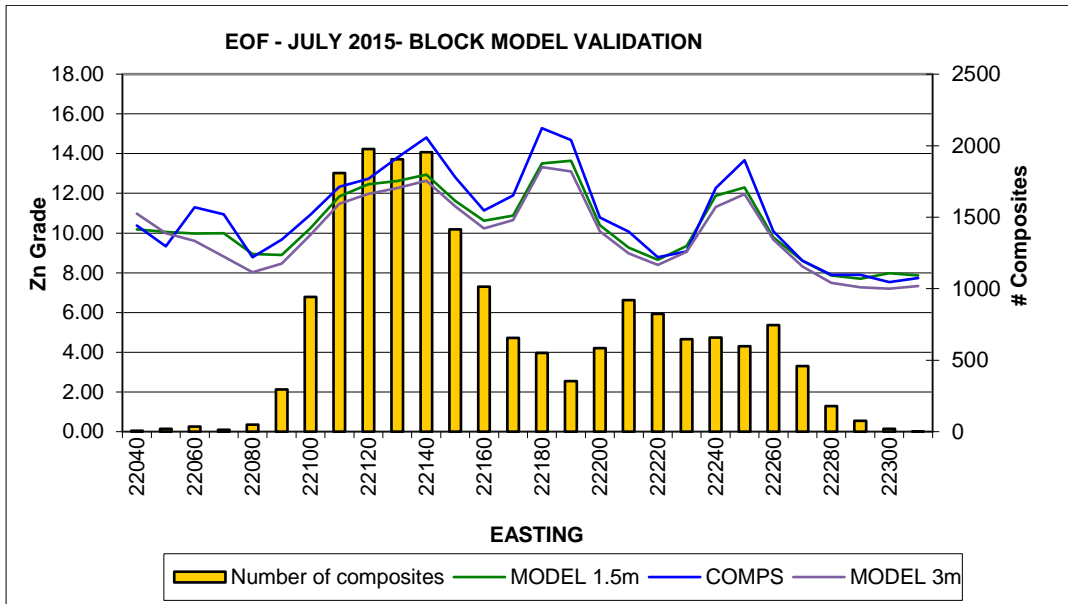
Zn Variogram for Domain 1 in the intermediate direction



Zn Variogram for Domain 1 in the minor direction



Zn and Pb swath plots in the easting direction



APPENDIX Z

Ag swath plot in the easting direction

